THE EFFECT OF FINS ON FLUIDELASTIC INSTABILITY IN IN-LINE AND ROTATED SQUARE TUBE ARRAYS

THE EFFECT OF FINS ON FLUIDELASTIC INSTABILITY IN IN-LINE AND ROTATED SQUARE TUBE ARRAYS

By

ROBERT HAYDEN LUMSDEN, B. Eng.

A Thesis

Submitted to the School of Graduate Studies

in Partial Fulfilment of the Requirements

for the Degree

Master of Applied Science

McMaster University

MASTER OF APPLIED SCIENCE (2008) McMaster University

(Department of Mechanical Engineering) Hamilton, Ontario

TITLE: The effect of fins on fluidelastic instability in in-line and rotated square tube arrays

AUTHOR: Robert Hayden Lumsden, B. Eng.

SUPERVISOR: David S. Weaver

NUMBER OF PAGES: xiv, 121

Abstract

The study of fluidelastic instability in tube arrays has been ongoing for four decades. Although much research has been conducted, a full understanding of the mechanisms involved is still not available. Designers of cross-flow heat exchangers must depend on experience and empirical data from laboratory studies. As new designs are developed, which differ from these experimental facilities, there is an increased risk of failure due to fluidelastic instability.

An experimental program was conducted to examine fluidelastic instability in in-line and rotated square finned tube arrays. Three arrays of each geometry type were studied; two with serrated, helically wound finned tubes of different fin densities, and the third, a bare tube which had the same base diameter as the finned tubes. The tube pitch was kept constant to reduce the number of test sections required under this investigation. As a result, the bare tube array has a larger tube pitch ratio than that of previous researchers.

The finned tubes under consideration were commercial finned tubes of a type typically used in the fossil and process industries. The addition of fins to tubes in heat exchangers enhances heat transfer due to the increased surface area and the turbulence produced by the flow moving over the fins. The resulting flow pattern/distribution due to the fins is therefore much more complicated than in bare tube arrays. Previous research has shown that an effective diameter of a finned tube is useful in the prediction of vortex shedding. This concept is used to compare the finned tube results with the existing bare tube array guidelines for fluidelastic instability. All of the tube arrays in the present

study have the same tube pitch, and have been scaled to have the same mass ratio. Results for the rotated square arrays show that the use of an effective diameter is beneficial in the scaling of fluidelastic instability and the finned tube results are found to fit within the scatter of the existing data for fluidelastic instability. For in-line square arrays, the results indicate that fins significantly increase the stability threshold.

Acknowledgements

The author would like to thank many individuals for their contributions toward the completion of this thesis.

Professors:
Dr. Ross L. Judd – Mentoring and encouragement
Dr. David S. Weaver – Supervision, mentoring & encouragement
Dr. Samir Ziada – General help with acoustic emissions

Technicians:
Andrew Buyers – Welding/Guidance
Ron Lodewyks – Manufacturing/Design for manufacturing advice/guidance
Mark MacKenzie – Welding of tubes
Jim McLaren – Building of jigs for machining threaded rods
Dave Schick – Help with anything
Joe Verhaeghe – Soldiering/Electronics support

Post Doctoral:
Dr. Paul Feenstra – Assistance with strain gauge installation and with the wind tunnel
Dr. Rafael Bravo – MATLAB assistance

Peers:
Joaquin Moran – Sounding board, mentoring & encouragement
Youssef Ziada – General sounding board

Flow-Induced Vibration and Noise Group:
The weekly meetings of the group have helped myself immensely with public speaking and are beneficial as a sounding board for new ideas and solving problems.

Finally, I would like to thank my parents and family for their encouragement and continued support during this time.

Whomsoever you see in distress, recognize in him a fellow man

Royal Life Saving Society of Canada

Table of Contents

Nomenclature

A - Amplitude of vibration
D - Diameter or Characteristic length
E - Young's Modulus of Elasticity
f - Frequency or natural frequency of the tube
fpi - Fins per inch
F - Fluid flow area
h - Fin height
I - 2nd area moment of Inertia
k - Stiffness
K - Proportionality constant
l - Threaded rod length
L - Test Tube length
m - Tube mass per unit length
n - Power
p - Fin pitch
P_t - Tube pitch
P - Perimeter of flow area in contact with finned tube
Re_D - Reynolds Number
s - Serration length
St - Strouhal Number
t - Fin thickness
U - Velocity
w - Serration width
δ - Logarithmic decrement of damping
ρ - Density
ω - Circular frequency

Subscript

b - Bare
$crit$ - Critical
D - Datum
eq - Equivalent
eff - Effective
f - Fin
n - Natural
p - Pitch
red - Reduced
u - Upstream
V - Variable
vs - Vortex Shedding

List of Figures

List of Tables

1.0 Introduction

Flow-induced vibrations can cause damage in tube bundles over a long period of time, due to turbulent buffeting or vortex shedding in gas flows, or they can produce high levels of noise due to acoustic resonance. However, none of these compare to the tube failures caused by fluidelastic instability. Fluidelastic instability occurs once a critical velocity is exceeded within a cross-flow tube bundle. The resulting vibration amplitudes of the tubes dramatically increase with increasing flow velocity. Many experiments have been conducted and several guidelines have been proposed to give industry safe/stable operating velocities for cross-flow tube arrays. The majority of this research has been conducted using bare tubes. However, designers of heat exchangers have been using finned tubes without experimental fluidelastic threshold data. This current study investigates the critical velocity for two different finned tube bundle geometries: an in-line and a rotated square array each with two different fin densities. Due to the lack of data available in finned tube array research, the comparison of finned tubes to bare tubes has been made using an effective diameter. Studies which suggest the use of an effective diameter have considered finned tubes mainly under vortex shedding. The same effective diameter was used in this study of fluidelastic instability in finned tube bundles. Preliminary results from this study were reported in Lumsden and Weaver (2006). The experimental results of this thesis are published in Lumsden and Weaver (2007).

Section 2 is the literature review. Sections 2.1 and 2.2 discuss flow-induced vibrations and the history of the study of fluidelastic instability, presenting the

mechanisms, the effect of different variables, modeling and the different guidelines which have been used for the prevention/prediction of fluidelastic instability. Sections 2.3, 2.4 and 2.5 discuss the literature pertaining to the use of finned tubes, such as the applications and previous flow-induced vibration research. Section 3 pertains to the experimental apparatus and procedure used during the capture of the experimental results. Section 4 presents the results of the current study and discusses how the results relate to the existing literature. Section 5 explains the conclusions and recommendations from the current study. Section 6 lists the references. Section 7, the appendices, lists the supporting information for this thesis.

2.0 Literature Review

Fluidelastic instability is a much researched, but still incompletely understood type of flow-induced vibration. This literature review will discuss the early studies along with the current recommendations and guidelines used in industry relating to fluidelastic instability. It will also address some of the deficiencies that have occurred in the research of this instability.

Finned tubes will also be discussed to explain their use and the effect that they have on flow and flow-induced vibrations, with most attention on fluidelastic instability studies in finned tube bundles.

Due to the amount of research available on fluidelastic instability, some forty years worth, not all the information can be included in this review. General concepts and trends will be presented, but not all areas are complete in their description. Normally the earliest results found will be mentioned. The papers are generally presented chronologically to show the progression of the state of research and understanding.

2.1 Flow-Induced Vibration

There are typically four different types of flow-induced vibrations in heat exchangers in cross flow: turbulent buffeting, vortex shedding, acoustic resonance and fluidelastic instability.

Turbulent buffeting is a process which occurs over a wide band of frequencies. The damage that can be attributed to this phenomenon will typically be fretting wear at tube supports and occurs over a long period of time.

Vortices are shed from cylinders ($40 \leq Re_D \leq 3 \times 10^5$, Blevins (2001), pg. 46). The frequency of release of a vortex is governed by the Strouhal number ($St = f_{vs}D/U$, $0.18 \leq St \leq 0.22$ for a single right circular cylinder). In tube arrays, two or more Strouhal numbers can be found depending on the Reynolds number, array geometry and the tube pitch to diameter (P_t/D) ratio. If the frequency of vortex shedding is equal to the natural frequency of the cylinder, resonance occurs, which in liquid flows can cause significant vibration amplitudes. In air, the response is typically less significant.

If the frequency of vortex shedding is equal to the acoustic natural frequency of the surrounding heat exchanger shell, an auditory response can occur at levels above the allowable health and safety working limits. This acoustic resonance can exceed sound pressure levels of 165 dB and can cause structural damage as well.

Fluidelastic instability will be discussed in the following section. Since it is the topic of this thesis, a more in depth background is provided.

2.2 Fluidelastic Instability

2.2.1 Definitions, Early Studies and Restrictions

Fluidelastic instability is a flow-induced vibration problem which occurs when a critical flow velocity is reached. At this velocity, the tubes within a row (cascade) or bundle of tubes are excited by the flow at or near their natural frequency, causing large amplitude vibration. If the flow velocity continues to increase, the tube (or tubes) may reach high amplitudes, or more importantly, stresses that result in failure of the components (See Figure 2.1).

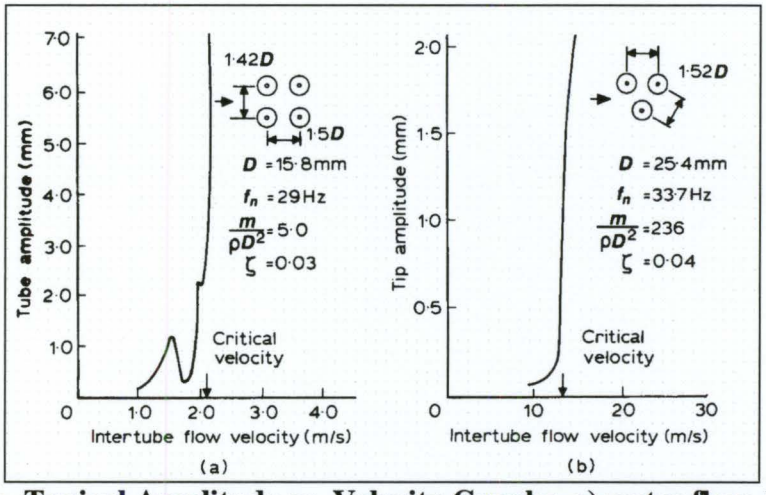

Figure 2.1: Typical Amplitude vs. Velocity Graphs, a) water flow, b) air flow (Blevins (2001), pg. 155)

Not all issues pertaining to fluidelastic instability are addressed in this review. An excellent, concise paper written by Païdoussis (1982) lists many issues pertaining to past studies of this phenomena.

2.2.1.1 Jet Switching

Jet switching, which has been described as a "coanda-like"[1] phenomenon and also as a "time-lag mechanism"[2], was first described by Roberts (1966). Roberts tested a row of tubes in cross flow, with the row perpendicular to the flow (also known as a cascade of tubes). With every other tube fixed in the row, he moved the un-fixed tubes and looked at the associated flow pattern and the forces applied to the tubes. As he moved the tube downstream by only a small amount, the flow was drawn behind the upstream cylinders, reducing the wake behind those cylinders and the wake behind the downstream tube grew larger. As the un-fixed tube was moved upstream of the fixed tube, the wake behind it diminished and the wake behind the fixed tube increased in length. This flow resembles a jet between two cylinders, and as one of the cylinders is moved downstream the jet direction arcs behind the upstream tube. From this action, it can be seen that if the tubes are vibrating in the streamwise direction, out-of-phase with each other, the jet will switch back and fourth, which explains this phenomenon's name.

Roberts related jet switching by two parameters. One is the damping ratio (ζ) which is measured in *"vacuo"* or in a vacuum. He stated that this parameter "represents the amount of energy lost by the system during a steady-state vibration"[3]. The other parameter is:

$$\lambda = \frac{\rho U_0^2}{2m\omega_0^2} \tag{2.1}$$

[1] Païdoussis (1982), pg. 41
[2] Blevins (2001), pg. 154
[3] Roberts (1966), pg. 20

which "is proportional to the amount of energy available from the air stream to over come the energy loss (ζ)", "Intuitively, one might expect that the ratio of these two energy parameters to be a realistic variable."[4] "The variable (ζ/λ) may be replaced by the more practical variable of ($m\delta/\rho D^2$)."[5] Roberts plotted his experimental data on a graph (log-log plot) of the reduced velocity against this parameter, which is usually referred to as the mass-damping parameter. He also plotted his theoretical model (semi-empirical) of jet switching on the graph, which was in pretty good agreement with the experimental data. This plot is for the stability of a row of tubes for jet switching.

One interesting issue pertaining to this effect is that as the jet switches, the separation point on both tubes move. As both of the separation points move, the components of drag on each tube will change. As the tube is moved downstream, the separation points move toward the front stagnation point, decreasing the skin friction drag and oddly the pressure drag also decreases. Roberts suggests that there is a "cavity or bubble" formed behind the downstream cylinder, reducing the pressure drag. The opposite occurs for the tube that is upstream.

[4] Ibid, pg. 20
[5] Ibid, pg. 25

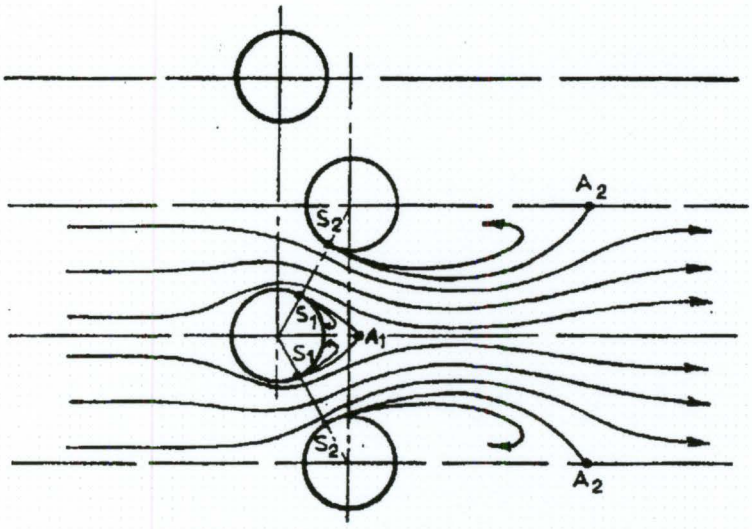

Figure 2.2: Sketch of Steady Flow through a Staggered Cascade of Cylinders, S_1 and S_2 are the Separation Points, A_1 and A_2 are the Stagnation Points, (Roberts (1966), pg. 3)

In the diagrams shown by Roberts (Figure 2.2), the wake size on the upstream cylinder is larger than the downstream cylinder and the separation points (the S_1's) for the upstream tube are behind the tube. The jet is directed behind the upstream cylinder.

Starting with a cascade of cylinders in line with each other, if one of the cylinders is displaced upstream, the total drag force on this cylinder increases and the total drag force on the downstream cylinder decreases. This will continue to cycle at the natural frequency of the cylinders until: 1) the fluid and structure are able to damp out the vibration, 2) something breaks (the cylinder or its support) to dissipate the energy in the system.

Jet switching is an instability which results in the tubes that are side by side to behave in an out-of-phase streamwise vibration relative to each other. A question which

should be asked is what happens if the tube is displaced in the transverse direction? This will be answered in the next section.

2.2.1.2 Fluidelastic Excitation

Connors in 1970 described fluidelastic excitation in the following way: "if during a cycle of vibration, the energy extracted from the flowing fluid by the tubes exceeds the energy dissipated by damping, a fluidelastic vibration will be established. The vibration is self-excited, and once initiated will grow in amplitude."[6] This is quite similar to Roberts' explanation of jet switching and under this definition; jet switching is a type of fluidelastic excitation. Connors suggests that there are two different fluidelastic mechanisms: 1) a tube position-dependent mechanism that is time-independent and 2) a time-dependent mechanism.[7] The first mechanism would suggest that fluidelastic excitation could be independent of the lag in the system. Connors associates the second mechanism with jet switching.

Connors studied a single row of five tubes, three of which were flexible, with a P_t/D=1.41. He found that the tubes went unstable at a critical velocity of 70 ft/s. The tubes were not just moving in the streamwise direction (like Roberts), but were in fact orbiting in the streamwise and transverse to flow directions. Connors described the orbiting as "not chaotic, but" "are quite repetitive and steady in certain flow ranges"[8]. He also found that as the flow velocity increased, the vibrations in the streamwise direction went as high as a quarter of the tube diameter, which was arrested when the tube hit the

[6] Connors (1970), pg. 45

clearance holes in the wall of the test section. Connors also observed different tube motion patterns of the five tubes during different experimental runs, but found that the critical velocity was still virtually the same.

He also found that when visually inspecting the amplitude of vibration relative to the flow velocity, he was able to easily pick off the critical velocity, as the velocity before the amplitude increased sharply.

Connors next experimented with five tubes in a quasi-steady investigation, similar to Roberts, but instead, he had a fixed central tube, which he monitored in the drag and lift directions, and moved the tubes above and below it out-of-phase with each other in the lift (transverse) direction. When moving the tubes away from the central tube, the force in the streamwise direction reduced, which would cause the central tube to move forward (if it wasn't fixed). Also, when the tubes were returned to their original position and then brought transversely towards the central tube, the streamwise force increased. The motion of the two tubes in the transverse direction, if cycled in the above manner, would cause the central tube to have forces that result in the tubes' motion in the streamwise direction in a cyclical fashion. Connors plotted these force values against the deflection of the moved tubes (Figure 2.3).

---

[7] Ibid, pg. 45
[8] Ibid, pg. 47

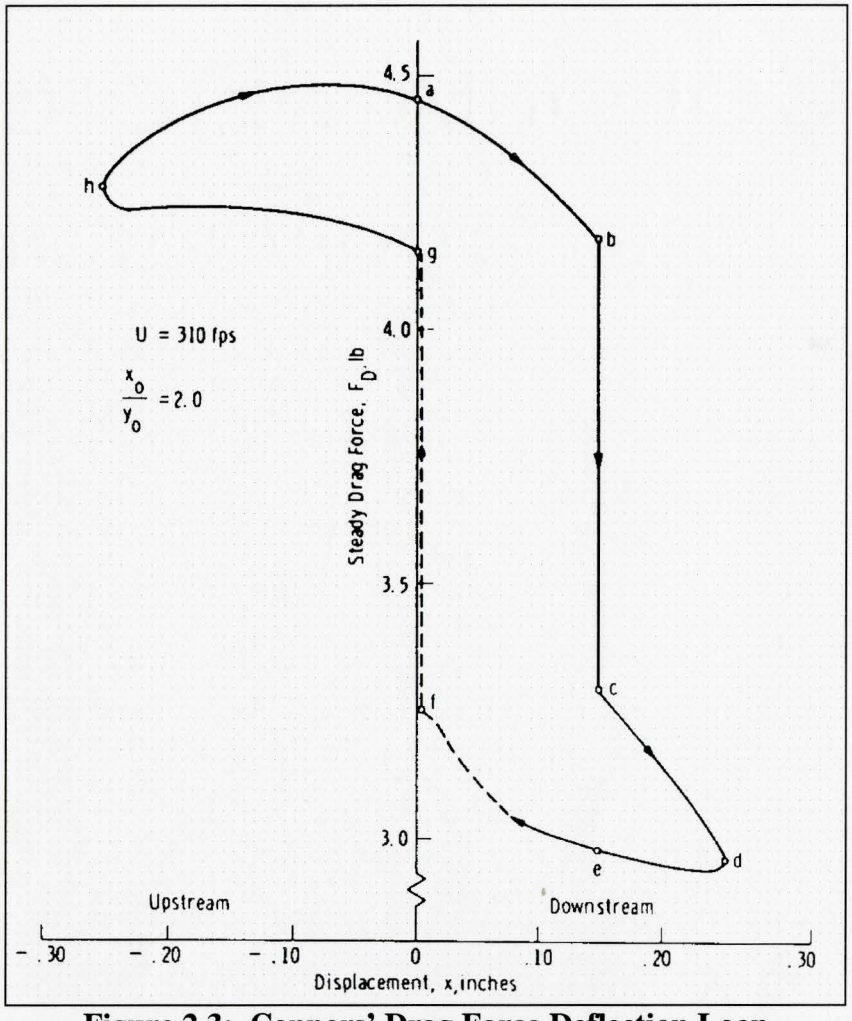

Figure 2.3: Connors' Drag Force Deflection Loop (Connors (1970), pg. 51)

He assumed that the amplitude of the measured tube would be twice that of the amplitude of the side tubes. Connors then fixed the tubes above and below the central tubes and ran the experiments again and plotted these results (Figure 2.4), noting that jet switching occurred in both experiments, but his displacement mechanism does not occur in the second case.

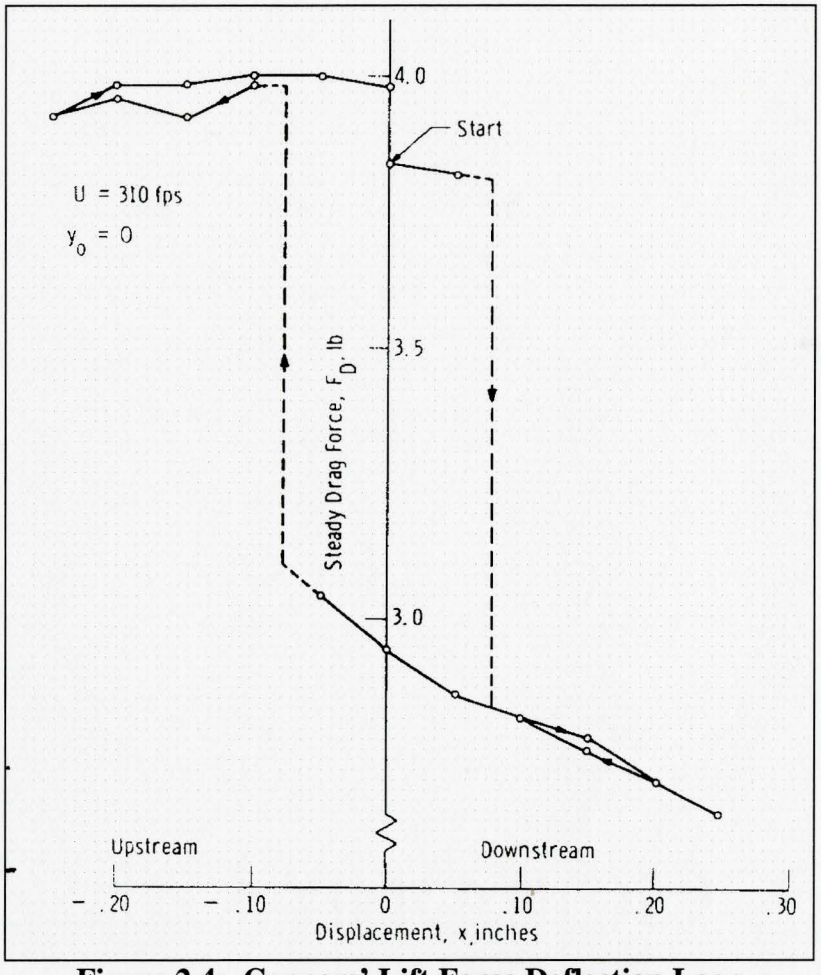

Figure 2.4: Connors' Lift Force Deflection Loop (Connors (1970), pg. 51)

He then plotted a third graph (Figure 2.5) which was created by removing the jet switching mechanism. This new graph was the contribution of the displacement mechanism alone.

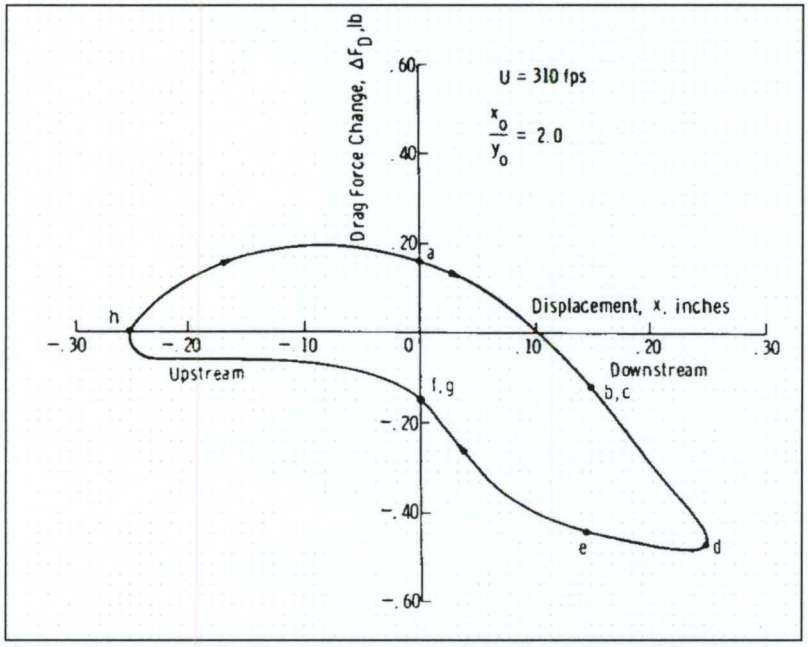

Figure 2.5: Connors' Deflection Loop: Displacement Mechanism Alone (Connors (1970), pg. 52)

Another experiment was also run, where the tube above and tube below the central tube were displaced in the streamwise direction out-of-phase with each other. It was found that the central tube would move in the transverse direction toward the side tube that was moving upstream in the streamwise direction and again as the side tubes continued to be moved (out-of-phase) back and forth in the streamwise direction, the central tube would continue to move in the transverse direction, toward the upstream side tube. Connors plotted these results again on a force-displacement graph (Figure 2.6) and came up with experimental results that somewhat resembled his earlier graph of the displacement mechanism, when removing jet switching as before.

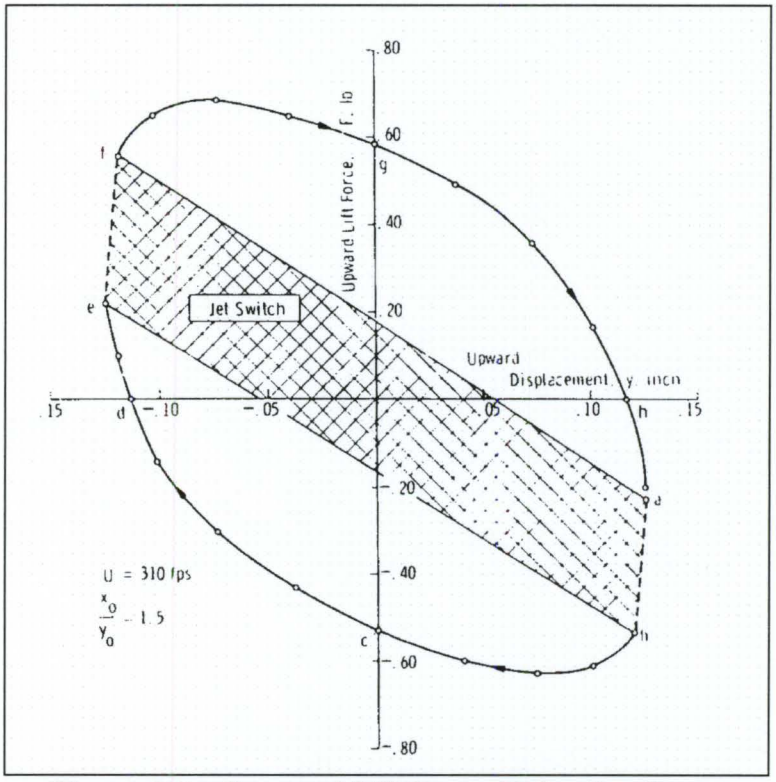

Figure 2.6: Connors' Lift Force Deflection Loop, Shaded Area is Work Done by Jet Switching, Rest of Area is Work Done by the Displacement Mechanism (Connors (1970), pg. 52)

The area enclosed in each graph of the displacement mechanism is stated to be the work done by the mechanism during a cycle.

Connors created a semi-empirical solution for the displacement mechanism, based on the coefficient of lift and drag values which he had obtained experimentally. The result of this work was:

$$\frac{U_{crit}}{fD} = K\left[\frac{m\delta}{\rho D^2}\right]^n \tag{2.2}$$

where U_{crit} is the threshold flow velocity, f is the natural frequency of the tube, D is the tube diameter, m is the mass per unit length of the tube, ρ is the density of the fluid in

cross flow and δ is the logarithmic decrement of damping. Equation 2.2 is commonly known as Connors' equation. Connors' suggested $K = 9.9$ and $n = 0.5$, as a result of his experiments on a single row of cylinders and using the upstream velocity (U_{up}) as the critical velocity. The left hand side of equation (1) is the critical reduced velocity and the bracketed term on the right hand side is the mass-damping parameter. It is important to note that when calculating the value of K in Connors' model, the value for transverse instability is 9.85 and for streamwise is 9.88 (using the numbers available in the report), which would suggest that instability could happen in either direction.

Connors plotted the data from all of the different configurations of his model, conserving his pitch ratio, on a graph of reduced velocity versus mass-damping parameter. The data appears to fit well with the slope of the line represented by his equation, although it is a log-log plot.

Connors also states that jet switching was not the cause of the vibration in his experiments, even though it was observed. It should be asked, can the two phenomena be separated if they both occur at the same time?

According to Blevins (1974), "jet switching has apparently only been observed for reduced velocities ... of order 100. The jet switch mechanism may not be operative for reduced velocities less than 75 due to the time required for the switch. Connors observed no jet switch for reduced velocities less than 30."[9]

In this same work, Blevins suggested that the same type of analysis that Connors applied to a single rows could be extended to tube arrays by obtaining the fluid force

[9] Blevins (1974), pg. 263

coefficients. He extended Connors' work in order to address irregularities in natural frequency and damping between tubes/within the cascade. He suggested that as the difference between natural frequencies increased (by a small percentage), the critical velocity would be delayed. He extended this thought by suggesting that single flexible tube with fixed tubes beside would not be unstable because the neighbouring tubes would not be able to generate the required interactive forces required to generate an instability. One final observation that was made by Blevins was that "as the number of tubes in a row increases, the critical velocity of the tube row decreases"[10].

Although this last observation may occur in some tube arrays, it must be noted that as the number of elements are added to a tube array two factors are introduced: an additional tube element can couple with the other tubes, reducing the stability as indicated by Blevins, but also an additional damping element can stabilize the array. Therefore Blevins' statement is only conditionally true.

In Weaver and Lever (1977), it was suggested that Blevins and Connors work was "based on the assumption that the fluid forces on a tube are only dependent on the relative displacements of the two nearest tubes in the same row" and also that the "predicted dependence of the critical flow velocity on the damping parameter is exaggerated"[11] (n=0.5 in Equation 2.2 for both the mass ratio and the logarithmic decrement is not appropriate, the two parameters should have different powers).

This study was to address Blevins' suggestion that as the difference in natural frequencies between adjacent tubes was increased, the stability of the array would

[10] Ibid, pg. 267

increase accordingly. Weaver and Lever's results are presented in Figure 2.7, where f_D is the natural frequency of the datum tubes (frequency remains the same for all tests) and f_V is the natural frequency of the variable tubes (frequency is adjusted for each test).

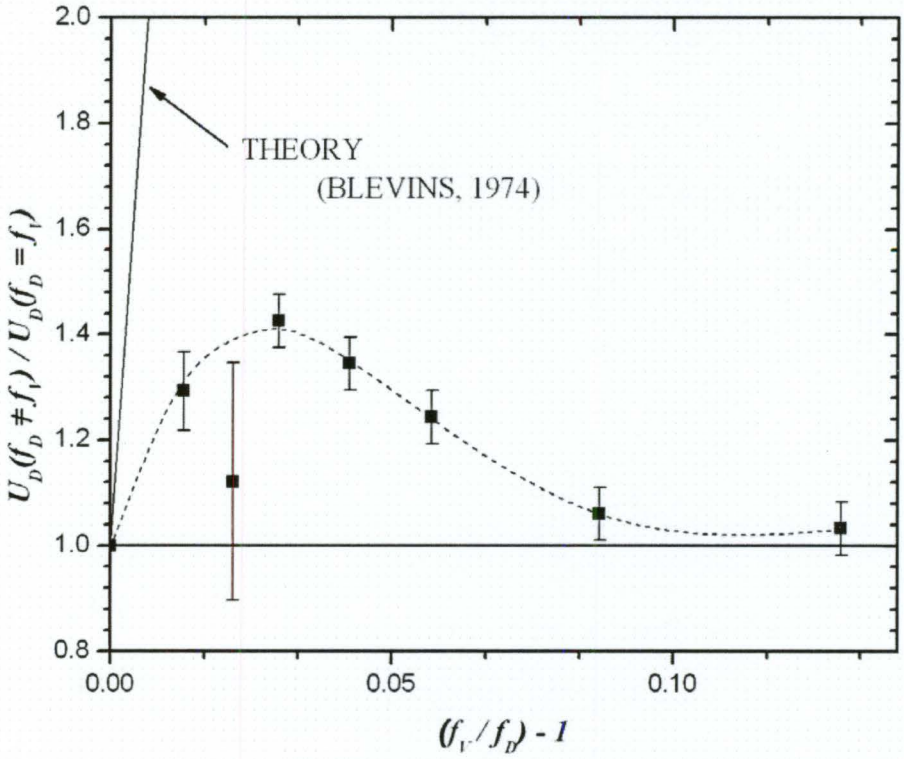

Figure 2.7: Critical Velocity Ratio versus Frequency Difference, • – Experimental Results (Adapted from Weaver and Lever (1977), pg. 328)

The vertical axis is the flow velocity of the experiment normalized by the case where the natural frequency of the datum tubes is equal to that of the variable tubes. On the horizontal axis the difference between the natural frequencies is normalized by the datum tube natural frequency. As can be seen in Figure 2.7 for small differences in natural frequency (near 1%) there will not be significant effect to the stability threshold, which is in agreement with Blevins. But, as the difference between the natural frequencies

[11] Weaver and Lever (1977), pg. 323

reaches approximately 10%, the difference in natural frequencies has essentially no effect on the stability threshold, not agreeing with Blevins theory.

Weaver and Lever suggested that "this was an important observation because it indicates that fluid coupling with adjacent tubes is not necessary for fluidelastic instability in tube banks"[12]. As a result of this, in the paper's discussion section from the Symposium Proceedings a question was asked which covered the requirements for the study of fluidelastic instability. The response was that "only one flexible tube in an array of at least 5 rows of rigid tubes are required to study the fluid-elastic instability". However, Weaver suggested that he would "recommend the use of more flexible tubes ... at least the tube monitored plus its nearest surrounding neighbours"[13].

2.2.1.3 Effect of P_t/D Ratio

In a later paper Connors (1978) presented the effect of changing the pitch to diameter ratio (P_t/D) in a three row in-line square array. The result was that as the ratio was increased, the critical velocity increased linearly when the mass-damping ratio was held constant, in a range from 1.41 to 2.12 (P_t/D).

The critical velocity for tube arrays is typically quoted as the gap or pitch velocity (U_p), which is the mean velocity in the gap between tubes:

$$U_p = U_u \left[\frac{P_t}{P_t - D} \right] \tag{2.3}$$

[12] Ibid, pg. 328
[13] Ibid, pg. 331

where U_u is the upstream velocity and P_t is the tube pitch. Equation 2.3 is derived using the continuity equation.

In Figure 2.8, Soper (1983) suggests that different array geometries behave differently with respect to the P_t/D ratio. The parallel triangle array (listed as rotated triangle in the figure) is shown to have a constant K value. The rotated square array's K appears to increase and then plateau as the P_t/D ratio is increased. The normal triangle array's K simply increases and the in-line square array's K behaves in a parabolic fashion with increasing P_t/D ratio.

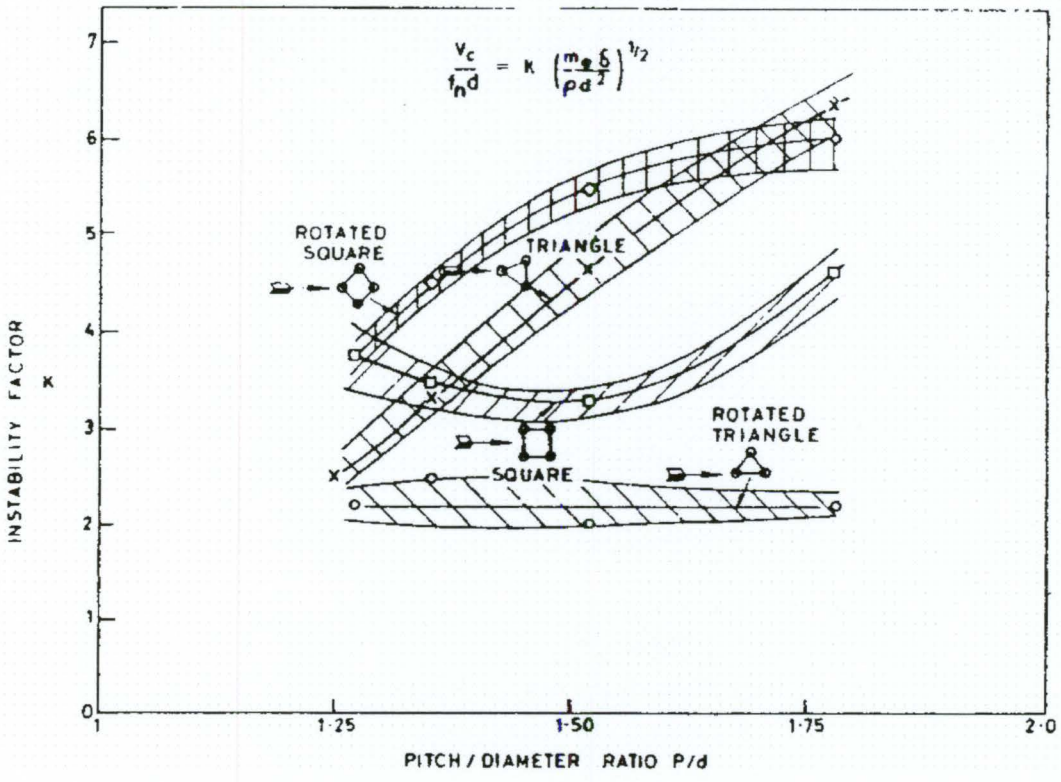

**Figure 2.8: The Effect of Pitch Ratio on *K*,
The Parallel Triangle Array is Listed as Rotated Triangle,
The Normal Triangle Array is listed as Triangle,
(Soper (1983), pg. 747)**

Guidelines for fluidelastic instability with regards to the P_t/D ratio are discussed in Section 2.2.3.2.

2.2.1.4 Effective Velocity (Partial Admission)

Also, Connors (1978) presented an effective velocity. If the flow across a bundle of tubes is not uniform, or if only part of the bundle is exposed to flow, the critical velocity, which was able to excite the bundle under a uniform flow, would not be enough to cause the bundle to go unstable. He proposed an effective velocity, which is the summation of the work extracted from the flow along the exposed tube span divided by the kinetic energy of a tube with a uniform flow distribution. This was an early attempt at the study or evaluation of the partial admission effect. Further investigations have been done on partial admission for instance, by Waring and Weaver (1988) since Connors.

2.2.1.5 Flow direction

The effect of flow direction was also demonstrated in Connors (1978). It is reported that differences of about 15% in the critical flow velocities were observed when flow direction was switched from a forward flow to a reversed flow. The critical velocity was higher for the single rows and the normal triangle arrays when the flow direction was reversed. For the in-line square array, the critical velocity lowered when the flow direction was reversed. In general, Connors states that the flow direction has no affect on the critical velocity which is not generally true. The effect of the approach flow direction

for triangular tube arrays are presented in Yeung and Weaver (1983) and for square arrays in Weaver and Yeung (1983).

2.2.1.6 Number of Rows Required to Study Fluidelastic Instability

In Weaver and ElKashlan (1981a), the number of tube rows required to study different flow-induced vibration phenomena in tube arrays representing heat exchangers are presented. They present an experiment in which a multi-row normal triangle array is monitored for different flow-induced vibrations. The main experimental apparatus consisted of ten rows of tubes with many instrumented tubes. Upstream of these tubes there were nine rows of fixed, but removable, tubes and downstream there were eight rows of removable fixed tubes. Once data was captured for the fully assembled tube array, one tube row was removed and another set of data was captured. This method of removing tubes versus adding rows ensures that irregularities in assembly are eliminated.

The results suggest that for fluidelastic instability, the third and fourth rows are crucial, and that the tubes in the downstream rows have very little effect on stability. This is not the case for other flow-induced vibrations such as vortex shedding. The main recommendation put forth by this paper is that six rows of tubes should be used for the study of fluidelastic instability, and at the very least five rows are required.

This suggests that the early work of Roberts and Connors is not representative of fluidelastic instability in large multi-row tube bundles, such as the ones used in industrial applications.

2.2.1.7 Effect of Damping on Fluidelastic Instability

The value of damping that is used seems to be one of the most inconsistent measurements made, or at least in earlier work. The lack of a standard method of measurement is discussed in Païdoussis. Damping has been measured in a "*vacuo*" like Roberts (which is typically just done in static air), in static water, (when it is the working fluid for the experiments) and in flowing fluid.

One problem with damping measurements is with possible non-linearities in its measured value. If damping is measured at larger vibration amplitudes, the damping may be quite high compared to lower values such as ones measured at $1\%D$ amplitudes, value used by Weaver and ElKashlan (1981b).

The value of damping measured under static conditions is very important to measure, because it was shown in Weaver and ElKashlan (1981b) that the total damping at the critical velocity is zero. At velocities beyond this point, the total damping value measured is negative, causing the amplitudes to increase instead of reduce.

Another problem is associated with the definition of the critical velocity. In some cases the critical velocity is hard to determine, especially when there is a great deal of turbulent buffeting or vortex shedding resonance occurring close to the critical velocity value. The other issue is pertaining to prediction of the critical velocity amplitudes.

There have been multiple studies suggesting that Connors' equation should not include damping under the same power as the mass ratio (Weaver and ElKashlan (1981b) and Chen's (1984) guidelines, along with many others). This is an example of one of

many reasons that Connors' equation is said to not represent the true nature of fluidelastic instability.

2.2.1.8 Effect of Mass Ratio on Fluidelastic Instability

The effect of mass ratio was also studied in Weaver and ElKashlan (1981b). With damping, the natural frequency and the tube diameter held constant, they increased the mass ratio and found that once the critical velocity was reached, the amplitude of vibration reduced with increasing mass ratio ($A/D \propto \rho D^2/m$). They also found that before the critical velocity, the tube buffeting reduced as the mass ratio was increased. These two findings would have to be associated with the inertial effects of the tubes and energy conservation.

2.2.1.9 Effect of Frequency on Fluidelastic Instability

Païdoussis (1982) comments on the effect of detuning and that if the natural frequencies of the tubes are different enough, it has a stabilizing effect. But, at the same time, he quotes a study that suggests that "the effect disappears if detuning is greater than a small percentage of the basic frequency"[14].

In experimental studies, the tubes are typically tuned within 1% of the natural frequency, but in actual industrial heat exchangers the tubes are not tuned and the tubes can be of different lengths, resulting in different natural frequencies.

[14] Païdoussis (1982), pg. 43 – was commenting on Weaver and Lever (1977).

2.2.1.10 Single Flexible Tube in a Fixed Bundle

Weaver *et al.* (2001) studied a single flexible tube in a fixed bundle with a P_t/D=2.01, in-line array. First, the bundle was fully flexible and instability was met by 6.7 m/s. In a single flexible column of tubes, in which the rest of the tubes were fixed, instability was reached by 7 m/s (about a 4% increase). Finally the single flexible tube was tested and there was no clear instability. 2% of the tube diameter was not reached until almost 12 m/s. This shows that a single flexible tube can not always represent a fully flexible bundle.

2.2.2 Models

One of the goals of the research into fluidelastic instability is the creation of a theoretical model for the prediction of the critical velocity, to prevent tedious and costly examination of experiments on each and every bundle geometry and parameter.

When Connors' equation is used for multiple rows of tubes and in different tube array arrangements, the value of K and n (Equation 2.2) have been found to vary. The values for a single row of tubes has been found not to represent those of a full bundle through experimentation. This being the case, the theories or models put forth by Connors and Roberts do not represent a full bundle of tubes. For this reason, different models have been presented to explain the interaction of tube bundles with the flow and between neighbouring tubes.

Païdoussis (1982) discussed the early theoretical models of Lever and Weaver (1982), Tanaka and Takahara, Chen, and Price and Païdoussis.

Tanaka and Takahara's, and Chen's models were based purely on experimental coefficients (a very large number of them). When comparing these models with other experimental results, Païdoussis suggested that the results were in good agreement, which is not surprising. The problem with such a model is the need for multiple, carefully controlled experiments, in multiple array configurations and working fluids, to feed into the model. It would be much simpler to build a model of each heat exchanger required for industry and experimentally find the critical velocity under different working conditions.

Chen's model suggests that there are two types of instabilities. The first is called the "fluid-damping-controlled" instability, which is controlled by negative damping. It is suggested that instability of a single flexible tube in a fixed array may go unstable under this type. It is dominant at low mass ratios, detuning of tubes is not an issue and it depends on the motion of the tube, hence damping is related. This also makes sense since a low mass ratio usually occurs in liquid flows where the fluid damping is the major component of the total damping. The second instability is called "fluidelastic-stiffness-controlled", which is dependent of the motions of the tubes and their interactions. This instability is dominant at high mass ratios and since the tubes must interact, it is less likely for a single flexible tube to go unstable in an array of fixed tubes, depending on the array geometry.

The Lever and Weaver model is "truly analytical", "requiring virtually no input from measurements"[15]. The model involves a parallel triangle array and "the forces leading to destabilization are considered to arise from flow redistribution in the "channel" formed by the dividing streamlines of the sub-channel flows"[16]. Païdoussis states that the agreement with experimental results is "remarkably good, especially for high mass-damping ratios".

The final model discussed by Païdoussis is his model with Price. Their model is quasi-static which means that fewer coefficients are required compared to Tanaka and Takahara. For low values of mass-damping, the model is not very dependent on mass-damping ratio, but for high values of mass-damping ratio, the results become close to the

[15] Païdoussis (1982), pg. 47

results using Connors' equation, which is in agreement with Chen's model. A more recent review of the available models has been completed by Price (1995).

2.2.3 Guidelines

The results of previous researchers have been collected by various authors who have presented their own relationships, or sets of equations for the prediction of the critical velocity for fluidelastic instability using non-dimensional parameters.

2.2.3.1 Single Row

In Païdoussis (1982), a comparison of the work of Roberts and Connors was shown. When plotting the data from various studies on single rows of tubes, along with the curves from Roberts' and Connors' theories, it was found that Connors was deficient in predicting the work of three other studies. Roberts' theory was the better of the two at predicting the results, but it falls short at low mass-damping ratios.

2.2.3.2 Tube Bundles

There are various guidelines for the prediction/prevention of fluidelastic instability but only four will be discussed here. Figure 2.8 shows the typical array geometries used in cross-flow heat exchangers.

---

[16] Ibid

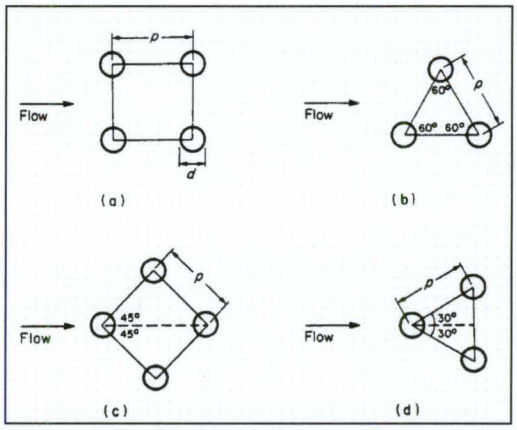

Figure 2.9: Typical Array Geometries: a) In-Line Square, b) Parallel Triangle, c) Rotated Square, d) Normal Triangle (Weaver and Fitzpatrick (1988), pg. 74)

Chen's guidelines suggest that for rotated square and normal triangle arrays, the critical velocity is dependent on the P_t/D ratio and that for in-line square and parallel triangle arrays, the P_t/D ratio is not important. For all array geometries except for the rotated square array, the n value on the mass-damping parameter is between 0.1 and 0.17 for lower values of mass-damping (n = 0.5, for rotated square arrays). For higher mass-damping ratios, it is suggested that n = 0.5 independent on the array geometry, which is in agreement with Connors relationship (Equation 2.2).

Weaver and Fitzpatrick's guidelines (Figure 2.10) do not use the P_t/D ratio. Considering the lines placed under the data on Weaver and Fitzpatrick's graph at lower mass-damping values, the line is flat, which would suggest that the relationship is constant or that the reduced velocity is independent of the mass-damping parameter. This agrees with one of the types of fluidelastic mechanisms that Connors' suggested: "tube position-dependent mechanisms that are time-independent". The other guidelines, with the exception of Pettigrew and Taylor (which will be discussed below), also have

different slopes at lower mass-damping values than at higher values, which could suggest that there are two (at the very least) different mechanisms at work.

The n-value (Equation 2.2) relating to the mass-damping ratio varies for the different array geometries in Weaver and Fitzpatrick.

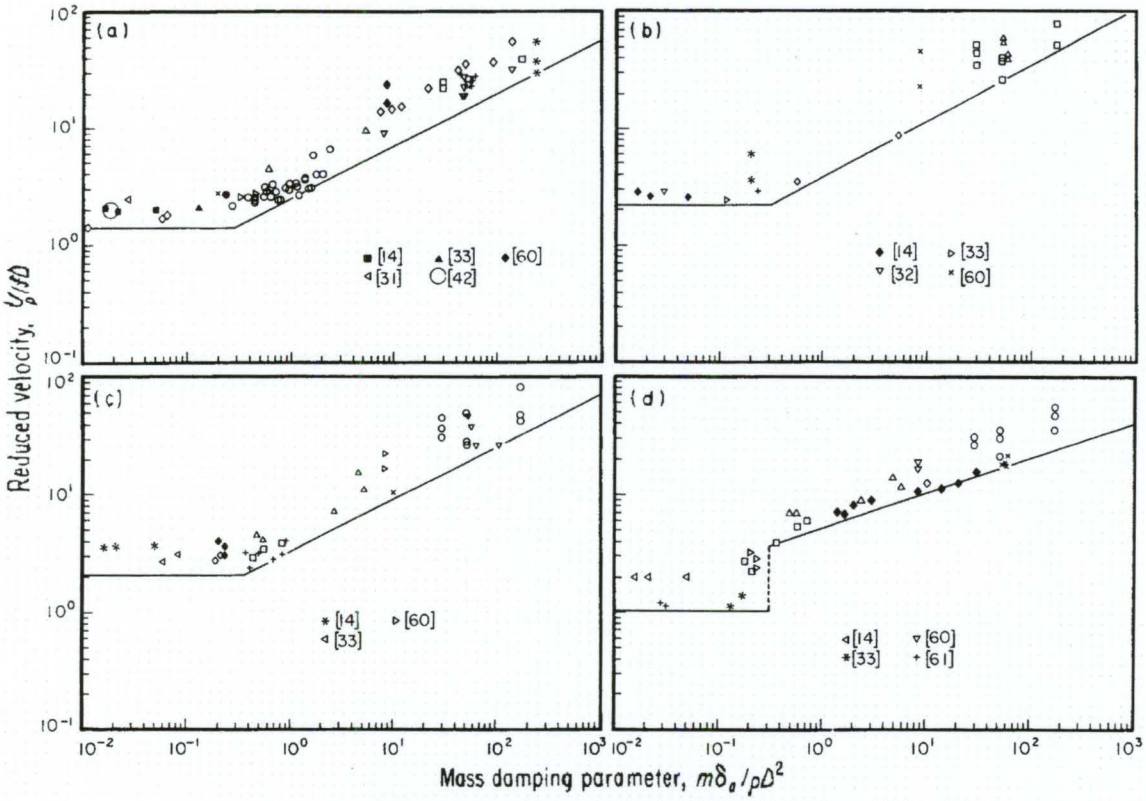

Figure 2.10: Stability Maps,
a) In-Line Square, b) Rotated Square,
c) Normal Triangle, d) Parallel Triangle,
Adapted to reflect the current Nomenclature
(Weaver and Fitzpatrick (1988), pg. 85)

Schröder and Gelbe (1999) present a revision to their work presented in VDI-Wärmeatlas guideline, which incorporates more data. They use a P_t/D ratio dependent K (for all arrays except for parallel triangle), which is different if the fluid is a gas or a liquid flow, which makes it more similar to Chen than Weaver and Fitzpatrick. For

liquid flows, the n-value of the mass-damping parameter is 0.15 for all arrays. In gas flows, the n-value of the mass-damping parameter is 0.5 for normal triangle and rotated square, and 0.4 for in-line square and parallel triangle. Schröder and Gelbe suggest that "the best existing guidelines are in one case that of Chen", for normal triangle arrays in gas flows, "and in all other cases those of Weaver and Fitzpatrick"[17]. A comparison between Chen and Schröder and Gelbe is made in the Section 2.5.6.

Pettigrew and Taylor (2002) have presented the latest published guideline, but it seems to have changed little over the years with the exception of new application for use with finned tubes. They do not plot the data of the different array geometries on separate graphs, but instead every study is plotted on one graph. The scatter is quite large compared to the other guidelines, but with a K value of 3.0 (which is suggested for all types of tubes and fluids, even two-phase flows), and using $n = 0.5$, over 90% of the data plotted is above the stability line. This suggested value of K is not that different from Connors' $K = 2.9$ in 1978.

Pettigrew and Taylor's guideline requires almost no knowledge of the geometry of the tube bundle and if heat exchanger designers use this guideline and do not look at other guidelines or research on the subject of fluidelastic instability. The designer will not realize the complexity of the phenomena and assume that Connors' equation with K=3.0 is all that is required to prevent failure of the heat exchanger.

Dropping the stability line below all existing data should prevent failure due to fluidelastic instability, but it restricts the maximum operational velocity, which can

[17] Schröder and Gelbe (1999), pg. 375

impact heat transfer, which in-turn reduces profit potential and efficiencies. For some larger pitched tube arrays, this approach may lead to limits on flow velocities which are conservative by a factor of five or more. This is safe but very poor in terms of cost competitiveness.

2.3 Types of Finned Tubes

Heat exchangers with bare tubes are not as efficient as finned tubes at removing heat from the fluid flowing around them for two reasons: the first being the increased surface area and the second being the turbulence generated by the flow over the fins.

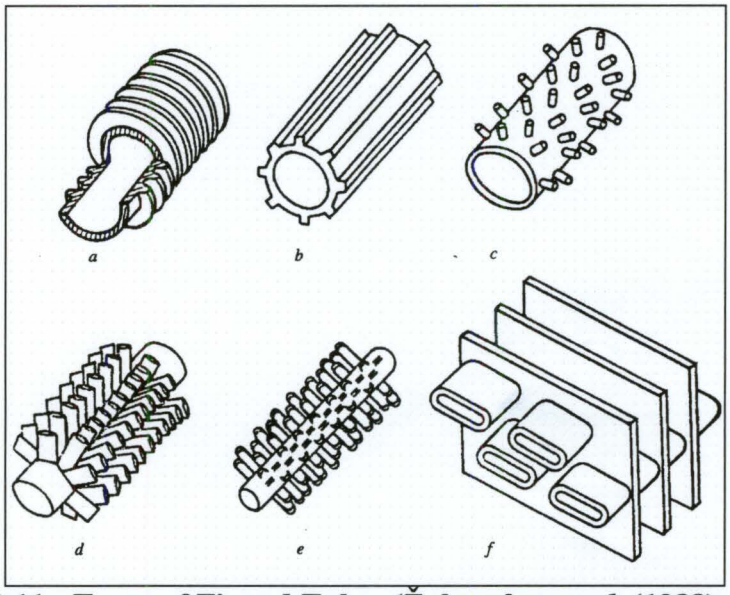

Figure 2.11: Types of Finned Tubes (Žukauskas *et al.* (1988), pg. 162)

Different types of finned tubes are shown in Figure 2.11. They are used in different heating and cooling applications.

In the early 1970s, ESCOA (Extended Surface Company of America, now part of Fintube Corp.) introduced the serrated, helically wound finned tube (typically referred to an "I" type fin) to the American marketplace (Figure 2.12, lower image).

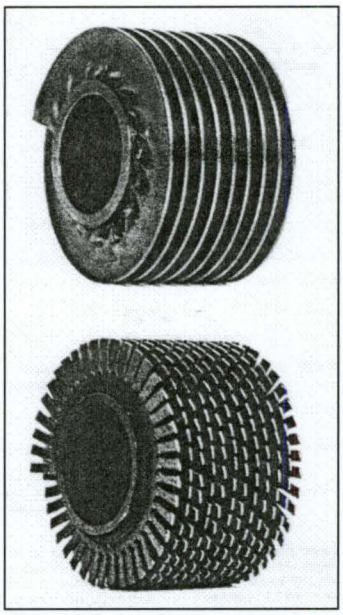

Figure 2.12: Comparison of Helically Wound Finned Tubes, Unserrated (Upper) and Serrated (Lower), (Reid and Taborek (1994), pg. 407)

The tubes use high frequency resistance welding which reduces the overall weld size and therefore allows for tighter fin pitches to be produced (Figure 2.13).

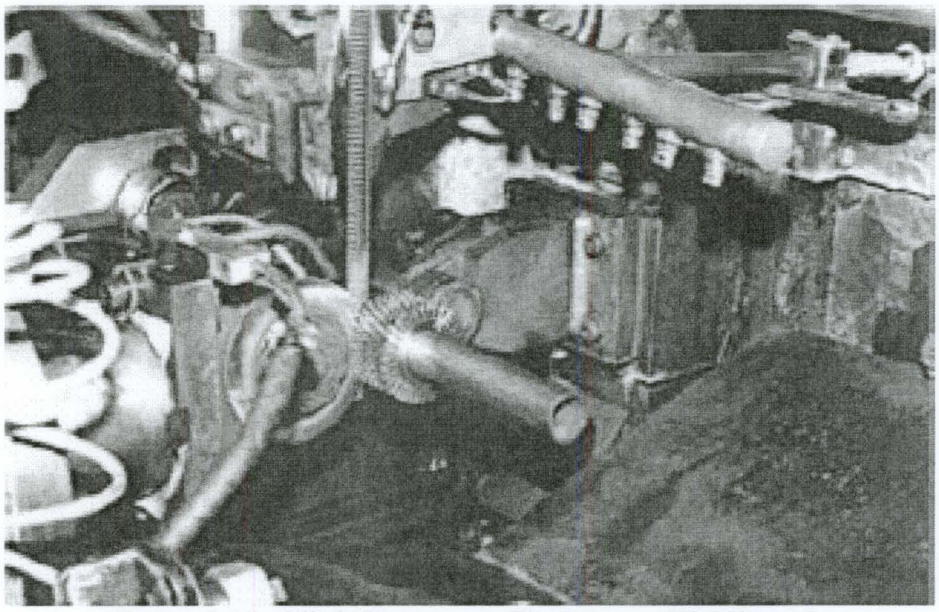

Figure 2.13: High Frequency Resistance Welding of a Serrated, Helically Wound Finned Tube
(http://www.dti.gov.uk/files/file18742.pdf, Reaccessed: March 8th 2007)

The pre-serration of the strip of fins requires no crimping or stretching of the strip before welding so the maximum fin height is much less restricted by the manufacturing process, unlike plain helical finned tubes.

Heat Recovery Steam Generators (HRSG) are a major user of this technology. The fin pitch used depends on the fluid used in cross flow, the main decision depending upon the amount of particulate in the flow which can clog up the gap between fins during operation. The finned tubes in the present study are suggested for heavy oil combustion (3.3 fins per inch along the tube span) and natural gas and light oil combustion (5.7 fins per inch along the tube span) according to Reid and Taborek (1994) (Table 2.1).

Table: 2.1: Recommended Fin Densities (Reid and Taborek (1994), pg. 409)

Fin-side fluid type	Fins/in	mm/fin
Clean air	8 - 11	3.0 - 2.3
Nat. gas combustion	6 - 8	4.2 - 3.0
Light oils combustion	4 - 6	6.3 - 4.2
Heavy oils combustion	3 - 5	8.5 - 5.0
Solid fuel combustion	1 - 2	25 - 12

2.4 Single Finned Tube

An early study by Dye and Abrahams found that vortices were shed from the gap between fins on a single finned tube. They also studied two finned cylinders side-by-side and even with a small clearance of 0.015" between fins (no other tube dimensions available), they found that vortices were shed from the sides of the pair of tubes as well as from between the two tubes, in the gap (using flow visualization).

2.4.1 Effective Diameter and Vortex Shedding

As finned tubes have been adopted for their increased heat transfer performance, researchers have attempted to define an effective diameter which will allow the users of finned tubes to convert their finned tube into an equivalent bare tube, which will allow the designers of heat exchangers to use the existing bare tube data available to predict the response of finned tubes.

Halle *et al.* (1975) tested two bare tubes and a finned tube. The bare tubes were of 44.5 mm (1.75") and 37.3 mm (1.47") in diameter and the finned tube had the same fin diameter as the larger tube and bare tube diameter as the smaller tube. They found that the finned tube shed vortices at a frequency that was between the frequencies of the two tubes. An estimate of an effective diameter, based on the frequency of the vortices shed off the finned tube and a Strouhal number of 0.2, was backed out as 39.4 mm (1.55"). In Halle *et al.* (1984), it was explained that the effective diameter that they used was the equivalent bare tube having the same volume as the finned tube (including the inner tube

diameter). This diameter will now be referred to as the "volumetric effective diameter (D_{vol})".

Mair *et al.* (1975) conducted a study of different annular finned tubes, by stacking different sized spacers and washer like fins on a fixed tube. The finned tube elements were placed at the central section of the tube that spanned the wind tunnel. The finned section made up only a quarter of the tube and end plates were used to isolate the finned tube from the bare part of the tube. Results of this study show that the Strouhal numbers of the different finned tubes tested colapsed using an effective diameter. The proposed effective diameter was based on the projected area of the tube per unit length and can be calculated using:

$$D_{eff} = \frac{1}{p}\left[t\left(D_f - D_b\right) + pD_b\right] \tag{2.4}$$

where p is the fin pitch, t is the fin thickness, D_f is the fin diameter, D_b is the bare tube diameter. Noted that Equation 2.4 can also represent the ratio of fin spacing to the tube diameter. Mair *et al.* commented that the fins increase the sharpness of the peak in the power spectrum.

Although the definition for the volumetric effective diameter is different from the effective diameter of Mair *et al.*, the difference between the two values is between 4 and 6% for the current finned tubes under investigation. Note that both definitions were derived for plain (un-serrated, non-helical) finned tubes.

A third model proposed by Harrison (1948) has been used in heat transfer for comparing different types of finned tubes, including plate and tube heat exchangers. This

model is a weighted average of the surface areas of the tube and fins. The heat transfer results of different finned heat exchangers colapse quite well using this method. The calculation of this effective diameter is quite lengthy for a serrated, helically wound finned tube. The relationship that Harrison used was:

$$D' = \left[\frac{D_b S_b + L_H S_f}{S_b + S_f} \right] \tag{2.5}$$

where S_b = area of surface, D_b = pipe diameter, S_f = area of fin surface, and L_H = diameter or equivalent diameter of fins. "For plate or spiral wound strip fins, L_H is taken as the square root of the area of one side of a fin or of that part of a fin which is associated with one pipe."[18].

In Eid (2004), a study of plain fins suggested that the addition of "fins reduces the strength of vortex shedding from single cylinders" and that there is an "increase in the broadband turbulence" which "becomes significant with increasing fin density"[19]. It was also suggested that the fins cause a reduction in the sound pressure at resonance.

Eid also studied the effect of fins on tandem cylinders. In this case, the fins caused the sound pressure to increase before the onset of resonance, though the sound pressure level was lower than the bare tandem cylinder with the same P_t/D_{eff} ratio of 1.5. For a P_t/D_{eff} ratio of 2, it was found that the sound pressure level was higher for the finned tubes than for the bare tube case and the same was true for the P_t/D_{eff} ratio of 3 case.

[18] Harrison (1948), pg. 33
[19] Eid (2004), pg. 120

Katinas *et al.* (1991HT) studied a single finned tube with a trapezoidal cross-section that was helically applied (the appearance is similar to a threaded rod). It was suggested that fluidelastic instability occurred at a reduced velocity of 10. It is not very clear whether or not this did occur, as the maximum amplitude of vibration reached is approximately $0.15\%D$ in their water tunnel experiments. Fluidelastic instability or galloping is not possible for single right cylindrical bare tubes.

Katinas *et al.* observed vortex shedding at lower flow velocities that were greater in the streamwise direction for their bare tube and their finned tube results. At higher velocities, the tendency was for vibration in the transverse to flow direction.

2.4.2 Vortex Shedding and a Single Serrated Finned Tube

Hamakawa *et al.* (2001), Ryu *et al.* (2003) and Jebodhsingh *et al.* (2004) have all conducted experiments on serrated finned tubes.

Flow visualization was completed by Ryu *et al.* for various fin pitches and fin heights. They found that a hydraulic diameter (Equation 2.6) collapsed the time mean velocity and the turbulent intensities better than Mair *et al.*'s effective diameter or using the outer or inner tube diameters.

$$D_h = D_f - 2\left[\frac{4h(p-t)}{p-t+2h}\right] \qquad (2.6).$$

The use of Mair *et al.*'s effective diameter for vortex shedding over serrated finned tubes was found to correlate well in Ryu *et al.* and Jebodhsingh *et al.*'s results.

Jebodhsingh *et al.* found that the span-wise correlation of vortices along the span of the tube was different as the tube was rotated relative to the direction of the approach flow velocity. This was thought to be an effect of the serration pattern. When visually inspecting the tubes along the span, a "wavy pattern" was seen. This pattern was different for different fin pitches and for tubes with the same serration width, which were tested in this study. The serration occurred at a fixed width (w), so as the pre-serrated ribbon was wrapped around the tube, some fins did not fully flay out, causing the distance between the serrated fins to be non-uniform at the tips. This non-uniformity, and the fact that these notches were not lined up along the span, caused the wavy pattern, and hence if the tube were rotated, the relative flow fin pattern changed, changing the span-wise correlation length of the vortices.

Hamakawa *et al.* (2001) suggested that the scale of the vortices coming off the tubes was considerably larger than one fin pitch and that when the fin pitch was reduced, the wake width increased. It was also proposed a relationship for an effective diameter, but this relationship was the same as Mair *et al.*.

2.4.3 Vortex Suppression Using Different Fins

In 1981, Zdravkovich reported an extensive study of different fins attached to or placed near single tubes. Figure 2.14 shows the tubes which were studied. The tubes with a plus beside them were able to suppress vortex shedding, whereas the tubes with a minus beside them indicated that suppression did not occur. Some of the designs are

more effective than others. A few of these suppressor designs are used frequently on smoke stacks.

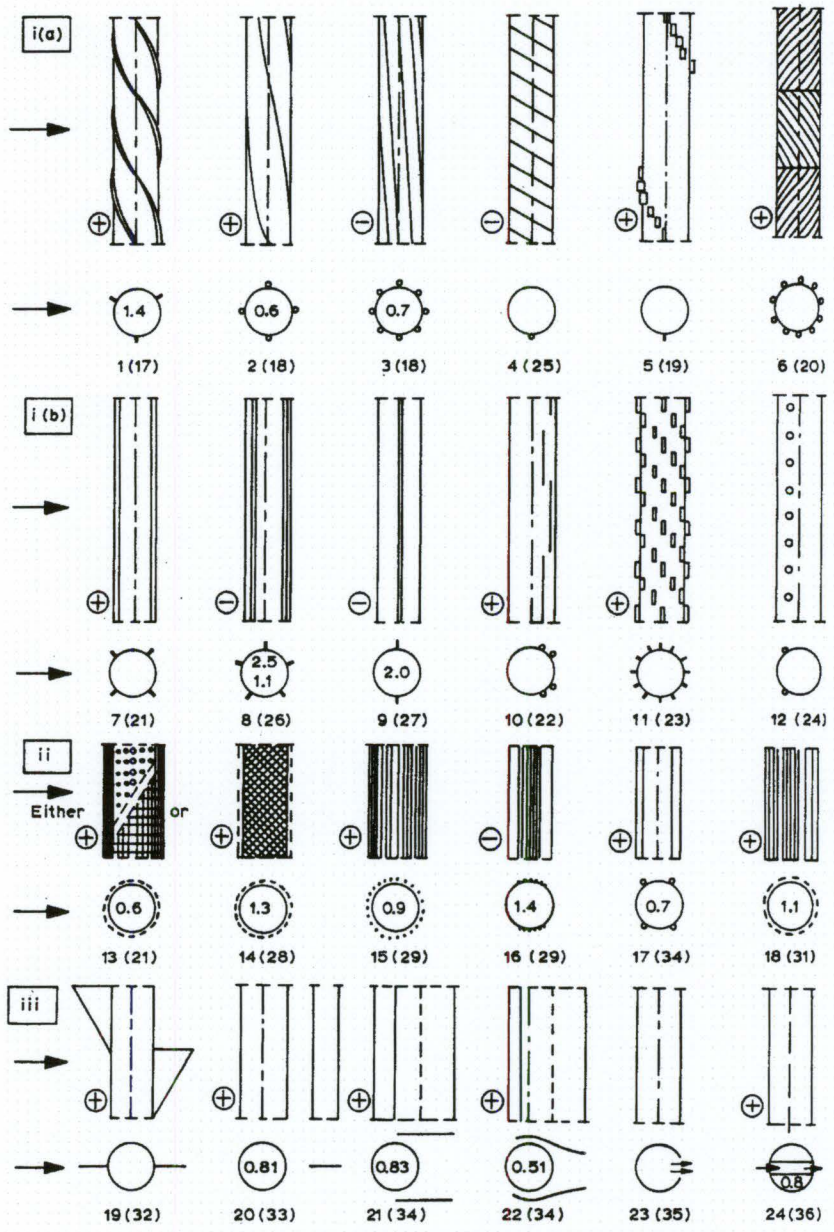

Figure 2.14: Interfering with Vortex Shedding,
(i) Surface Protrusions, (ii) Shrouds, (iii) Near Wake Stabilizers,
(+ Effective, - Ineffective)
(Zdravkovich (1981), pg. 148)

2.5 Finned Tube Arrays

2.5.1 Flow in Finned Tube Arrays

Figure 2.15 shows the fouling pattern around a plain finned tube (a), versus a bare tube (b). The material that has built-up onto the tubes, due to fouling, can represent the regions of stagnation. For the bare tube, the accumulation of fouling material will be of a similar thickness along the span of the tube, whereas looking at the sectioned views, it can be seen that along the span of the finned tube, the thickness of the fouling material varies considerably at the intersect of the fins and the tube. This variation of the flow pattern along the span of the finned tube is what complicates the analysis of finned tubes. Note in the *I-I* sectioned view, the particulate has much less build up at the rear of the tube compared to the front. This is most likely due to the wake behind the cylinder minimizing accumulation.

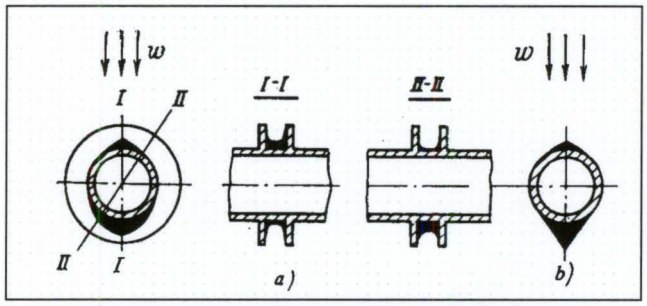

**Figure 2.15: Fouled Finned Tubes,
Typical Shape of Deposits in Tube Bundles
a) Finned, b) Bare Tubes,
(Lokshin *et al.* (1979), pg. 141)**

The flow in a normal triangle array of tubes in shown in Figure 2.16, results were measured between the third and fourth rows of the bundle.

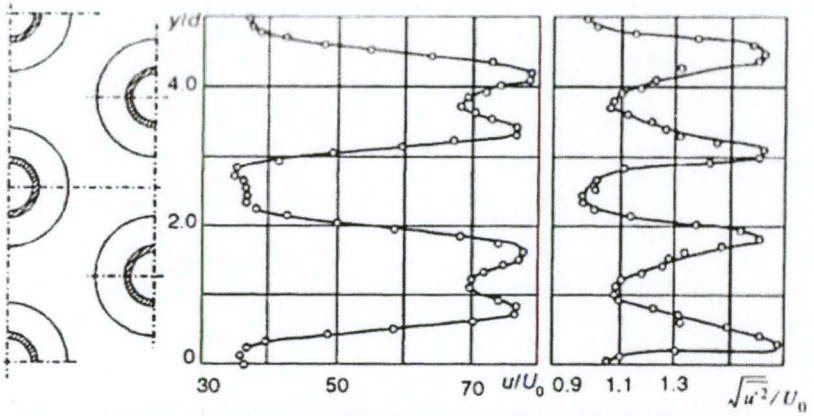

Figure 2.16: Flow Distribution in a Finned Tubes Array, Variation in the Local Velocity of an Air Flow and in its Fluctuating Component Behind Finned Tubes of the Third Row of a 1.61 x 1.38 Staggered Bundle, (Katinas (1997), page 139)

In bundles of finned tubes a hydraulic diameter has been suggested for flow calculations, which is illustrated in Figure 2.17 ($D_h=4F/P$).

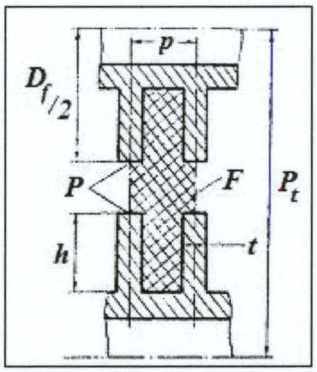

Figure 2.17: Finned Tube Hydraulic Diameter Adapted to reflect the current Nomenclature (Žukauskas *et al.* (1988), pg. 165)

2.5.2 Friction Factor in Finned Tube Arrays

There is a great deal of literature available on the friction factor and heat transfer through finned tube bundles, especially from the old Soviet block, where the development of finned tube technology took place around the same time as it did in the United States. The friction factor information presented herein is from American studies of the finned tube type presently under investigation.

In Weierman (1977), the results are presented from experiments at ESCOA Fintube Corporation, for the friction factor through serrated helically wound finned tube bundles. Some of the results of this study are shown in Figure 2.18. The intent of these graphs was to find out the minimum number of rows required to study the friction factor through a bundle of in-line and staggered finned tube arrays. This was similar to what was done by Weaver and ElKashlan (1981a) for fluidelastic instability. The average friction factor per row added in the experiments was normalized by the average friction factor per row for a seven row test section. It can be seen from Figure 2.18 that for the in-line arrays tested, the five row bundle has approximately the same result as the seven row bundle, and that for in-line arrays, there is a definite effect if fewer rows than five are used. For the staggered arrays tested, the value of friction factor per row does not follow the trend of the in-line array, and five rows is sufficient to measure the friction factor in a staggered array, although fewer rows appear to be acceptable.

What is interesting about this outcome is that the minimum number of rows required to study friction factor in a bundle of tubes is the same that which is suggested

for fluidelastic instability, although this does make sense since it is related to the number of tube rows required to produce fully developed flow in a tube bundle.

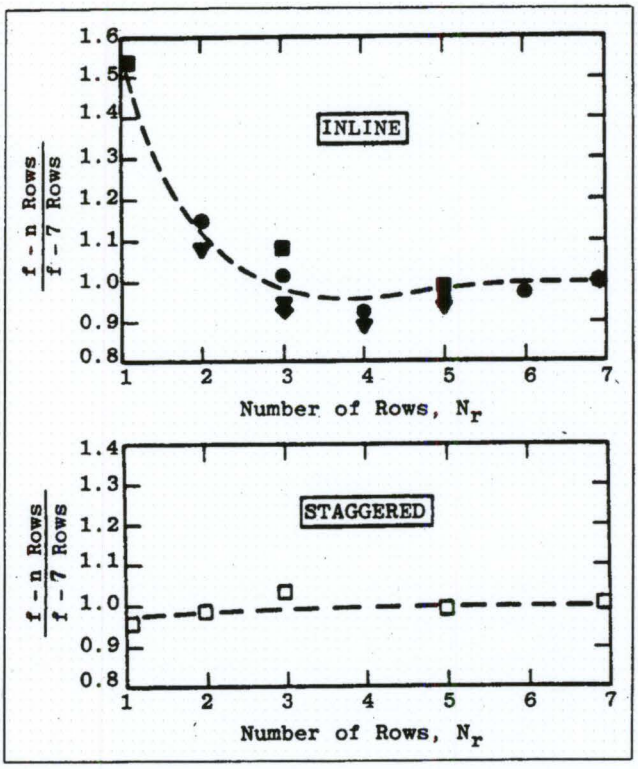

Figure 2.18: The Effect of the Number of Rows of Tubes on the Friction Factor, In-Line Array (Upper), Staggered Array (Lower) (Weierman (1977), pg. 71)

Ganapathy (1996) has a table of coefficients to calculate the friction factor through a serrated in-line and a serrated staggered finned tube bundle. It should be noted that there are errors in three of the five coefficients given for the calculation of friction factor. These same coefficients are used in sample calculations within this paper, which are still incorrect, but surprisingly the final result of each calculation ends up with the proper value (even though the math does not compute).

One interesting suggestion that is made in Ganapathy, is the use of multiple rows of different types of tubes. "Fin density and height should be reduced in the hot gas region and gradually increase as the gas cools. In high gas-temperature applications, for example, bare tubes are used for the first few rows, followed by tubes with a low fin density (2 to 3 fpi) and then tubes with higher fin density (4 to 6 fpi) to reduce tube wall and fin tip temperatures."[20] The idea of increasing the surface area of the tubes as the temperature gradient decreases is very logical, but there is no indication in the literature that this idea has been adopted by industry.

The ESCOA Engineering Manual is a downloadable executable (available on-line from Fintube Corp.) which has been created to aid industrial users of serrated finned tubes in the design of their heat exchanger for their particular application. The user is able to change parameters of the heat exchanger and find the number of rows of tubes, the heat transfer coefficients and the friction factor through the bundle. This application is said to be based on experimental results, and the equations along with their coefficients are provided. The calculations for the friction factor listed in the program are the same for the serrated, un-serrated, twisted and the studded finned tubes but this seems unlikely (these equations and coefficients are provided in the Appendix of this thesis). When using these calculations to obtain a friction factor for ambient wind tunnel experiments, the predicted results were found to be 5 to 30% off for in-line and 30 to 60% off for staggered finned tube arrays (see Appendix 7.3). The experiments which were used to create these formulas may not have included data under ambient conditions.

[20] Ganapathy (1996), pg. 104

2.5.3 Flow-Induced Vibrations in Platen Fin Tube Arrays

A study of vortex shedding and fluidelastic instability was completed by Weaver *et al.* (2001). This study was of platen fins, which are tubes with thin plates affixed to them in the span-wise direction. Two rectangular fins were used, one upstream of the tube and the other downstream.

First a bundle of bare tubes in an in-line rectangular (not a typical array geometry, $(P_t/D)_{transverse}$ = 2.01, $(P_t/D)_{streamwise}$ = 3.56) arrangement was investigated and vortex shedding and fluidelastic instability were observed (in Figure 2.19).

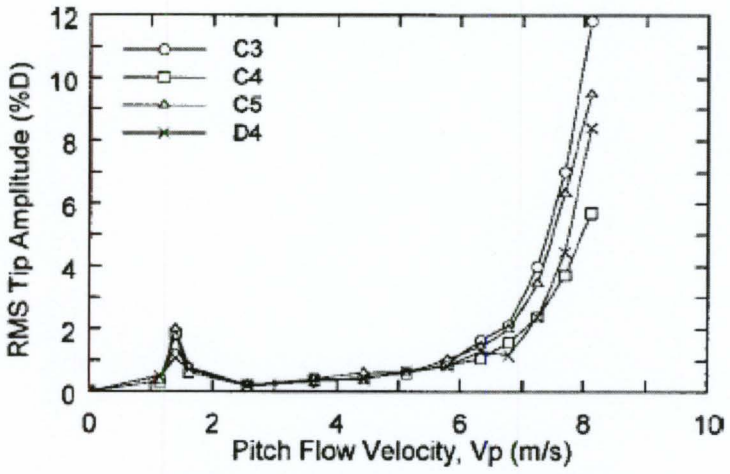

Figure 2.19: Bare Tube Bundle, C3 – 3rd Row, C4 – 4th Row, C5 – 5th Row, D4 – 4th Row beside C4, (Weaver *et al.* (2001), pg. 438)

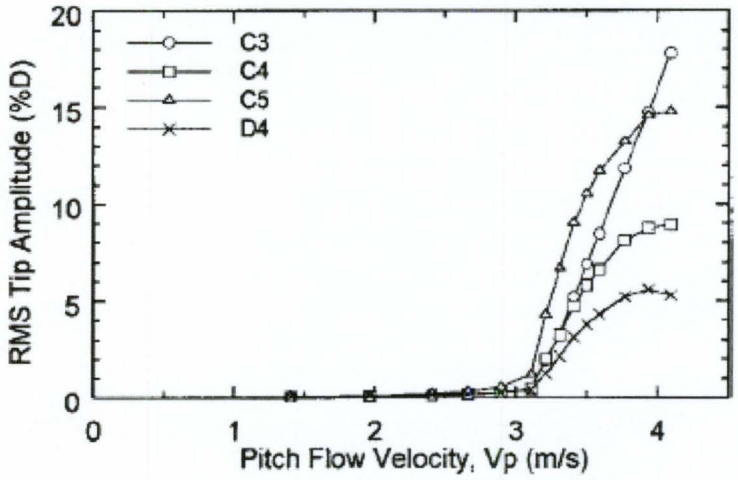

Figure 2.20: Platen Finned Tube Bundle,
C3 – 3rd Row, C4 – 4th Row,
C5 – 5th Row, D4 – 4th Row,
(Weaver *et al.* (2001), pg. 439)

The platen fin tubes tested were scaled to the same mass and were tuned to the same frequency as the bare tubes. This left two non-scaled variables, the critical velocity and the damping. As seen in Figure 2.20, the platen fin tubes displayed no evidence of resonance due to vortex shedding. It was expected that the vortices behind each tube would not be able to couple since the plate fin prevents coupling across the tube wake. This could also be expected due to earlier work by Zdravkovich (1981).

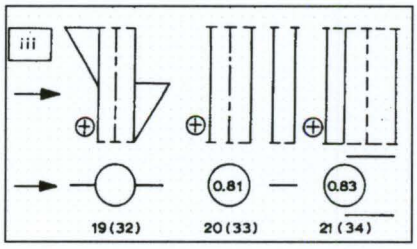

As it can be seen in the figure above (part of Figure 2.13), all three of the tube and vertical plate arrangements are effective at suppressing vortex shedding.

Also, as seen in other studies of preventing/reducing vortex shedding and acoustic resonance, the addition of baffle plates has been successful. The platen fins resemble a baffle plate fore and aft of each tube.

For fluidelastic instability in platen fin tube arrays, it was found that the platen fin tube went unstable earlier than the bare tube, even though the damping of the platen fin tubes was double that of the bare tubes (this doubling of the damping was attributed to the windage effect caused by the platen fins). It was suggested that the platen fins increased the coupling of the tubes in the transverse direction. In Figure 2.20, the behaviour of the 4^{th} and 5^{th} row tubes after the critical velocity is exceeded is quite peculiar, in that the trend of the amplitude of vibration begins to level off instead of the more typical rapid climb of the 3^{rd} row tube. The amplitude of vibration was measured only in the transverse to flow direction. The streamwise vibration was minimal, since larger amplitudes of vibration would have caused the ends of the fins to touch.

The cases of a single flexible column and single flexible tube within a rigid bundle were also tested. The single flexible column of tubes went unstable sooner than the fully flexible bundle when using the platen fin tubes and the single flexible tube did not go unstable. The single platen fin tube did not vibrate at as high an amplitude as the bare tube previously tested in the study.

The final experiment that was conducted connected the platen fin tubes in the stream wise direction in pairs and groups of three. The result was that the more tubes that were tied together, the greater the stability of the bundle (increase in stability by a factor of: 1.9 for pairs and 4.7 for threes). The fluid damping forces were applied to a greater

surface area which would increase the total damping and in turn increase the stability of the bundle, as was seen in this study.

When calculating K, when the tubes were tied, the mass was doubled and tripled for the two cases. The diameter used was the bare tube diameter of the platen fin tubes. From an aerodynamic point of view, it would seem reasonable that the total length of the platen fin tube in the streamwise direction should be the characteristic length, since the vibrations were dominant in the transverse or lift direction,

$$D_{eff,platen\_Lift} = D_b + 2h$$

as opposed to the drag direction characteristic length.

$$D_{eff,platen\_Drag} = D_b$$

However, the results using just the mass adjustment and the bare tube diameter seems to make sense (when plotting using the lift direction as the characteristic length ($3.5D_b$), the values of reduced velocity reduce to values that do not seem comparable to the bare tube results).

2.5.4 Vortex Shedding and Acoustic Resonance in Finned Tube Arrays

Nagamatsu and Rolsma (1982) said that they found acoustic resonance that was caused by vortex shedding and turbulent buffeting, in a normal triangle, un-serrated helical finned tube array. The study reports three different Strouhal numbers for the array tested. It is suggested that the acoustic resonance was linked with turbulent buffeting, and the data appears to show that it is brought upon at a single frequency found in the power spectral analysis. This frequency was apparently predicted by Owen's turbulent

buffeting equation. One of the three Strouhal numbers was linked with vortex shedding and the third Strouhal number was twice the value of the second Strouhal number, which it was suggested was associated with turbulent buffeting (Figure 2.21).

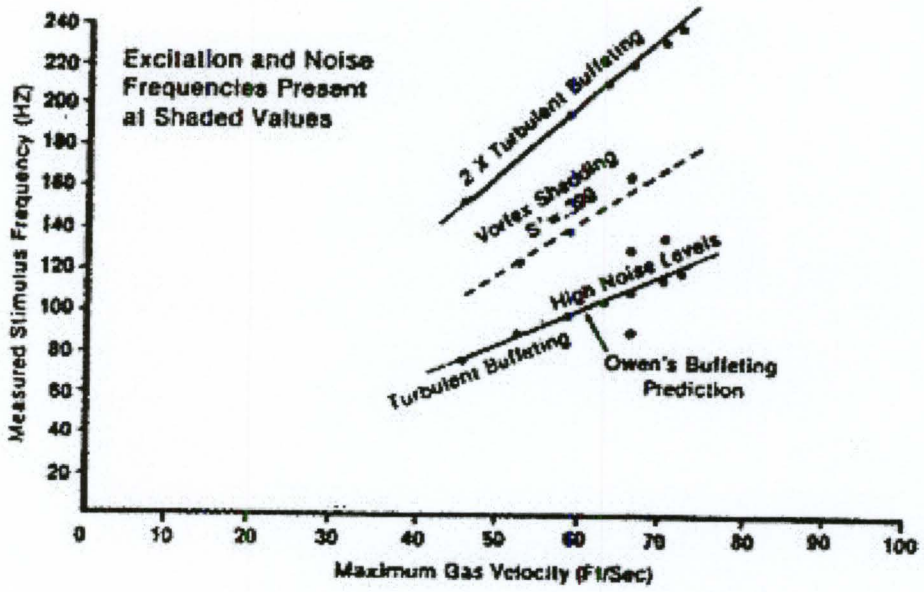

Figure 2.21: Strouhal Numbers for 12 Row Normal Triangle Finned Tube Array (Nagamatsu and Rolsma (1982), pg. 5)

Kouba (1986) studied three normal triangle finned tube arrays and suggested that the results were similar to bare tube arrays when comparing with the bare tube diameter in calculation of the Strouhal number. Each array had different fin heights: 3.5, 4.5 and 11 mm respectively.

In Powell and Sohaney (1989), an industrial gas finned tube heat exchanger was said to have failed due to vortex shedding. Using strain gauges, they assessed that the failure was in the second mode of vibration of the tubes. The problem was fixed by adding two span supports to prevent the second mode of vibration. Unfortunately no flow velocity data is available, so Strouhal and fluidelastic parameters are not available.

Apparently "the flow induced problem only occurred during the last five minutes of the operational cycle during cool down when the pressure was high, thus increasing the density"[21]. It is unlikely that this failure was due to vortex shedding, since it involved a gas flow heat exchanger and it is more likely that this failure was due to fluidelastic instability.

Katinas *et al.* (1991FM) studied a staggered array of finned tubes (same type as mentioned in Katinas *et al.* (1991HT) in Section 2.4.1) under vortex shedding. They found two different Strouhal numbers for the bundle under investigation. They also suggested that in their water tunnel experiments, they were unable to excite fluidelastic instability, even though their experiments went up to a reduced velocity of 30 (not enough information is given to calculate the mass damping ratio).

Nemoto and Yamada (1992) found similar results to that of Kouba and also studied the use of baffle plates to prevent acoustic resonance. Nemoto and Yamada (1994) is a continuation of their previous paper, using the same tube array geometries, in which it is suggested that "the level of sound generation has no bearing on fins"[22] and instead it is dependent on array geometry. Nemoto and Yamada also reported that they found two or more Strouhal numbers in their experiments.

In Nemoto *et al.* (1997), multiple types of finned tubes were tested and in this study they indicate that fins can assist or suppress acoustic resonance. They also state that the fins themselves do not emit noise.

[21] Powell (2005), Electronic Communications, Also fins are un-serrated, helical and their thickness is 1/32".
[22] Nemoto and Yamada (1994), pg. 281

Fan (2002) studied six different finned tubes with three different fin pitches and two fin heights and found that acoustic resonance could be excited by either vortex shedding or turbulent buffeting. The fins used are an "L" type, spot welded fin that is serrated twisted. It was found that increasing the fin height enhanced the turbulent buffeting peak, weakened the vortex shedding peak and produced a weaker resonance than the shorter fin height investigated. As the fin density was increased, the excitation existed at multiple frequencies. Fan found that using Mair et al.'s effective diameter was adequate for comparing his results with other bare tube array results.

2.5.5 Fluidelastic Instability in Helical Finned Tube Arrays

There are only a few studies published on fluidelastic instability in finned tube bundles, and all of the known studies are presented here. Note that all of the finned tube dimensions of these fluidelastic instability studies can be found in Table 2.2, at the end of this section and the associated array geometries, pitches and non-dimensional values can be found in Table 2.3.

Halle *et al.* (1975) tested 5 U-tubes (10 tubes connected by 5 U-tube ends) in a wind tunnel at Argonne National Laboratory in Illinois, and found fluidelastic instability. Their damping measurement was done in air at various flow velocities. When reporting the K value, they used the damping ratio instead of the logarithmic decrement, in Connors' equation. Since the U-tubes did not have the same natural frequency in the streamwise direction (6.3 Hz) as the transverse direction (3.6 Hz), they used both frequencies in the calculation of K. On review of the data that they included in their

paper, it seems that at their critical velocity, the tube started vibrating at a frequency of around 5 Hz. This may be a coincidence, but the average value of their two frequencies is 4.95 Hz. Using this frequency to calculate K results in a value of 15.1. If U-tube ends behave like two tubes tied together, then as in Weaver *et al.* (2001), the mass per unit length of two tied tubes should be doubled. This results in a K=10.6 for a P_t/D_{eff} = 1.33, which is not far from K=9.9 for a P_t/D = 1.41 found by Connors (1970) for a single row of tubes.

Kienböck (1982) examined an actual heat exchanger tube bundle with fins that were rolled out of the tube material. The fins are very small (h/D_b = 6.6%, where h is the fin height), compared to modern industrial finned tubes (h/D_b = 50% in this thesis). Kienböck went on the assumption that an array of finned tubes behaves similarly to an array of bare tubes. When the logarithmic decrement was measured for the bundle, the values of damping were found to range from 0.3 to 0.64, which is extremely high. They said that they had struck the array to measure the value, so this value of damping may be a result of all the tubes acting together, as opposed to a damping measurement where only the tube that is being tested is flexible and only its measurement is measured. When Kienböck tested a single tube, it seems as though this tube was not inside the bundle, the logarithmic decrement was found to be from 0.05 to 0.06, which is a much more appropriate value. The final value given for their damping was listed as the same value as the single tube.

The information that is presented in the Tables 2.2 and 2.3 are from the "test layout" experiments that Kienböck mentions in his paper. The resulting K value was said

to be found by Jülich Nuclear Research Station. A limit on the amplitude of 4% of the bare tube diameter was set as a conservative design guideline for fluidelastic instability. The paper notes that there was never any tube-to-tube contact recorded. This paper does not list the reduced velocity or mass-damping value, but it states that the K value is valid for a range of the logarithmic decrement between 0.02-0.05. It may be possible to back out the reduced velocity and the mass-damping parameter, but the density of the working fluid (steam) was not given.

Halle *et al.* (1984) did a massive study of fifteen different tube bundles, with varying array geometries, different baffle plate set-ups and two different tubes (one bare and the other finned). These were water flow experiments made on the shell side of a six pass shell-and-tube heat exchanger. Two of the fifteen configurations were of finned tubes, with fin length of 1.6 mm (again extremely small fins, h/D_b = 10%). One of the experiments was in an in-line square and the other was in a normal triangle array.

The finned tubes used seem to be cut-out of a smooth tube, somewhat like a thread cutting operation. The fin thickness is missing, and therefore the volumetric effective diameter value, supplied by Halle *et al.* (1984) is used in Table 2.2 and 2.3. The other tubes that were used in the thirteen other experiments had the same outer diameter as the fin diameter of the finned tubes.

Hirota *et al.* (2002) studied two rows of tubes in a normal triangle array. Their experiments were conducted in a wind tunnel, with only one monitored tube in the two rows. Two cases were studied. The first case was a higher damping case where the end of the cantilever tube was put in water. In the second case, the water was removed to

reduce the damping. As a result, the damping in the first test was about 26% higher. Hirota *et al.* also switched the flow direction acting on the two rows of the tunnel. This meant that the monitored tube that was once in the second row, was now in the first row (these results were not included in Tables 2.2 & 2.3). The interesting result was found that the critical velocity was approximately the same, independent of the flow direction, for cases with high and low damping. This may be a result of the number of rows used, which is acknowledged by the authors. They also state that these results do not represent a full tube bundle, due to the results of Weaver and ElKashlan (1981a).

Hirota *et al.* (2002) used and suggested the use of a volumetric effective diameter as the diameter to be used for fluidelastic instability of finned tube bundles since it predicted a K value lower than the value suggested by S.S. Chen ($K=7.3>6.3$). They defined the volumetric effective diameter as:

$$D_{vol,plain} = \sqrt{\left(D_f^2 - D_b^2\right)\frac{t}{p} + D_b^2} \tag{2.7}$$

No reason was stated as to why it was decided to use this effective diameter. Halle *et al.* (1984) was cited. As stated earlier, Halle *et al.* (1984) suggested the use of a volumetric effective diameter for vortex shedding.

Examining the definition of the effective diameter, it seems that the equation is for a plain finned tube (even though their tube was helically finned). Volumetrically based equations that have been derived for helically wound finned tubes are presented below.

$$D_{vol,helical} = \sqrt{D_b^2 + \frac{4th}{\pi}\sqrt{1+\left[\frac{\pi D_f}{p}\right]^2}} \tag{2.8}$$

$$D_{vol,serr} = \sqrt{D_b^2 + \frac{4th}{\pi}\sqrt{1+\left[\frac{\pi\left(D_f - 2s\right)}{p}\right]^2}} \tag{2.9}$$

The first equation is for helical finned tubes and the second is for serrated helical finned tubes (note that if $s=0$, then Equation 2.9 reduces to Equation 2.8).

Fischer (2003) presents equations for the calculation of the stiffness of a helically finned tube, including the contribution that the fin has on the total stiffness of the finned tube. The results of a study of eight tubes in a water tunnel is also presented. One of the experiments involved three rows of tubes in a normal triangle array, below recommendations of Weaver and ElKashlan (1981a) and the second had five rows of finned tubes in a parallel triangle array arrangement. Fischer used four steel tubes with copper fins and the other four were steel tubes with steel fins. The fin pitch is different for each tube according to his tables (fin densities listed: 4 fpcm (10.16 fpi) for the copper tubes and 3 fpcm (7.62 fpi) for the steel tubes over tube span of 0.230 m (9.055"). The tube pitch was 39.26 mm[23] (1.546") and a fin diameter of 40 mm (1.575"). Since the fin diameter is greater than the tube pitch, it is possible for fins to be in contact, and with different fin densities, the possibility of fin contact with pristine fins (unmodified from manufacturing specifications) is guaranteed over the tube span used. When consulting Fischer[24] about the possibility of the fins being in contact to ensure that the finned tube specifications were correct in his paper, the author said that they were but also that he did

not conduct the experiments himself (Fischer did not seem to be interested in answering any further inquires about his paper).

These two different helical finned tubes had different natural frequencies (120 and 157 Hz), his tube array is shown in Figure 2.22.

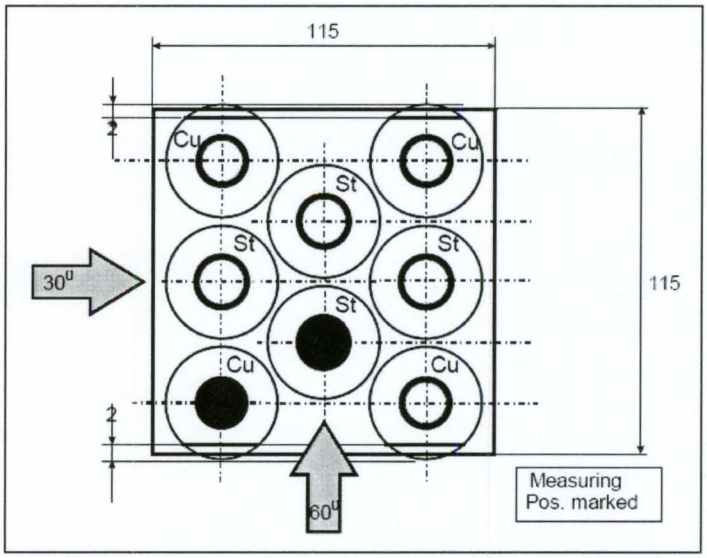

Figure 2.22: Fischer's Finned Tube Bundle, Cu – Copper Tubes, St – Steel Tubes (Fischer (2003))

The tubes with the solid centres are monitored with accelerometers. The monitored copper finned tube is the tube on which Fischer based his fluidelastic analysis, since the copper tubes have the lower natural frequency. Note that it is in the first row of each array.

Fischer does warn that Connors' equation should be used with care, as it was developed for bare tubes. The water tunnel tests resulted in K values of 2.92 and 3.37 for the normal and parallel triangle arrays respectively. The values of K of 3.43 and 3.96

[23]Fischer (2004), Electronic Communication, value for, but not listed in Fischer (2003)

were actually reported by Fischer, since he divided his K values by 0.85 in his calculations. Also it should be noted that the calculations for K were based on the maximum pitch velocity obtainable in the water tunnel for the two different tube arrangements. The amplitudes of vibration was starting to increase in a manner similar to a typical fluidelastic vibration curve, but the bundle did not actually show unstable amplitudes. Without more data, it is unclear whether or not instability was met. The amplitude of vibration is extremely low (less than $0.2\%D_{eff}$) which is too low to suggest that the bundle is close to the critical velocity. Fischer suggests that it is not possible to have vortex shedding in the bundle because of the fins and the tube pitch to diameter ratio. Irrespective of whether or not it is possible to have vortex shedding, vortex shedding could not be seen since the flow velocity corresponding to one of the Strouhal numbers for this array was not yet met by the water tunnel. Fischer's data is absent from Tables 2.2 and 2.3 because there is not sufficient proof that fluidelastic instability was seen in his study.

Fischer also talked about an industrial case where a tube bundle made up of finned tubes that have fins which are loosely connected to the tube were replaced with finned tubes with fixed fins. It was found that the loose fins added additional damping, most likely due to friction/relative motion between the fins and the tubes, so the damping was high enough that under operating conditions the bundle was stable. When the tubes were changed to the fixed fin tubes, for improved conductive heat transfer, the damping was reduced and tube rupture occurred.

---

[24]Fischer (2004), Additional Electronic Communication

Table 2.2: Finned Tube Fluidelastic Instability Studies – Finned tube Dimensions (mm/inches)

Author	D_b	h	t	p	D_{eff}	h/D_b
Halle et al., 1975	38.1 (1.50)	2.8 (0.11)	1.0 (0.04)	2.31 (11 fpi)	40.6 (1.60)	0.073
Kienböck, 1982	22.2 (0.87)	1.46 (0.06)	0.35 (0.01)	1.34 (19 fpi)	23.0 (0.91)	0.066
*Halle et al., 1984**	15.9 (0.63)	1.6 (0.06)	N/A	1.34 (19 fpi)	16.9 (0.67)	0.101
Hirota et al., 2002	42.7 (1.68)	19 (0.75)	1.6 (0.06)	5.08 (5 fpi)	54.7 (2.15)	0.445

**D_{eff} could not be calculated due to missing data, instead used D_{vol} provided by Halle et al., 1984*

Table 2.3: Finned Tube Fluidelastic Instability Studies - Results

Author	P_t/D_{eff}	U_{red} (D_{eff})	$m\delta/\rho D_{eff}^2$	K	*Fluid*	*Array*	*# Rows*
Halle et al., 1975	1.33	227.5	477.6	10.4	Air	Single Row	5 U-tubes
Kienböck, 1982	1.35	N/A	N/A	6.5	*Steam @ 10 Bar*	Normal Triangle	Actual Exchanger
*Halle et al., 1984**	1.41	4.94	0.742	5.7	*Water*	Normal Triangle	Actual Exchanger
	1.41	3.92	0.721	4.6	*Water*	In-Line Square	Actual Exchanger
Hirota et al., 2002	1.57	47.5	51.7	6.6	*Air*	Normal Triangle	2
		68.6	65.2	8.5	*Air*	Normal Triangle	2

2.5.6 Guidelines for Fluidelastic Instability in Finned Tube Arrays

In 2002, Pettigrew and Taylor included Guidelines for finned tube arrays. They suggest using a "hydraulic diameter". The equation for the hydraulic diameter presented in Pettigrew and Taylor is that of Mair *et al.* This diameter is suggested for use in all "vibration excitation parameters such as Strouhal number, dimensionless flow velocity, random excitation, etc..." and also in the pitch to diameter ratio. These

recommendations are based on the limited data on finned tubes, which do not have h/D_b ratios similar to modern industrial finned tubes.

When it comes to the calculation of the total damping in the system, it was reported that the estimation for the friction damping ratio is 80% of the bare tube value for finned tubes. This is reported as a result of an unpublished study by Hartlen and Barnstaple, and there is no indication on how they came to this conclusion in Pettigrew and Taylor. Hartlen and Barnstaple's 80% value was suggested because the finned tube and the support are not in full contact with each other so that the bearing area is reduced compared to bare tubes.[25]

Pettigrew and Taylor also include an equation for calculating the flexural rigidity of a finned tube (from Bolleter and Blevins work). This was also quoted in Fischer (2003), but Fischer expanded the calculation for helically wound finned tubes.

[25] Communication with Pettigrew (2005)

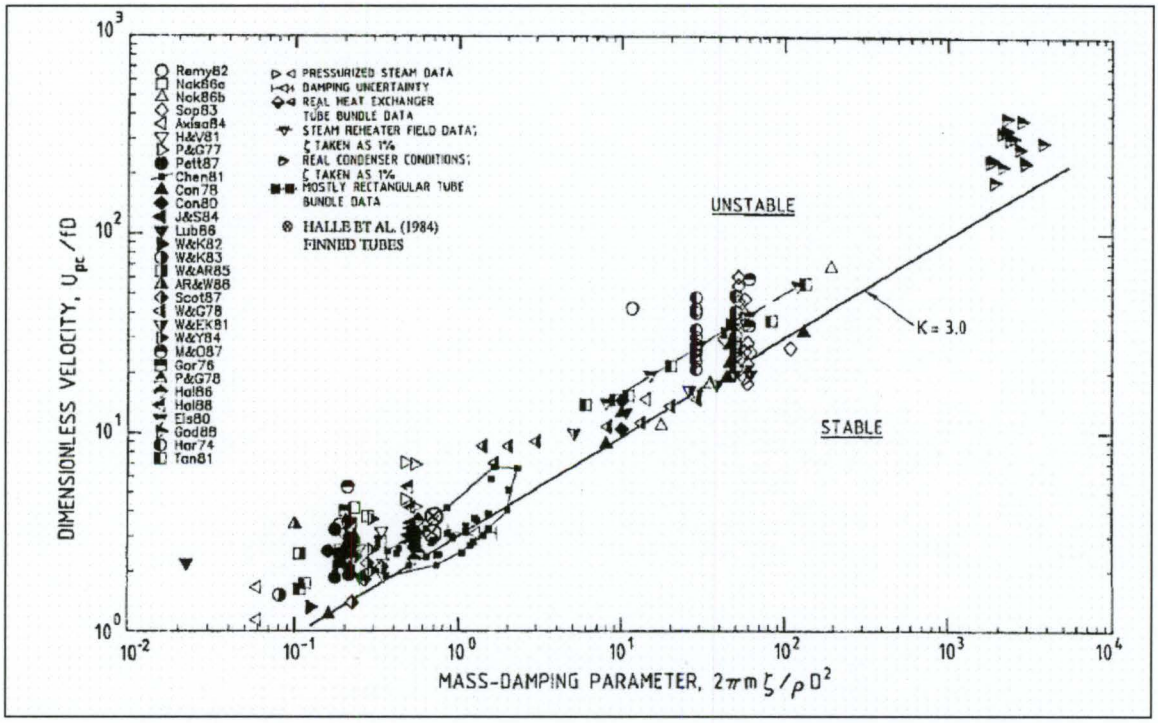

Figure 2.23: Pettigrew and Taylor's Fluidelastic Guidelines (2002)

Pettigrew and Taylor note the scarce finned tube data available, and plot Halle *et al.* (1984) (in above Figure 2.23) with all of the rest of the data. The K value which is also suggested for bare tubes in single and two-phase flow is 3.0. All of the data from the different array geometries are plotted together.

The available data of normal triangle finned tube arrays is plotted below in Figures 2.24 and 2.25, if the guideline requires a P_t/D ratio, P_t/D_{eff} was used and both the highest and lowest ratios are plotted.

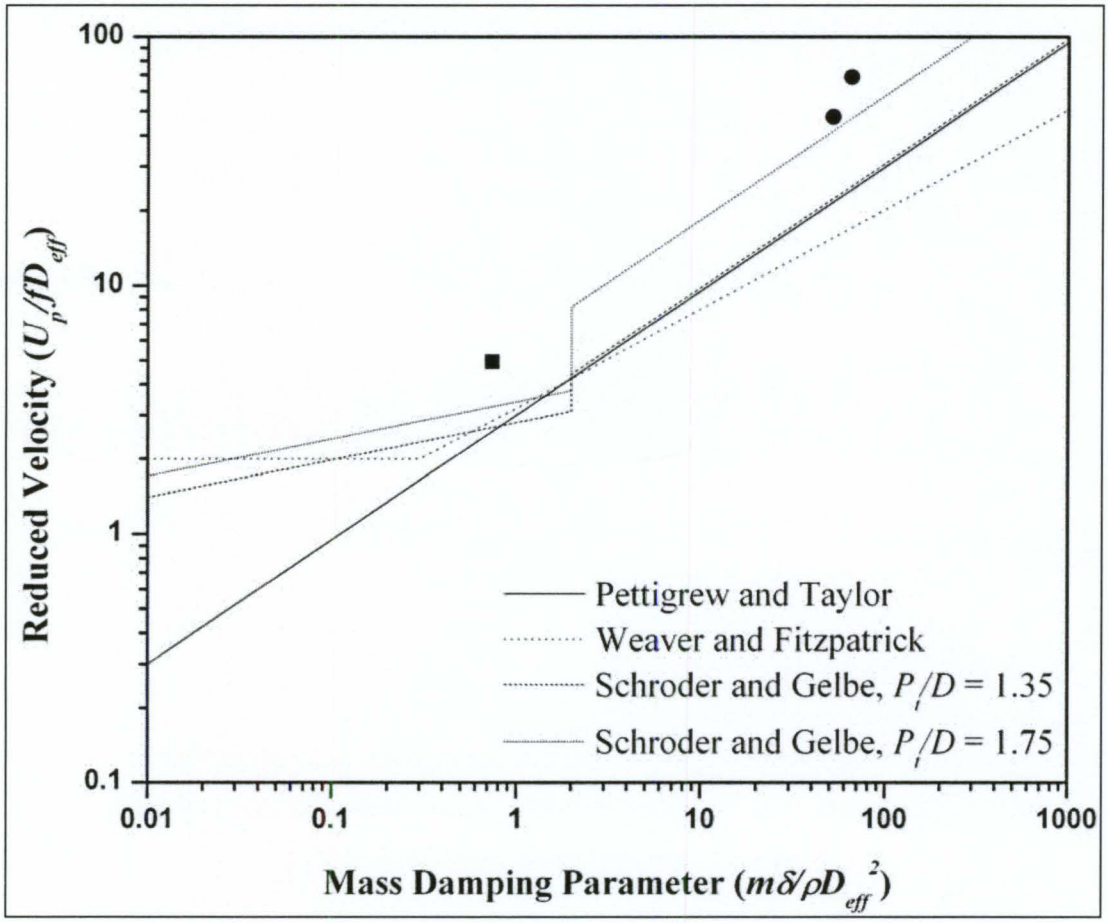

Figure 2.24: Fluidelastic Instability in Normal Triangle Finned Tube Bundles
■ – Halle *et al.* (1984), ● – Hirota *et al.* (2003)
(Chen, 1984, not included for clarity, see next graph)

Examining Figure 2.24, the data by Hirota *et al.* and Halle *et al.* (1984) fall well above all of the guidelines.

When examining the new guidelines of Schröder and Gelbe (1999), compared to Chen's (Figure 2.25), there is little difference between the P_t/D=1.75 slopes. There is a major difference in the P_t/D=1.35 case when the mass-damping parameter is below 0.3, Chen's guideline is much lower than Schröder and Gelbe's.

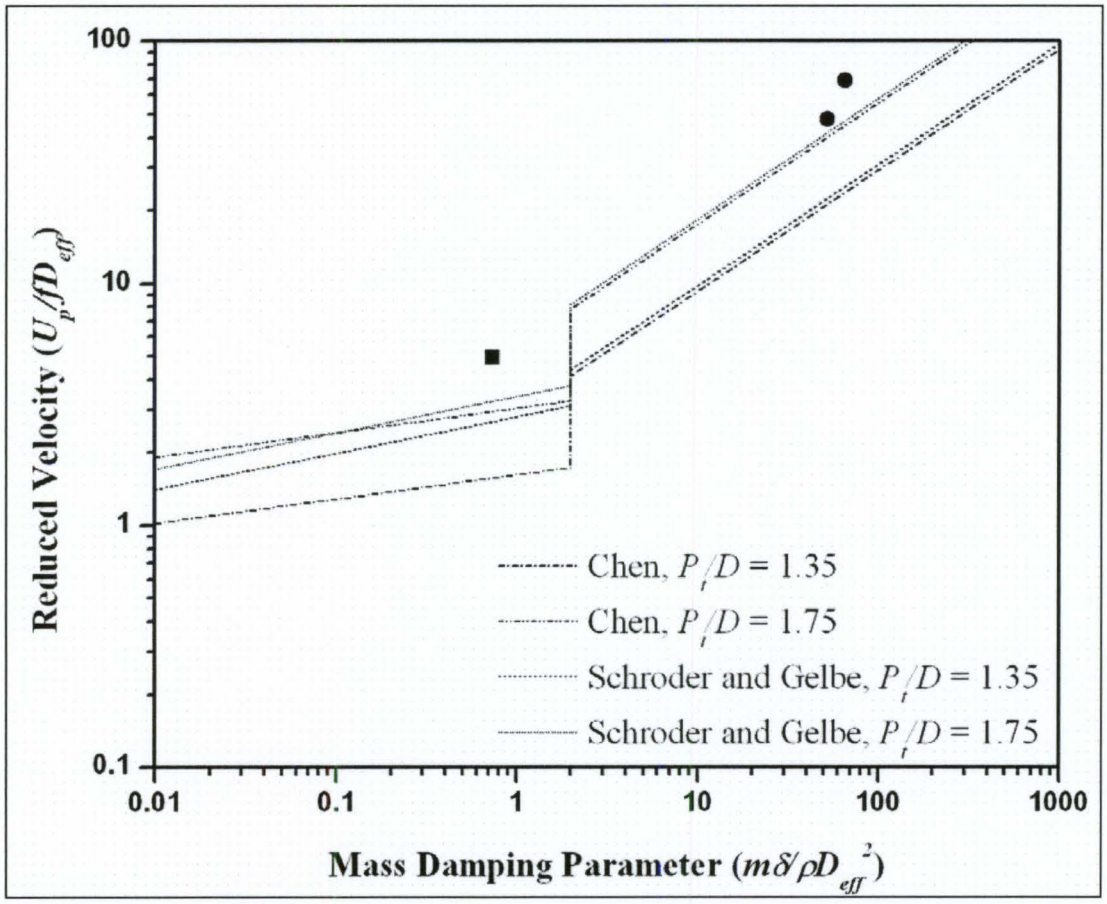

Figure 2.25: Fluidelastic Instability in Normal Triangle Finned Tube Bundles, ■ – Halle *et al.* (1984), • – Hirota *et al.* (2003)

2.6 Conclusions

From this literature review it can be seen that fluidelastic instability in finned tubes has not been studied to the same extent that have been established for the study of fluidelastic instability in bare tube arrays. The recommendation of Pettigrew & Taylor of using Mair et al.'s effective diameter is based on previous results from vortex shedding over a single finned tube and therefore the use of an effective diameter for the prevention of fluidelastic instability is suggested with the absence of any precedent. With very little

ground to start on, the present study of fluidelastic instability in finned tube arrays will be the fundamental study that is required to build our knowledge of fluidelastic instability with finned tubes.

The measurement of damping will be the greatest challenge that will be faced for fluidelastic studies. Without the proper measurement of the loss of energy in the system, finding a value of net damping equal to zero will be an extremely difficult task and will make the comparison of data from different researchers, using different methods of measurement, quite difficult.

3.0 Experimental Apparatus and Procedure

Six different tube arrays were studied in the low speed wind tunnel located in JHE 208 at McMaster University. This wind tunnel has been used for various studies and has been found to have an upstream turbulence intensity of 1%.

3.1 Test Sections

The test section has a square cross section of 0.618 m (24.31"). The inline arrays (see Figure 3.1) consist of 42 tubes, 25 of which are flexible (fixed tubes are indicated by a solid center in Figure 3.1 and 3.2) and the rotated square arrays (see Figure 3.2) consist of 33 tubes, 21 of which are flexible. The test section was designed to accommodate the three different tubes and two different array geometries, so that only one test section would be required (instead of six). Only one test section and support structure are employed to reduce the manufacturing required which means that the tube pitch is 88.2 mm (3.47") for all arrays. Each tube array has six rows of tubes, as per the recommendations of Weaver and ElKashlan (1981a). The test section has the ability of being rotated 45 degrees, with the removal and reassembly of certain components, to convert from an in-line to a rotated square array.

The side walls have four different configurations, two of these configurations can be used for the in-line arrays (both configurations result in flat walls), one is used for the rotated square finned tube array and the last configuration is used for the rotated square bare tube array. The rotated square configurations were designed so that half tubes

would not be required; instead the tubes closest to the walls are set inside the wall, so that the flow only interacts with half of a tube. For the in-line array the gap between these tubes and the wall is equal to half of the gap between tubes ($[P_t - D_{outer}] / 2$). This ensures a uniform pressure drop across each tube bundle.

3.1.1 In-Line Square

The in-line square arrays contain six rows and seven columns of tubes. The tubes closest to the walls are fixed (not dynamic), to ensure that the acrylic walls are not damaged during operation. The last row of tubes (the furthest downstream) is also fixed, to reduce the number of tubes required to be tuned. The fixing of the last row of tubes will not effect the fluidelastic phenomenon according to the research done in Weaver and ElKashlan (1981a), in that the addition of rows of tubes beyond the fifth row do not affect the fluidelastic threshold.

The tube arrays have twenty-five flexible (dynamic) tubes, four of which are monitored (numbered 1-4 in Figure 3.1) for capturing the frequency and amplitude of vibration of the tubes. They are all tuned to a similar natural frequency (±1%).

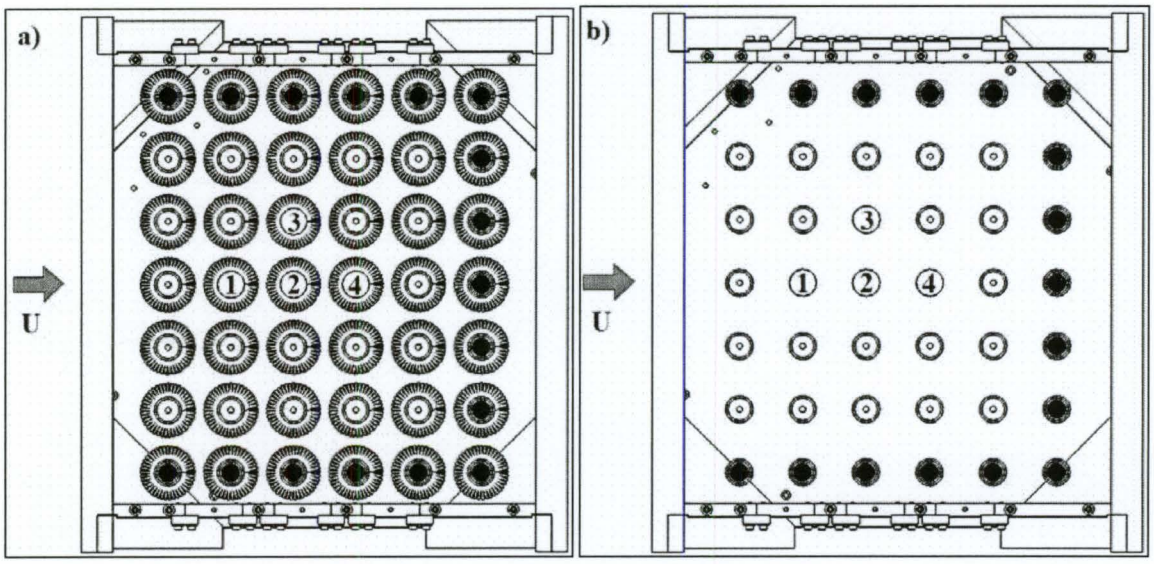

Figure 3.1: In-Line Square Tube Arrays,
a) 3.3 and 5.7 fpi , b) Bare
Note: fixed tubes are indicated by a solid center

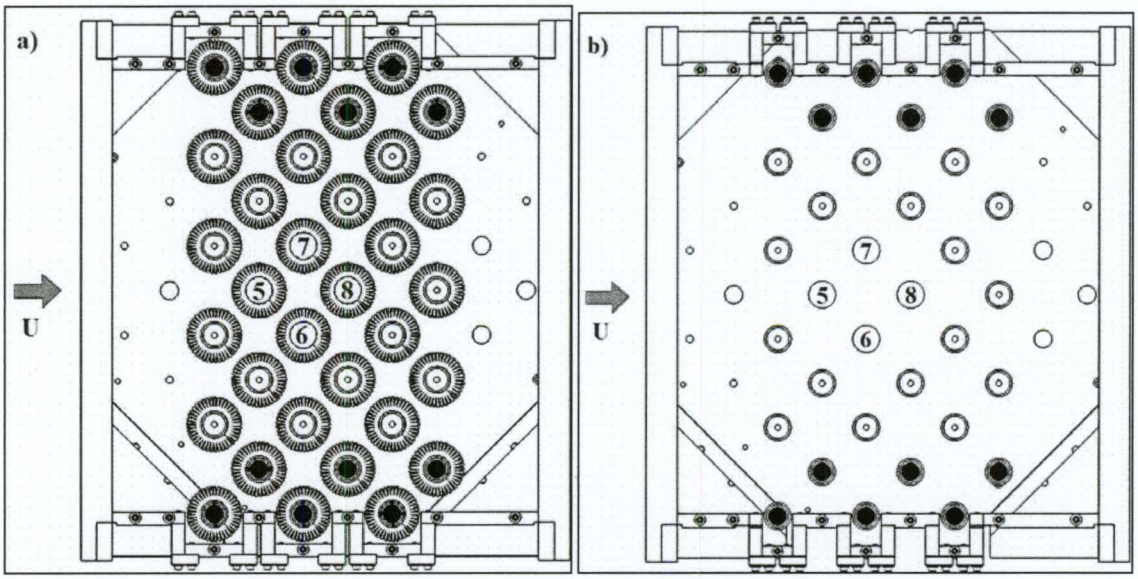

Figure 3.2: Rotated Square Tube Arrays,
a) 3.3 and 5.7 fpi, b) Bare

3.1.2 Rotated Square

In the rotated square arrays, the two columns of tubes closest to the walls of the test section are fixed to prevent damage of the acrylic walls and the other twenty-one tubes are flexible. The tubes numbered 5-8 in Figure 3.2 are monitored and again all the flexible tubes are tuned to a similar natural frequency (±1%).

3.1.3 Test Tubes

The tubes were supplied by Foster Wheeler Power Group, manufactured by Biraghi Canada of Bécancour, Quebec, which is a subsidiary of Fintube Corp (Finned Tube Corp. also owns ESCOA which was previously mentioned in Section 2.3).

The tubes were cut to 0.610 m (24") and a 9.53 mm (3/8") fine threaded rod was welded to a bung, which was then welded to the end of one of the tubes, resulting in a cantilever (fixed-free) arrangement. For the monitored tubes the threads were removed from a section of the threaded rod (close to the support base) and a strain gauge was applied in the streamwise and transverse to flow directions to capture the respective amplitudes of vibration (see Figure 3.3).

The threaded rods used are 3/8"-24 mild steel for 3.3 & 5.7 fpi tubes and 3/8"-24 B7 alloy for the bare tubes. The higher alloy was used for the bare tubes since the vibrational amplitudes can be larger for the bare tubes (tube to tube clashing versus fin to fin or fin to tube clashing). The modulus of elasticity of the different steel alloys is approximately the same, not affecting the natural frequency, but the yield strength is higher for the B7 alloy. The threaded rods are fastened by two nuts with washers above

and below the support structure (see Figure 3.3), which are all torqued to the pre-load value of 20.4 N·m (15 ft-lbs).

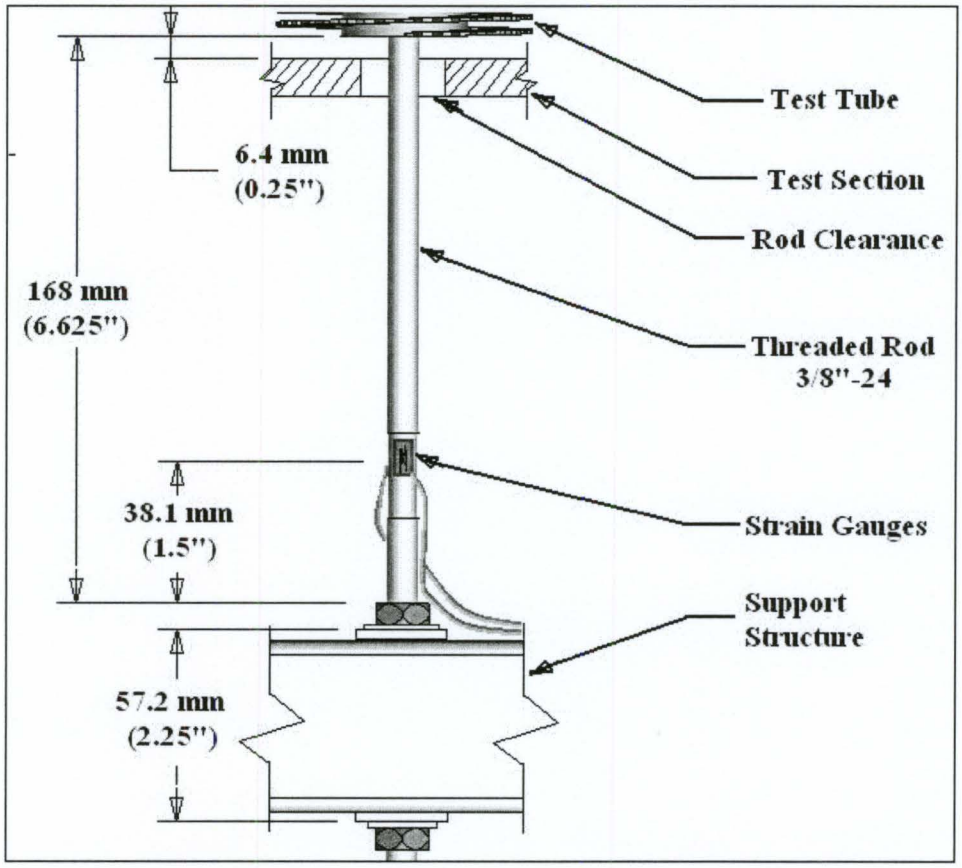

Figure 3.3: Schematic of the Fixation of the Tubes, the Strain Gauges and Tunnel Clearance (5.7 fpi)

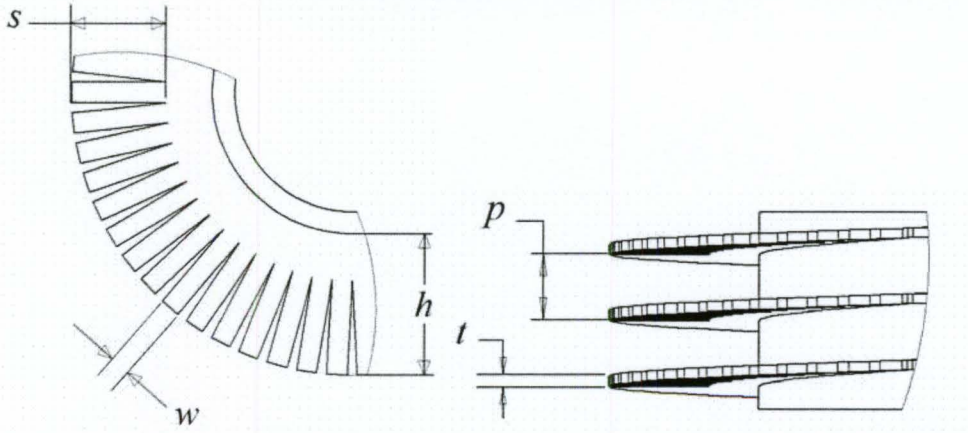

Figure 3.4: Geometry of Finned Tubes

The geometry of the finned tubes is shown in Figure 3.4 and pictures of the steel finned tubes under investigation are shown in Figure 3.5. The bare tube diameter, D_b, is 38.3 mm (1.508"). The fins are 1.3 mm (0.051") thick, t. The serration, s, starts 12.7 mm (0.5") from the end of the fin. Table 3.1 shows the other specifications for the finned tubes, w is the fin serration width and fpi is fins per inch. The bare tubes used (not shown) have the same outer diameter as the bare tube diameter of the finned tubes.

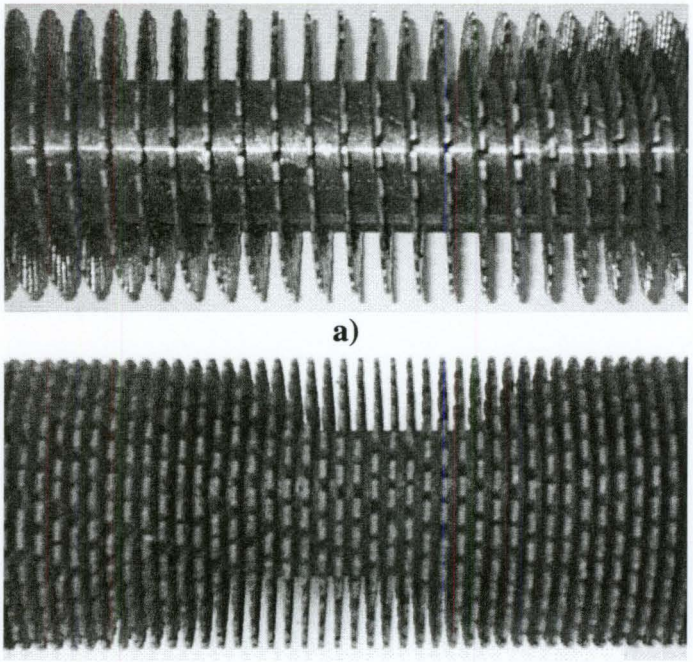

a)

b)

Figure 3.5: Photo of Finned Tubes Under Investigation, a) 3.3 fpi, b) 5.7 fpi

Table 3.1: Finned Tube Specifications [mm (inch)]

Tube	h	w	p
3.3 fpi	18.5 (0.727)	4.4 (0.172)	8.4 (0.321)
5.7 fpi	19.1 (0.750)	4.5 (0.176)	4.2 (0.173)

Since the tubes are full scale, the tubes are quite heavy, compared to previous studies of fluidelastic instability. The total test section, support structure and tubes weigh approximately 273 kg (600 lbs) for the 5.7 fpi in-line square array.

3.2 Modelling of Tube

The test tubes were modelled to predict their natural frequency through the use of analytical and finite elements methods. The latter model was used to predict the size of the end masses for tuning purposes.

3.2.1 Analytical

An analytical model was developed with beam deflection equations (Castigliano). The resulting stiffness associated with the threaded rod is:

$$k_{eq} = \frac{3EI}{l^3}\left[\left(\frac{l}{L/2}\right) + 3\left(\frac{l}{L/2}\right)^2 + 3\left(\frac{l}{L/2}\right)^3\right]^{-1} \tag{3.1}$$

where E is the Modulus of Elasticity, I is the 2nd Area Moment of Inertia, l is the length of the threaded rod and L is the length of the test tube. The stiffness associated with the test tube is not included, as it is much stiffer compared to the stiffness of the threaded rod ($I_{threaded\ rod} << I_{test\ tube}$).

The equivalent mass for the analytical model did not include the mass of the threaded rod since the latter is negligible in comparison with that of the tube. Note that the equivalent mass of a cantilever beam acting at its free end is 33/140 of its total mass.

Thus, $$m_{eq} \cong M_{tube} \quad (3.2).$$

The resulting natural frequency is:

$$f_n \cong \frac{1}{2\pi}\sqrt{\frac{3EI}{M_{tube}l^3\left[\frac{l}{L/2}+3\left(\frac{l}{L/2}\right)^2+3\left(\frac{l}{L/2}\right)^3\right]}} \quad (3.3).$$

3.2.2 Finite Element

Since the analytical model was not able to predict the measured natural frequency of the tubes better than about 9%, a more precise analysis was carried out. A finite element model was created in FEMAP v9.0 and the appropriate values associated with the mass (density) and stiffness (geometry and material properties) were entered into the program. The number of elements was selected based upon the resulting natural frequency; as the number of elements increase, the value of the natural frequency converges to a constant value. The number of elements selected for the model was based on the actual measured natural frequency, and since the measured value is only valid up to 3 significant figures, the finite element model was designed to converge at 4 significant figures.

Damping can be added to the finite element model, but since the structural damping in the actual model is quite small, it was omitted.

3.2.3 Natural Frequency Comparison:

The results from the different models used are presented in Table 3.2.

Table 3.2: Comparison of the Natural Frequencies (Hz)

Method	Bare	3.3 fpi	5.7 fpi
Castigliano	5.896	2.813	2.747
FEA Model	4.398	2.505	2.499
Measured Value	4.50	2.51	2.51

It is known that the stiffness of a threaded rod is dependent on an effective diameter. This effective diameter was determined by tuning the predicted natural frequency for the 5.7 fpi tube to the measured value. This computation produced an effective diameter of 7.9 mm (0.3112"). This diameter was then used in computations for the natural frequencies of the other tube arrangements.

3.3 Similarity

Similarity was maintained between the models through the mass ratio using Mair et al.'s effective diameter ($m/\rho D_{eff}^2 = 2790$). 5.7 fpi has the highest mass per unit length, m, therefore the other test tubes were designed relative to it. End masses are added to the bare and 3.3 fpi tubes and the threaded rod lengths are adjusted to obtain the desired natural frequency. The bare tube's natural frequency is higher in order to ensure that the tube bundle will be unstable at an upstream velocity that could be measured with the current equipment and without the addition of viscous dampers; this was done at the design stage under the recommendations of the bare tube guidelines for fluidelastic instability (Weaver and Fitzpatrick (1988)). No additional damping was added, so

structural damping was the only damping available to stabilize the bundle. The finned tubes had the same natural frequency of 2.5 Hz and the bare tubes had a natural frequency of 4.5 Hz.

The procedure used to scale the tubes was as follows: First a uniform mass per unit length (M'_{tube}) was used in the finite element model, in place of the tube's true mass per unit length (M_{tube}), in order to calculate the threaded rod length required to obtain the desired natural frequency.

$$M'_{tube} = M_{6\,fpi}\left(\frac{D_{eff\_tube}}{D_{eff\_6\,fpi}}\right)^2 \tag{3.4}$$

Next the actual mass per unit length was used in the model with the established threaded rod length to compute the end mass required to produce the desired natural frequency. This end mass was adjusted to the computed value by varying its length and it was fixed to the inside of the free end of the tube using a set screw.

All the tubes were tuned to the same natural frequency ± 1% and the mass of each tube, prior to the addition of any end mass, was the same ± 1%. All the tube specifications are listed in Table 3.3. See Figure 3.4 for the threaded rod and end mass lengths.

Table 3.3: Tube Specifications

Tube	D_{eff} mm (inch)	f Hz	m kg/m (lbs/ft)
Bare	38.3 (1.508)	4.5	4.912 (3.294)
3.3 fpi	44.2 (1.740)	2.5	6.534 (4.381)
5.7 fpi	49.5 (1.949)	2.5	8.217 (5.510)

Table 3.4: Threaded Rod Lengths and End Mass Sizes m (inch)

	Bare	**3.3 fpi**	**5.7 fpi**
Threaded Rod Length	0.105 (4.125)	0.198 (7.800)	0.168 (6.625)
End Mass Length	0.077 (3.050)	0.020 (0.800)	N/A

3.4 Measurement Equipment

Strain gauges were affixed to the threaded rods attached to the test tubes in the streamwise and the transverse flow directions. Strain gauges: Vishay/Micro-Measurements Group, CEA-06-125UN-350 for finned tubes and ED-DY-062AK-350 for bare tubes. The bare tube strain gauges were of a different type because the maximum strain was much higher for tube to tube clashing and the gauge size was smaller because of the lead time/availability associated with the gauges. Data from the strain gauges was captured by way of a Vishay 2310 signal conditioning amplifier and a Hewlett Packard/Agilent 34570A dynamic signal analyzer.

For the tuning of the test tubes, an accelerometer (PCB Piezotronics ICP 352 B22) was affixed to the top of each tube with wax and the tube was plucked and the response

frequency was captured by way of a Kistler 5134 power supply and an Agilent 54621A oscilloscope.

RPM of the fan motor was measured by way of an optical tachometer (Lutron Digital Tacho DT-2232C), measured at the shaft of the fan blades.

The upstream velocity was measured using a pitot-static probe attached to an Ashcroft XLDP differential pressure transducer. For the bare tube in-line square experiments, the upstream velocity could not be measured by this pressure transducer (too much uncertainty in the pressure measurement), so instead a water manometer was connected to a pitot static probe.

The pressure drop across the tube array was measured by four pressure taps that were installed in the upstream portion of the wind tunnel just prior to the test section and another four downstream of the test section. Each set of pressure taps were linked together by Tygon hoses so as to get an average measurement. Two hoses, one from each set of pressure taps, were then connected to a water manometer to measure the pressure drop.

The decay trace for measuring the damping was captured by using the Vishay 2310 strain gauge amplifiers and a DATAQ DI-205 data acquisition card along with the associated software (WINDAQ ACQ DI-200 Acquisition v.2.46).

3.5 Damping

The damping of the four monitored tubes was measured by pluck tests. All the tubes were fixed except for the tube that was under investigation. The tube was

subsequently plucked and the decay trace was captured. Three measurements were captured for each tube. The pluck amplitude was always larger than $2\%D_{eff}$ so that a measurement of the damping at this amplitude could be taken and to ensure that any non-linear damping was minimized.

When the tubes were plucked, there was a great tendency for the tubes to whirl or vibrate in patterns which could not be captured by a single strain gauge, so the decay traces of the streamwise and transverse to flow directions were both captured. This presented a problem when trying to obtain a value of the logarithmic decrement of damping. Different schemes were used to attempt to combine these two decay trace signals, but the best method seemed to be using a total amplitude of vibration method. This was originally derived through the summation of energy in the system (potential and kinetic). The results of this scheme appear as a cloud of data that is representative of the overall exponential decay curve, which is expected for damping. This data was then root-mean-square averaged for each full cycle. This procedure collapsed the cloud of data to a single exponentially decaying trend and a first order exponential curve was then fitted to obtain the logarithmic decrement.

As can be seen in Table 3.5 (Table 3.5 shows the values used for the plotting of the results in Section 4), the lowest measured damping value is that of the bare tubes which increases with the fin density, which can be attributed to "windage" effects. The sampling frequency for the pluck tests is 100 Hz for the finned tubes and 180 Hz for the bare tubes, 40 times the natural frequency of the tubes. Measurements of the logarithmic decrement, δ, are by way of an exponential curve fit to the acquired data at an amplitude

of $1\%D_{eff}$. Three trials were done per tube and the average from these results is presented in Table 3.5, along with an array average. All repeated tests produced results within 9% (see Appendix 7.4). The results for the In-line Square array are different from the Rotated Square array because when the array was re-arranged for changing between the two configurations, the tubes were loosened, rotated and re-tightened so that the strain gauges would measure in the new streamwise and transverse to flow directions (re-tuning was done as required).

Table 3.5: Logarithmic Decrement Damping of Tubes
(Refer to Figure 3.1 & 3.2 for tube location)

In-Line Square					
Tube	**1**	**2**	**3**	**4**	**Average**
Bare	0.0037	0.0024	0.0037	0.0024	0.0031
3.3 fpi	0.0047	0.0048	0.0046	0.0048	0.0047
5.7 fpi	0.0064	0.0062	0.0049	0.0073	0.0062
Rotated Square					
Tube	**5**	**6**	**7**	**8**	**Average**
Bare	0.0035	0.0029	0.0056	0.0026	0.0037
3.3 fpi	0.0050	0.0048	0.0055	0.0050	0.0051
5.7 fpi	0.0064	0.0049	0.0075	0.0063	0.0063

3.6 Experimental Procedure

Each experiment was conducted in a similar manner. The wind tunnel velocity was increased to a set value and measurements commenced after ten minutes for the finned tubes and eight minutes for the bare tubes. The amount of time is longer for the finned tubes due to their lower natural frequency. This period was allowed to elapse as it appeared that the tube amplitude of vibration reached a steady state response after this time. Limit Cycle Amplitude was approximately achieved. If measurements were taken earlier than this time, measurements would be below the long time value, since they

would be averaging a value that is increasing as the measurements progress. This procedure would yield a RMS amplitude that is lower than the actual value for the energy in the system at the flow velocity.

The velocity was determined using the pitot-static probe. The value was obtained before and after the previously mentioned build-up period for verification purposes. Afterward, measurements of the tube response for each of the monitored tubes in the streamwise and transverse direction were recorded by averaging 100 samples of the frequency spectra. The frequency resolution was 0.125 Hz. The RMS, root mean square, tube response amplitude is determined from the RMS streamwise and transverse components as:

$$RMS \quad Amplitude = \sqrt{streamwise^2 + transverse^2} \qquad (3.5).$$

Once the measurement was complete, the flow velocity was increased and another data point was captured in the same manner as previously described. The velocity was always increased and was not reduced between measurements, so as to prevent any hysteretic effect. If another point was required at a lower velocity, which would have required a reduction in velocity, the wind tunnel was stopped and the experiment was not restarted until a period of time had elapsed such that the amplitude of vibration dropped to a value well below the expected amplitude of vibration for the starting flow velocity. At least two data points were repeated, before or after the velocity which was being measured, to ensure that the new experimental results were representative of the previous data collected. This procedure not only validated the current data set, but also showed the repeatability of the previous measurements.

Since four tubes were monitored in the streamwise and transverse direction, which would require eight channels to capture all the tube response at once, and the HP dynamic signal analyzer only has four channels, experiments were conducted as follows: two tubes were monitored in two directions, the other tubes were monitored in two directions in a separate set of experiments and then a third set of experiments was conducted with one tube from each of the previous sets of experiments, to show that the behaviour of each set of the previous experiments was repeatable.

When the critical reduced velocity was unknown (the first set of experiments for each bundle), the velocity was varied with a coarse velocity step. A further experiment was then conducted, with a finer velocity step, where better resolution was required, so that a clearer critical velocity was achieved.

Measurements would be discontinued for two different conditions: 1) a tube within the array collided with another tube (fin-to-fin contact for finned tubes) which did not necessarily involve monitored tubes, 2) if the amplitude of vibration was significantly high enough (above $5\%D_{eff}$) and a significant change in slope of the amplitude versus velocity plot was observed. The second condition was only used for the bare tubes, since larger amplitudes of vibration can potentially cause plastic deformation of the tube support, which would yield non-linear stiffness effects.

3.7 Confidence Level

The certainty of measurements established the validity of the experiments, for comparison with the results of other researchers. The tolerances and uncertainties associated with the set-up and running of the experiments are summarized below.

Building and Assembly Tolerances:

Tube Mass: ± 1%

Tube Natural Frequency: ± 1%

Experimental Test Equipment:

Pressure Transducer: 0.0125 V (0.25 % of Full Span, Full Span = 5 V)

Water Manometer: ± 0.0127 mm (0.0005 in)

Vernier Height Gauge measurements: ± 0.05 mm

Voltmeter measurements: 0 to 2 V ± 0.0005 V, 2 V and up ± 0.005 V

Propagation of Error for Measured Values (See calculations in Appendix section 7.1):

Amplitude: 0.001 m ± 0.00005 m (for 5.7 fpi @ 2% D_{eff})

Upstream Velocity using Pressure Transducer (5.7 fpi Rotated Square Array): 2.32 m/s ± 0.03 m/s (at Critical Upstream Velocity) -> 1.3 %

Upstream Velocity using Water Manometer (Bare Tube In-Line Square Array): 2.33 m/s ± 0.06 m/s (at Critical Upstream Velocity) -> 2.6%

3.8 Calibration

A calibration for the pressure transducer was accomplished by applying a known pressure of two inches of water with a syringe (as a pressure piston) and a water manometer. The pressure was applied by the syringe into a rubber hose, which was split into two separate lines, one attached to the pressure transducer and the other attached to

the water manometer. This calibration was initially attempted using a commercial "piston" type calibrator, but the commercial calibrator was very difficult to employ as it was very sensitive to heat from the users hands and it was hard to ensure a constant known pressure of two inches of water (the span of the pressure transducer) was applied.

The strain gauges were calibrated by deflecting the tip of the tube by a known amount with a Vernier height gauge and measuring the resulting voltage output by the strain gauge. Multiple data points were captured to create calibration curves which fit well to a linear trend-line. The calibration curves can be found within Section 7.2 of the Appendix in Figure 7.1 and 7.2 for in-line and rotated square arrays respectively.

The natural frequency of each flexible tube within the tube array was obtained in both the streamwise and transverse to flow directions and natural period was measured over 11 cycles for the finned tubes and 19 cycles for the bare tubes to obtain an average value. If the tube's natural frequency was not within the set frequency range (± 1% of the natural frequency), the threaded rod length was adjusted until the proper value was achieved. In some cases a tube could not be successfully tuned. In this case, the tube was swapped with a fixed tube and this tube was marked as "not tuneable" or "defective" on the welded bung and the previously fixed tube was tuned in its place.

4.0 Experimental Results

Experiments were conducted with an in-line and a rotated square array geometry. The tube pitch to effective diameter ratio (P_t/D_{eff}) is different for each of the three tubes tested, but the tube pitch to bare tube diameter ratio was the same for all cases.

The nuclear steam generator industry has been driving the research of fluidelastic instability. The vast majority of available data has tube pitch ratios between 1.3 and 1.5. The fossil fuel industry, which supplied the finned tubes used, typically employs larger tube pitch ratios. Hence the larger pitch ratio in the current study. The mass ratio, $m/\rho D_{eff}^2$ was preserved and the P_t was kept constant, which means P_t/D_{eff} changes.

Table 4.1: Experimental Results

Tube	P_t/D_{eff}	$m\delta/\rho D_{eff}^2$		U_{crit}/fD_{eff}	
		In-Line	Rotated	In-Line	Rotated
Bare	2.32	8.6	10.3	19	62 ± 12
3.3 fpi	2.00	13.1	14.2	44	42
5.7 fpi	1.78	17.3	17.6	50 ± 3	35

The mass ratio and critical reduced velocity data from all the arrays is summarized in Table 4.1. The experimental results for each array are compared with the world data on the stability maps of Weaver and Fitzpatrick (1988) at the end of Section 4.1 and 4.2. The data is found to fall within or above the world data for the arrays tested; the plots have been adapted to U_p/fD_{eff} versus $m\delta/\rho D_{eff}^2$ to reflect the current study parameters.

The results from the in-line arrays are presented in Figures 4.1 to 4.3 and the rotated square arrays results are shown in Figure 4.5 to 4.7. These plots are RMS amplitude/D_{eff} versus reduced velocity (U_p/fD_{eff}).

4.1 In-Line Square

4.1.1 Bare

The graph in Figure 4.1 for the bare tube array is very typical of fluidelastic behaviour. It is extremely simple to determine the critical velocity for the array since the instability is very abrupt and all of the monitored tubes are unstable at roughly the same reduced velocity of about 19.

There is no clear distinction between the behaviour of the streamwise and the transverse to flow direction amplitude results, although the amplitude of vibration in the transverse direction is higher (double in the case of the fourth row tube) than the streamwise direction. Larger amplitudes in the transverse to flow direction, compared to the streamwise direction are typical of fluidelastic instability.

Although the present bare tube array has a larger pitch to diameter ratio than previously studied, the results appear to be similar to those of previous research in fluidelastic instability of bare tube arrays.

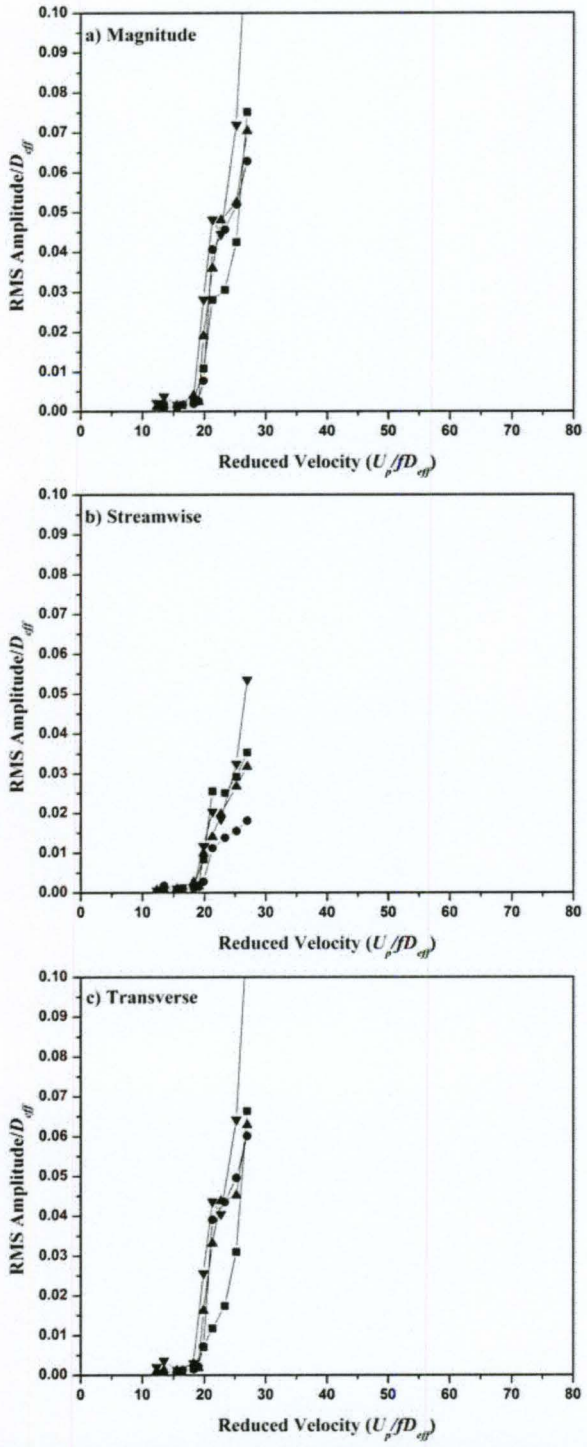

Figure 4.1: Bare Tube In-Line Square Array, a) Magnitude, b) Streamwise, c) Transverse, ■ – 1, ● – 2, ▲ – 3, ▼ – 4 (Refer to Figure 3.1)

4.1.2 3.3 fpi

The results for the 3.3 fpi in-line square array are summarized in Figure 4.2. The second row tube (number 1) shows an abrupt increase in oscillation amplitude in the transverse direction at a reduced velocity of about 44. This is typical behaviour seen in bare tube arrays. The other monitored tubes do not show such a sharp increase in rms amplitude although the amplitude-velocity slope does increase substantially for reduced velocities above about 44. It appears that the effect of these fins at 3.3 fpi is to substantially delay the stability threshold and to make this less distinct.

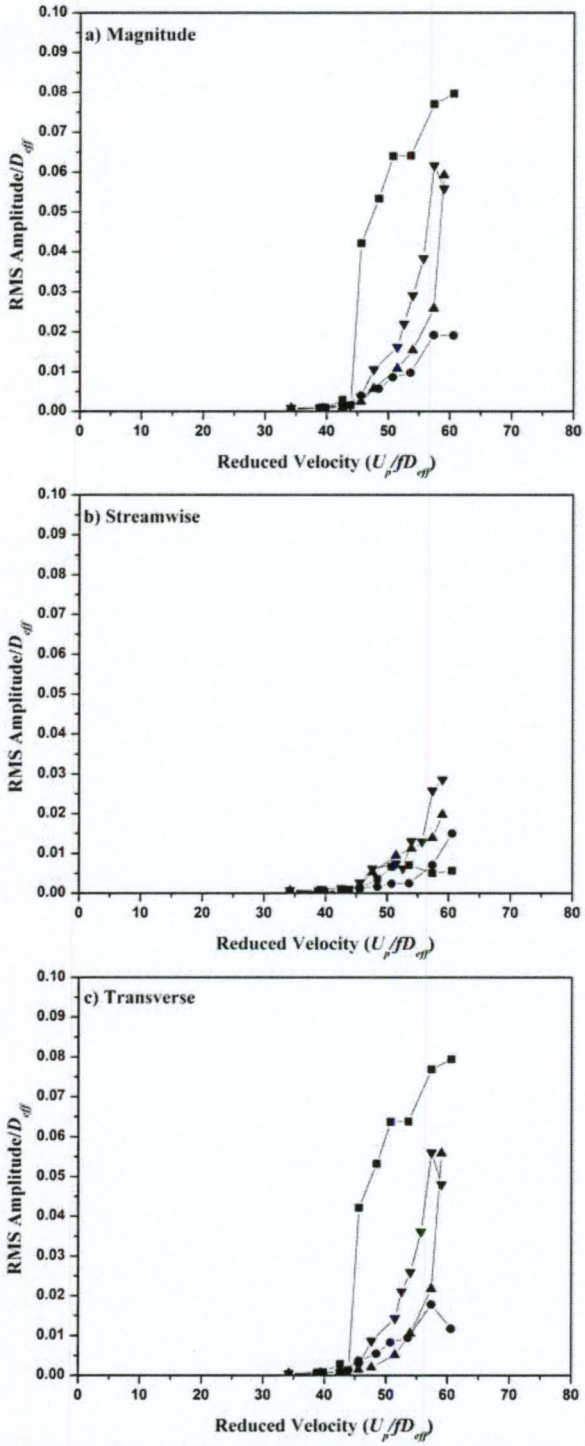

Figure 4.2: 3.3 fpi Finned Tube In-Line Square Array, a) Magnitude, b) Streamwise, c) Transverse, ■ – 1, ● – 2, ▲ – 3, ▼ – 4 (Refer to Figure 3.1)

4.1.3 5.7 fpi

The results for the 5.7 fpi in-line square array are summarized in Figure 4.3. Tube number 3 (3rd row) shows an increase in streamwise amplitude at a reduced velocity of about 43 but then levels off near an amplitude of 1%*D*. A streamwise response is somewhat unusual and the amplitude is rather small to consider that the tube is unstable. Tube number 1 (2nd row) shows an abrupt increase in transverse amplitude response at a reduced velocity of about 50. Subsequently, all of the tubes develop significant whirling amplitudes. Recognizing that there is some uncertainty in defining the stability threshold, the critical reduced velocity is taken as 50 ± 3.

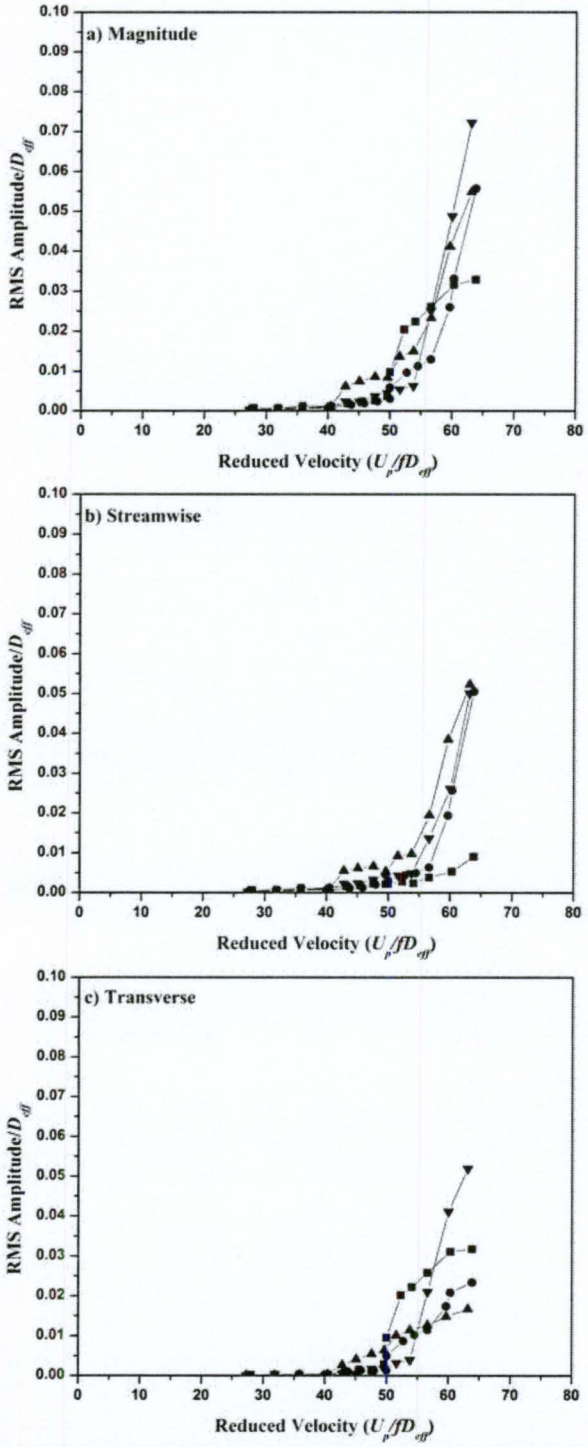

Figure 4.3: 5.7 fpi Finned Tube In-Line Square Array, a) Magnitude, b) Streamwise, c) Transverse, ■ – 1, ● – 2, ▲ – 3, ▼ – 4 (Refer to Figure 3.1)

Comparison with World Data: In-Line Square Arrays

The world data for in-line square arrays of bare tubes is plotted in Figure 4.4 (Weaver and Fitzpatrick (1988)). It is seen that the present bare tube data fits at the upper end of the scatter of the world experimental data.

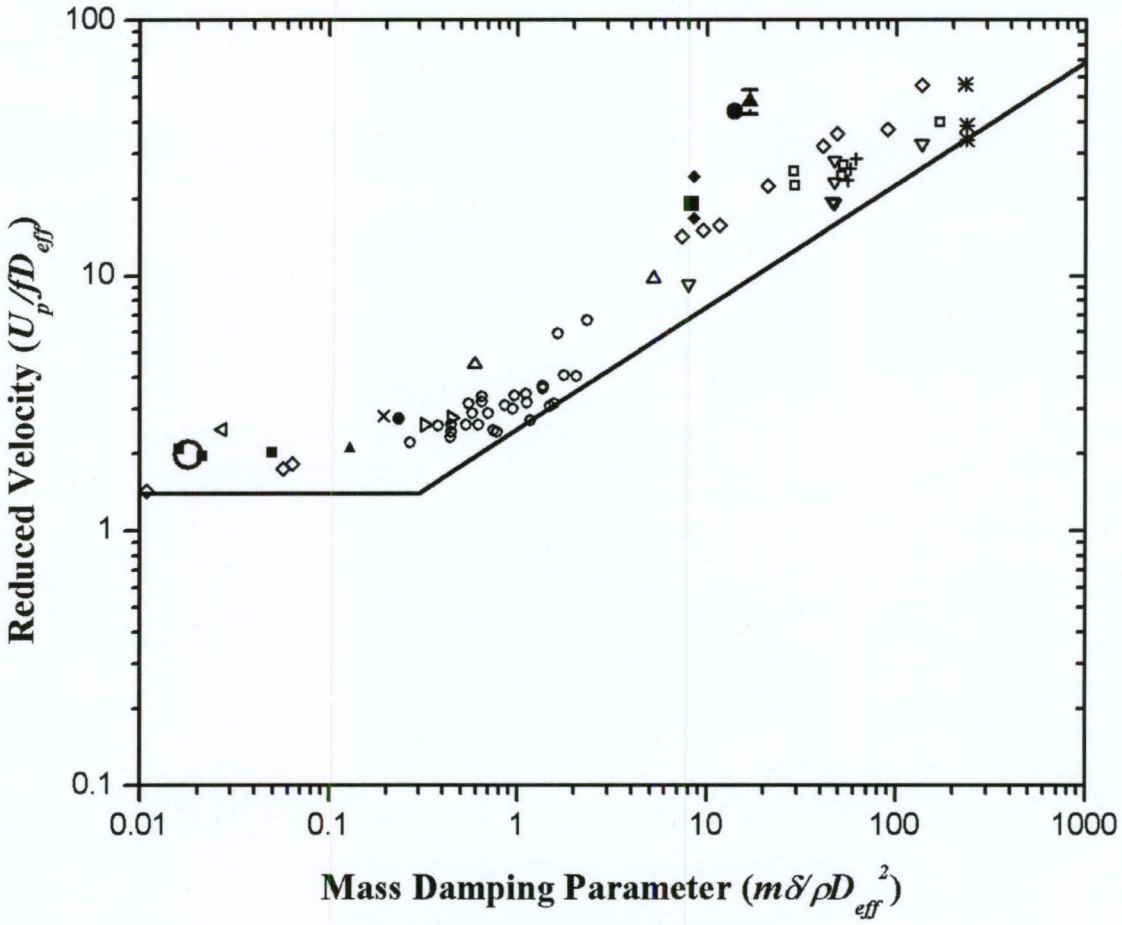

Figure 4.4: In-Line Square Arrays
■ – Bare, ● – 3.3 fpi, ▲ – 5.7 fpi
(Adapted from Weaver and Fitzpatrick (1988))

The data point sits between two other data points which have nearly the same mass-damping ratio (the ♦ data from ElKashlan (1984)). The current tube pitch to diameter ratio is 2.32, ElKashlan's data point below the current data has a P_t/D = 1.33 and the data point above has a P_t/D = 1.50. Although the current bare tube array has a

tube pitch ratio that is much higher than this other data, the trends relating to the tube pitch ratio (Schröder and Gelbe (1999)) for in-line square arrays in gas flows, suggests that there is a lower dependence on the tube pitch ratio. It must be noted that this comparison requires extrapolation since the data in Schröder and Gelbe is only available up to P_t/D = 1.8. Chen (1984) suggests that in-line square arrays are not strongly dependent on the P_t/D ratio. However, this may only be tube for smaller pitch ratios. The graph of Soper (Figure 2.8 in Section 2) suggests that there is a strong increase in critical velocity with pitch ratio for pitch ratios greater than about 1.6.

The 3.3 fpi and 5.7 fpi arrays have reduced velocities that are significantly higher than any of the previously collected bare tube data (Figure 4.4). This suggests that fins delay the threshold of instability by a factor of at least two compared to bare tube and using D_{eff} as the length scale. If the bare tube diameter were to be used as the length scale in the reduced velocity, the observed delay effect would be even greater.

4.2 Rotated Square

4.2.1 Bare

The results for the rotated square array of bare tubes are plotted in Figure 4.5. This was the last of the 6 arrays to be studied and it is possible that the strain gauges may have been damaged (See Figure 7.2 (b) in Appendix 7.2, the calibration curve for tube 7 in the bare tube array indicates that the transverse strain gauge is not behaving linearly). Unlike the other five tests, the turbulence excited vibration amplitudes (reduced velocities below 50) are much larger and different amongst the tubes monitored. In particular, the turbulence response amplitudes are expected to be less than about 0.2%D where as they are seen to be about 1%D in these bare tube experiments. The stability threshold is not clearly defined but the amplitude-velocity slope seems to increase at a reduced velocity of about 50 and the bundle is certainly unstable by a reduced velocity of about 74. While the rms amplitudes may be suspect, the change in amplitude with velocity should still be an indicator of instability. Thus, a reasonable estimate of the stability threshold is 62 ± 12, the large range recognizing the uncertainty in defining the threshold. Importantly, this uncertainty does not affect the conclusions drawn from this research.

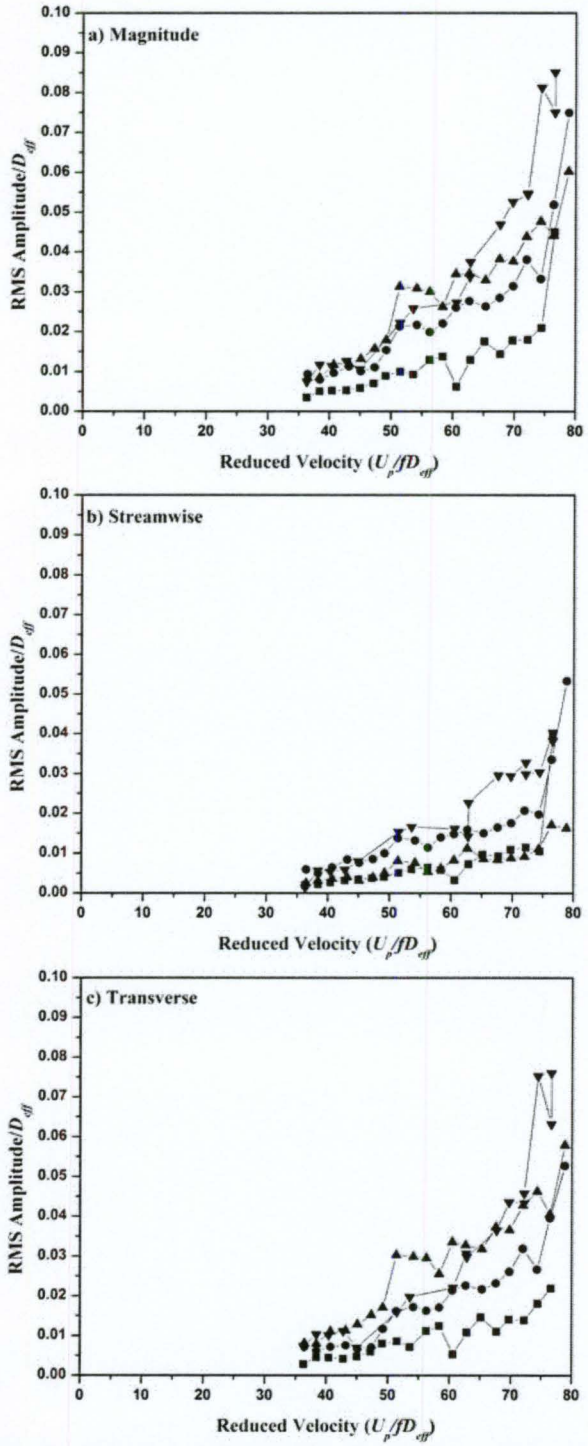

Figure 4.5: Bare Tube Rotated Square Array, a) Magnitude, b) Streamwise, c) Transverse, ■ – 5, ● – 6, ▲ – 7, ▼ – 8 (refer to Figure 3.2)

4.2.2 3.3 fpi

The results of the rotated square array of finned tubes with 3.3 fpi are summarized in Figure 4.6. The observed amplitude response behaviour as a function of flow velocity is much better behaved than for the bare tube array, lending credence to the suggestion that the strain gauge calibration in those experiments may have been compromised. All four monitored tubes behave similarly and the stability threshold is relatively well defined at a reduced velocity of about 42. Tube number 8 (4^{th} row) becomes unstable predominantly in the transverse direction but the other 3 monitored tubes appear to whirl with no preferred orientation.

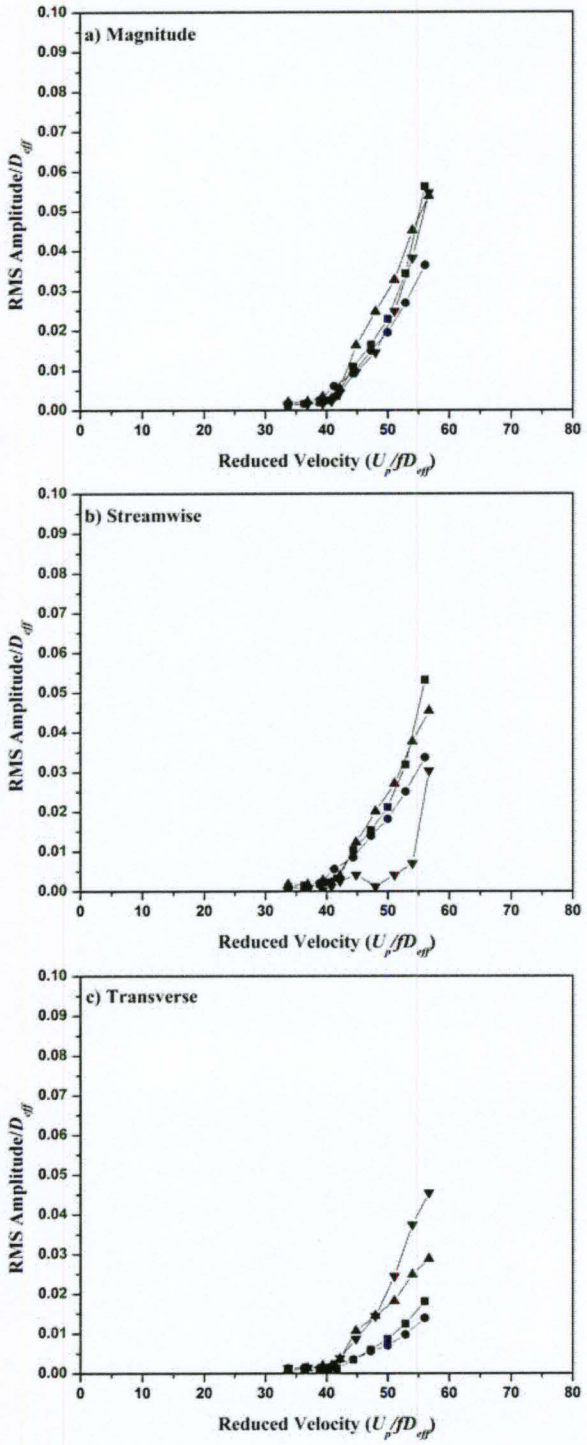

Figure 4.6: 3.3 fpi Finned Tube Rotated Square Array, a) Magnitude, b) Streamwise, c) Transverse, ■ – 5, ● – 6, ▲ – 7, ▼ – 8 (refer to Figure 3.2)

4.2.3 5.7 fpi

The results for the rotated square array of finned tubes with a fin density of 5.7 fpi are summarized in Figure 4.7. These plots show response behaviour which is even more regular than the 3.3 fpi array. The stability threshold is very clear at a reduced velocity of about 35 with all of the monitored tubes whirling at large amplitudes with no preferred orientation, similar to the behaviour of the 3.3 fpi array.

Interestingly, the increase in fin density for the rotated square array appears to regularize the tube response and reduced the stability threshold while the opposite behaviour was observed for the square in-line arrays.

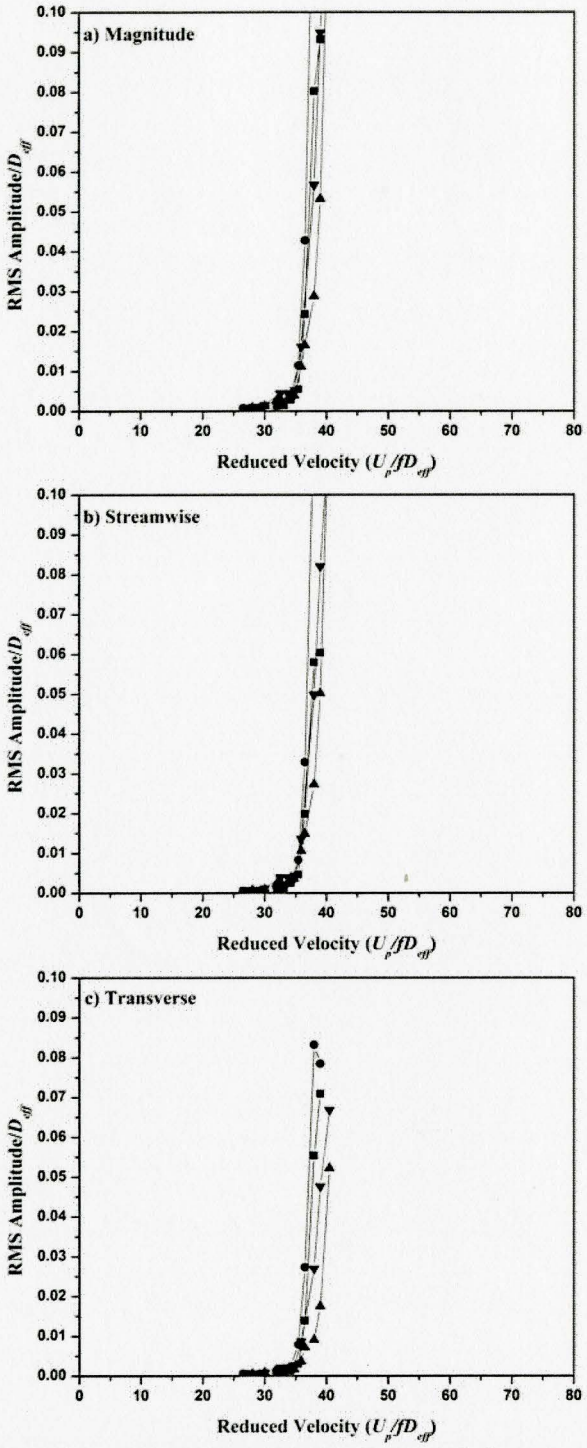

Figure 4.7: 5.7 fpi Finned Tube Rotated Square Array, a) Magnitude, b) Streamwise, c) Transverse, ■ – 5, ● – 6, ▲ – 7, ▼ – 8 (refer to Figure 3.2)

Comparison with World Data: Rotated Square Arrays

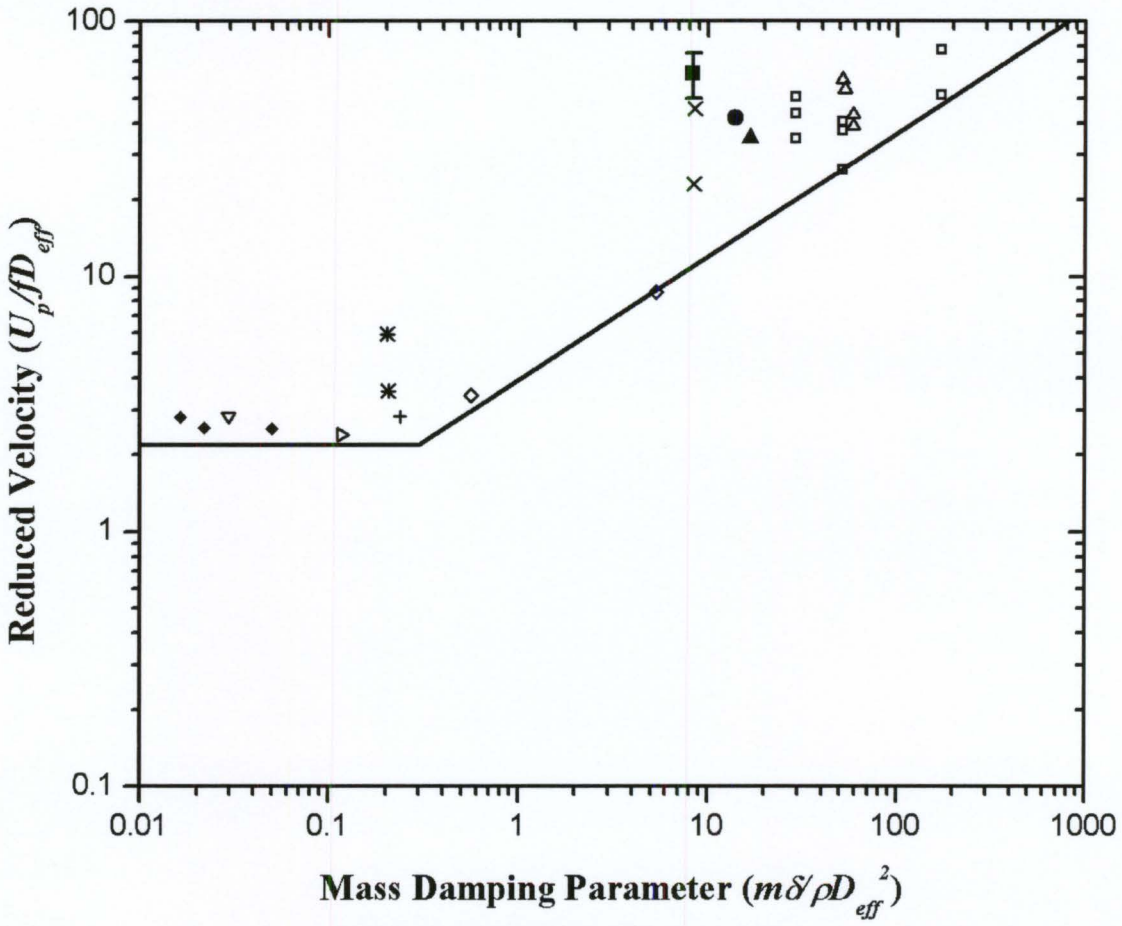

Figure 4.8: Rotated Square Arrays
■ – Bare, ● – 3.3 fpi, ▲ – 5.7 fpi
(Adapted from Weaver and Fitzpatrick (1988))

In Figure 4.8, the bare tube data captured in this current study (P_t/D = 2.32) sits above two other tube bundles (× data) from ElKashlan (1984). ElKashlan's lower data point has a P_t/D = 1.414 and the upper data point has a P_t/D = 1.70. This suggests that as the tube pitch ratio increases, the stability threshold increases which is consistent with Schröder and Gelbe (1999) and also in Chen (1984).

Stability threshold values for 3.3 fpi and 5.7 fpi (Figures 4.6 & 4.7) are well defined, unlike in the bare tube case. The results fall high but within the scatter of the

existing data, which suggests that the use of an effective diameter is appropriate for scaling fluidelastic instability results in rotated square arrays.

5.0 Conclusions and Recommendations

Experiments were conducted to study fluidelastic instability in in-line and rotated square finned tube arrays. For each array geometry, 3.3 and 5.7 fpi finned tubes and bare tubes were considered. The tube pitch (P_t) and the mass ratio ($m/\rho D_{eff}^2$) were kept essentially constant. For the first time, fluidelastic instability has been demonstrated in in-line and rotated square arrays of modern finned tubes. The principal conclusions drawn are:

1) The use of Mair *et al.*'s effective diameter appears appropriate for the scaling of fluidelastic instability in finned tube arrays.

2) The critical velocity in in-line arrays is substantially delayed by the addition of serrated fins, even though their effect is to significantly reduce the effective pitch ratio (P_t/D_{eff}). This effect increases with increasing fin density.

3) In rotated square finned tube arrays, the addition of fins appear to increase the coupling between neighbouring tubes and the stability threshold is reduced. This could be accounted for in part by the reduction in P_t/D_{eff}. This destabilizing effect increases with increasing fin density.

These results show the importance of the continued study of finned tube arrays, as well as the effects of the effective pitch ratio. It is particularity noteworthy that the effect of fins on in-line and rotated square arrays appears to be opposite, stabilizing in-line and destabilizing rotated square arrays. This behaviour is not understood and much more research is required to address the issue of fluidelastic instability in finned tube bundles.

As experiments in finned tube arrays progress, the differences between bare tubes and finned tubes will be observed, but attention should be given to finding common behaviour between the different tubes. This will ensure that the number of experiments required to understand the behaviour of finned tubes is kept to a minimum.

Attention should be given to the streamwise amplitude of vibration, as it has been shown in the 5.7 fpi in-line square array and both finned tube, rotated square arrays that the amplitude of vibration in the streamwise direction can be extremely large. Ignoring this tube vibration direction could produce misleading results.

The use of finned tubes in heat exchangers in general, will only increase with the on-going trend to recover wasted heat energy from processes and process by-products in a growing environmentally cautious world. The designers and users of these heat exchangers will always want the fluid to flow faster, which makes the tube arrays susceptible to fluidelastic instability and acoustic resonance.

For larger pitched bare tube arrays (P_t/D ratio larger than 1.8), there is a deficiency in the literature/previous data gathered. From the current study it has been shown that with a P_t/D ratio of 2.32:

1) For the in-line array the threshold could be predicted using the guidelines of Weaver & Fitzpatrick (1988). The fluidelastic behaviour was typical in that all of the tubes appear to have become unstable at approximately the same reduced velocity.

2) For the rotated square array it was difficult to select precisely the critical reduced velocity since the threshold was so poorly defined. This may be related to the greater

distance between neighbouring tubes. As the distance increases, the fluidelastic coupling between tubes decreases, causing the tubes to behave more independently.

6.0 References

Beers, Y., Introduction to the Theory of Error, Addison-Wesley Publishing Company Inc.: Cambridge Massachusetts, 1953.

Blevins, R.D., Flow-Induced Vibration, Second Edition. Krieger Publishing Company: Florida, 2001.

Blevins, R.D., "Fluid Elastic Whirling of a Tube Row", Journal of Pressure Vessel Technology, November 1974, 263-267.

Chen, S.S., "Guidelines for the Instability Flow Velocity of Tube Arrays in Crossflow", Journal of Sound and Vibration **93**(3), 1984, 439-455.

Connors, H.J., Jr., "Fluidelastic Vibration of Tube Arrays Excited by Cross Flow", Flow-Induced Vibrations of Heat Exchangers, ASME, December 1970, 42-56.

Connors, H.J., Jr., "Fluidelastic Vibration of Heat Exchanger Tube Arrays", Journal of Mechanical Design, Vol. 100, April 1978, 347-353.

Dye, R.C.F., and Abrahams, C.G.H., "An Investigation of the Aerodynamic Stability of a Cross-Flow Type Finned Tube Heat Exchanger", ASME Winter Annual Meeting and Energy Systems Expostion, Heat Transfer Division, New York, December 1-5, 1968, ASME 68-WA/HT-19, 5 pages.

Eid, M., Vortex Shedding From Single and Tandem Finned Cylinders. M.A.Sc. Thesis, McMaster University, 2004

ElKashlan, M. E. M., Array geometry effects on vortex shedding and instability in heat exchanger tube bundles. Ph.D. Thesis, McMaster University, 1984.

Fan, H., Vortex Shedding and Acoustic Resonance of an Array of Tubes with Twisted Serrated Fins. M.A.Sc. Thesis, McMaster University, 2002

Fischer, M., "Flow-Induced Vibration in Spiral Finned Gas Tube Bundle Heat Exchangers", PVP Vol. 460, July 20-24, 2003, Cleveland, Ohio, 253-259.

Ganapathy, V., "Design and Evaluate Finned Tube Bundles", Hydrocarbon Processing, September 1996, 103-111.

Halle, H., Boers, B.L., and Wambsganss, M.W., "Fluidelastic Tube Vibration in a Heat Exchanger Designed for Sodium-to-Air Operation", Journal of Engineering for Power **97**(4), October 1975, 561-568.

Halle, H., Chenoweth, J.M., and Wambsganss, M.W., "Flow-Induced Tube Vibration Thresholds in Heat Exchangers From Shellside Water Tests", ASME Symposium on Flow-Induced Vibrations, Vol. 3 December 9-14, New Orleans, Louisiana, 1984, 17-32

Hamakawa, H., Fukano, T., Nishida, E., and Aragaki, M., "Vortex Shedding From a Circular Cylinder With Fin", AIAA-2001-2215, May 26-30, 2001, 7 pgs.

Harrison, E., "Heat convection from finned tubes". Mechanical World Monographs, 46, Emmott & Co. Limited, Manchester, UK, 1948, 43 pgs.

Hirota, K., Nakamura, T., Kikuchi, H., Isozaki, K., and Kawahara, H., "Fluidelastic and Vortex Induced Vibration of a Finned Tube Array", Proceedings of IMECE2002, ASME International Mechanical Engineering Congress & Exposition, November 17-22, 2002, New Orleans, Louisiana. Paper: 32793, 7 pgs.

Jebodhsingh, D., The Effect of Fins on Vortex Shedding. M.A.Sc. Thesis, McMaster University, 2002

Jebodhsingh, D., Ziada, S., Weaver, D.S., and Eisinger, F.L., "The Effect of Fins on Vortex Shedding from a Cylinder in Cross-flow", In Proceedings of FIV 2004, 8th International Conference on Flow-Induced Vibrations, (ed. E. de Langre and F. Axisa), July 6-9, Paris, France, 2004, 6 pages.

Katinas, V., Perednis, E., and Svedošc(ius), V., "Crossflow-Induced Vibrations of Staggered Bundles of Finned Tubes", Fluid Mechanics-Soviet Research **20**(3), 1991, 80-88. – English translation from Trudy Akademii Nauk Litovskoy SSR. Ser. Energetika, (1), 1990, 82-89. – 1991FM

Katinas, V., Perednis, E., and Svedošcius, V., "Vibrations of Smooth and Finned Tubes in Crossflows of Viscous Fluids with Different Turbulence Levels", Heat Transfer-Soviet Research **23**(6), 1991, 844-851. – English translation from Litovskaya Akademiya nauk. Energetika, (2), 1990, 134-143. – 1991HT

Katinas, V., and Žukauskas, A., Vibrations of Tubes in Heat Exchangers, Begell House Inc., New York, 1997. (English Translation)

Kienböck, M., "Vibration Characteristics of Finned Tubes with Small Fins", VGB Kraftwerkstechnik 62, number 7, July 1982, 498-506. – English translation from German

Kouba, J., "Vortex Shedding and Acoustic Emission in Finned Tube Banks Exposed to Cross Flow", The 1986 Pressure Vessels and Piping Conference and Exhibition, Chicago Illinois, July 20-24, 1986, PVP, Vol. 104, 1986, 213-217.

Lever, J.H., and Weaver, D.S., "A Theoretical Model for Fluid-Elastic Instability in Heat Exchanger Tube Bundles", Journal of Pressure Vessel Technology, Vol. 104, 1982, 147-158.

Lokshin, V.A., Fomina, V.N., Ushakov, E.N., and Agress, B.A., "The Aerodynamic Resistances of Transversely Swept Tube Bundles with Irregular Pitches", Thermal Engineering **23**(12), 1976, 27-30. – English Translation from Teploenergetika 23(12), 1976, 30-34.

Lokshin, V.A., and Fomina, V.N., "Generalisation of Data From Experimental Investigation of Resistance of Finned Tube Bundles", Thermal Engineering **25**(6), 1978, 31-34. – English Translation from Teploenergetika 25(6), 1978, 36-39.

Lokshin, V.A., Zozulya, N.V., Fomina, V.N., and Portyanko, A.A., "Tests of an Economiser Manufactured of Tubes with Welded Strip-type Fins in a Boiler Operating on Ekibastuz Coal", Thermal Engineering **26**(3), 1979, 139-141. – English Translation from Teploenergetika 26(3), 1979, 10-13.

Lumsden, R.H. and Weaver, D.S., "Fluidelastic Instability in Finned Tube Bundles", Proceedings of CSME Forum 2006, Kananaskis Village, Alberta, Canada, May 21-24, 2006, 6 pages.

Lumsden, R.H. and Weaver, D.S., "The Effect of Fins on Fluidelastic Instability in In-Line and Rotated Square Arrays", Proceedings of PVP2007, ASME 2007 Pressure Vessels and Piping Division Conference, San Antonio, Texas, July 22-26, 2007, PVP2007-26597, 9 pages.

Mair, W.A., Jones, P.D.F., and Palmer, R.K.W., "Vortex Shedding from Finned Tubes", Journal of Sound and Vibration **39**(3), 1975, 293-296.

Nagamatsu, B.H., and Rolsma, B., "Row Depth Effects on Vortex Shedding and Turbulent Buffeting Formation in a Finned Tube Bank", AIAA/ASME 3rd Joint Thermophysics, Fluids, Plasma and Heat Transfer Conference, St. Louis, Missouri, June 7-11, 1982, AIAA-82-0982, 6 pages.

Nemoto, A., and Yamada, M., "Flow-Induced Acoustic Resonance caused by Fin-Tube Bundles", PVP Vol. 243, Symposium on Flow-Induced Vibration and Noise, Volume 4, ASME 1992, 137-152.

Nemoto, A., and Yamada, M., "Flow-Induced Acoustic Resonance in Staggered Tube Banks", PVP Vol. 273, Flow-Induced Vibration, ASME 1994, 273-282.

Nemoto, A., Takakuwa, A., and Tsutsui, M., "Flow-Induced Acoustic Resonance with Various Finned Tube Banks", AD Vol. 53-2, Fluid-Stucture Interaction, Aeroelasticity, Flow-Induced Vibration, ASME 1997, 311-320.

Païdoussis, M.P., "A Review of Flow-Induced Vibrations in Reactors and Reactor Components", Nuclear Engineering and Design **74**, 1982, 31-60.

Perednis, E., and Svyadosch, V., "Fluid Flows Over Bundles of Finned Tubes and Their Stability", Proceedings of the International Conference on Engineering Aero-Hydroelasticity, Prague, December 5-8, 1989, Vol. 1, Paper D-24, 169-173. (Republished in Heat Transfer–Soviet Research)

Pettigrew, M.J., Private Communication, CANCAM 2005, Montreal, Quebec.

Pettigrew, M.J., and Taylor, C.E., "Vibration Analysis of Steam Generators and Heat Exchangers: An Overview, Part 1: Flow, Damping, Fluidelastic Instability", Proceedings of IMECE2002, ASME International Mechanical Engineering Congress & Exposition, November 17-22, 2002, New Orleans, Louisiana. Paper: 32707, 11 pgs.

Powell, C.D., and Sohaney, R.C., "Modal Analysis and Strain Gage Testing of a Finned-Tube Heat Exchanger", Sound and Vibration, August 1989, 16-21.

Price, S.J., "A Review of Theoretical Models for Fluidelastic Instability of Cylinder Arrays in Cross-Flow", Journal of Fluids and Structures **9**, 1995, 463-518.

Reid, D.R., and Taborek, J., "Selection Criteria for Plain and Segmented Finned Tubes for Heat Recovery Systems", Journal of Engineering for Gas Turbines and Power, Vol. 116, 1994, 406-410.

Roberts, B.W., "Low Frequency, Aeroelastic Vibrations in a Cascade of Circular Cylinders", Mechanical Engineering Science, Monograph No. 4, Institution of Mechanical Engineers, September 1966, 32 pg.

Ryu, B.N., Kim, K.C., and Boo, J.S., "The Effect of Serrated Fins on the Flow Around a Circular Cylinder", KSME International Journal, Vol. 17(6), 2003, 925-934.

Schröder, K., and Gelbe, H., "New Design Recommendations for Fluidelastic Instability in Heat Exchanger Tube Bundles", Journal of Fluids and Structures 13, 1999, 361-379.

Soper, B.M.H., "The Effect of Tube Layout on the Fluid-Elastic Instability of Tube Bundles in Crossflow", Journal of Heat Transfer, Vol. 105, November 1983, 744-750.

Sviadosch, V., Katinas, V., and Perednis, E., "Vibrations of Smooth and Finned Tubes in a Cross Flow of Viscous Fluid at Different Turbulence Levels", PVP Vol. 202, Conference on Vibration Control of Mechanical, Structural, and Fluid-Structural Systems, ASME 1990, 69-74. (Republished in Fluid Mechanics–Soviet Research)

Waring, L.F., and Weaver, D.S., "Partial Admission Effects on the Stability of a Heat Exchanger Tube Array", Journal of Pressure Vessel Technology, Vol. 110, May 1988, 194-198.

Weaver, D.S., and ElKashlan, M., "On the Number of Tube Rows Required to Study Cross-Flow Induced Vibrations in Tube Banks", Journal of Sound and Vibration **75**(2), 1981, 265-273. – 1981a

Weaver, D.S., and ElKashlan, M., "The Effect of Damping and Mass Ratio on the Stability of a Tube Bank", Journal of Sound and Vibration **76**(2), 1981, 283-294. – 1981b

Weaver, D.S., and Fitzpatrick, J.A., "A Review of Cross-Flow Induced Vibrations in Heat Exchanger Tube Arrays", Journal of Fluids and Structures **2**, 1988, 73-93.

Weaver, D.S., and Lever, J.H., "Tube Frequency Effects on Cross Flow Induced Vibrations in Tube Arrays", Proceedings of the Fifth Biennial Symposium on Turbulence, October 1977, University of Missouri-Rolla, Missouri, 323-331.

Weaver, D.S., and Yeung, H.C., "Approach Flow Direction Effects on the Cross-Flow Induced Vibrations of a Square Array of Tubes", Journal of Sound and Vibration **87**(3), 1983, 469-482.

Weaver, D.S., Ziada, S., Sun, Z., and Feenstra, P., "The Effect of Platen Fins on the Flow-Induced Vibrations of an In-Line Tube Array", Journal of Pressure Vessel Technology, Vol. 123, 2001, 437-441.

Weierman, C., "Pressure Drop Data for Heavy-Duty Finned Tubes", Chemical Engineering Progress, Vol. 73(2), February 1977, 69-72.

Weierman, C., Taborek, J., and Marner, W.J., "Comparison of the Performance of In-Line and Staggered Banks of Tubes with Segmented Fins", American Institute of Chemical Engineers Symposium Series **174**(74), 1978, 39-46.

Yeung, H.C., and Weaver, D.S., "The Effect of Approach Flow Direction on the Flow-Induced Vibrations of a Triangular Tube Array", Journal of Vibration, Acoustics, Stress, and Reliability in Design, Vol. 105, 1983, 76-82.

Zdravkovich, M.M., "Review and Classification of Various Aerodynamic and Hydrodynamic Means for Suppressing Vortex Shedding", Journal of Wind Engineering and Industrial Aerodynamics 7, 1981, 145-189.

Žukauskas, A., Ulinskas, R., Katinas, V., Fluid Dynamics and Flow-Induced Vibrations of Tube Banks. Hemisphere Publishing Corporation: New York, 1988.

7.0 Appendices

7.1 Error Analysis

Amplitude:

$$Amplitude(m) = Amplitude(V) * \left(\frac{Calibration(m)}{Calibration(V)} \right)$$

For 5.7 fpi @ 2% $D_{eff} \approx 0.001$ m (0.00099 m, Calibration value at 1 mm will be used). Strain Gauge, Vernier Height Gauge and Voltmeter were used in this analysis (values in Section 3.7).

$$Amplitude(m) = 0.080 * \left(\frac{0.001}{0.080} \right) = 0.001 \text{ m}$$

$$Error_{Amplitude(m)} = Amplitude(m) * \sqrt{\left(\frac{Error_{Amplitude(V)}}{Amplitude(V)} \right)^2 + \left(\frac{Error_{Calibration(V)}}{Calibration(V)} \right)^2 + \left(\frac{Error_{Calibration(m)}}{Calibration(m)} \right)^2}$$

$$Error_{Amplitude(m)} = 0.001 * \sqrt{\left(\frac{0.0005}{0.080} \right)^2 + \left(\frac{0.0005}{0.080} \right)^2 + \left(\frac{0.00005}{0.001} \right)^2}$$

$$Error_{Amplitude(m)} = 0.00005 \text{ m}$$

Upstream Velocity using Pressure Transducer:

$$Velocity\left(\frac{m}{s} \right) = \sqrt{2 * \frac{\rho_{H_2O}\left(\frac{kg}{m^3} \right)}{\rho_{AIR}\left(\frac{kg}{m^3} \right)} * g\left(\frac{m}{s^2} \right) * \frac{0.0254(m)}{1(in)} * 2(in\_H_2O) * \left(\frac{Pressure(V) - 1.000(V)}{6.000(V) - 1.000(V)} \right)}$$

For 5.7 fpi Rotate Square Array @ at the Critical Upstream Velocity. Water Manometer and Voltmeter were used in this analysis (values in Section 3.7).

$$Velocity\left(\frac{m}{s}\right)=\sqrt{2*\frac{1000}{1.19}*9.81*\frac{0.0254}{1}*2*\left(\frac{1.032-1.000}{6.000-1.000}\right)}=2.315\ \text{m/s.}$$

$$Error_{Velocity\left(\frac{m}{s}\right)}=0.5*Velocity\left(\frac{m}{s}\right)*\sqrt{\begin{aligned}&\left(\frac{Error_{Density(kg/m^3)}}{Density(kg/m^3)}\right)^2+\left(\frac{Error_{Density(kg/m^3)}}{Density(kg/m^3)}\right)^2\\&+\left(\frac{Error_{Gravity(m/s^2)}}{Gravity(m/s^2)}\right)^2+\left(\frac{Error_{Calibration(in\_H_2O)}}{Calibration(in\_H_2O)}\right)^2\\&+2*\left(\frac{Error_{\Delta Pressure\_Calibration(V)}}{Pressure(V)-Pressure\_Calibration(V)}\right)^2\\&+2*\left(\frac{Error_{\Delta Pressure\_Calibration(m)}}{\Delta Pressure\_Calibration(V)}\right)^2\end{aligned}}$$

$$Error_{Velocity\left(\frac{m}{s}\right)}=0.5*2.315*\sqrt{\begin{aligned}&\left(\frac{0.5}{1000}\right)^2+\left(\frac{0.005}{1.19}\right)^2+\left(\frac{0.005}{9.81}\right)^2+\left(\frac{0.0005}{2.000}\right)^2\\&+2*\left(\frac{0.0005}{1.032-1.000}\right)^2+2*\left(\frac{0.0005}{6.000-1.000}\right)^2\end{aligned}}$$

$Error_{Amplitude(m)} = 0.026$ m/s

Upstream Velocity using Water Manometer (Bare In-Line Array):

$$Velocity\left(\frac{m}{s}\right)=\sqrt{2*\frac{\rho_{H_2O}\left(\frac{kg}{m^3}\right)}{\rho_{AIR}\left(\frac{kg}{m^3}\right)}*g\left(\frac{m}{s^2}\right)*\frac{0.0254(m)}{1(in)}*\Delta Pressure(in\_H_2O)}$$

For Bare Tube In-Line Square Array @ at the Critical Upstream Velocity. Water Manometer was used in this analysis (value in Section 3.7).

$$Velocity\left(\frac{m}{s}\right)=\sqrt{2*\frac{1000}{1.19}*9.81*\frac{0.0254}{1}*(4.793-4.780)}=2.333\ \text{m/s.}$$

$$Error_{Velocity\left(\frac{m}{s}\right)} = 0.5 * Velocity\left(\frac{m}{s}\right) * \sqrt{\left(\frac{Error_{Density(kg/m^3)}}{Density(kg/m^3)}\right)^2 + \left(\frac{Error_{Density(kg/m^3)}}{Density(kg/m^3)}\right)^2 + \left(\frac{Error_{Gravity(m/s^2)}}{Gravity(m/s^2)}\right)^2 + 2 * \left(\frac{Error_{\Delta Pressure(in\_H_2O)}}{\Delta Pressure(in\_H_2O)}\right)^2}$$

$$Error_{Velocity\left(\frac{m}{s}\right)} = 0.5 * 2.333 * \sqrt{\left(\frac{0.5}{1000}\right)^2 + \left(\frac{0.005}{1.19}\right)^2 + \left(\frac{0.005}{9.81}\right)^2 + 2 * \left(\frac{0.0005}{4.793 - 4.780}\right)^2}$$

$Error_{Amplitude(m)} = 0.064$ m/s

7.2 Strain Gauge Calibration Curves

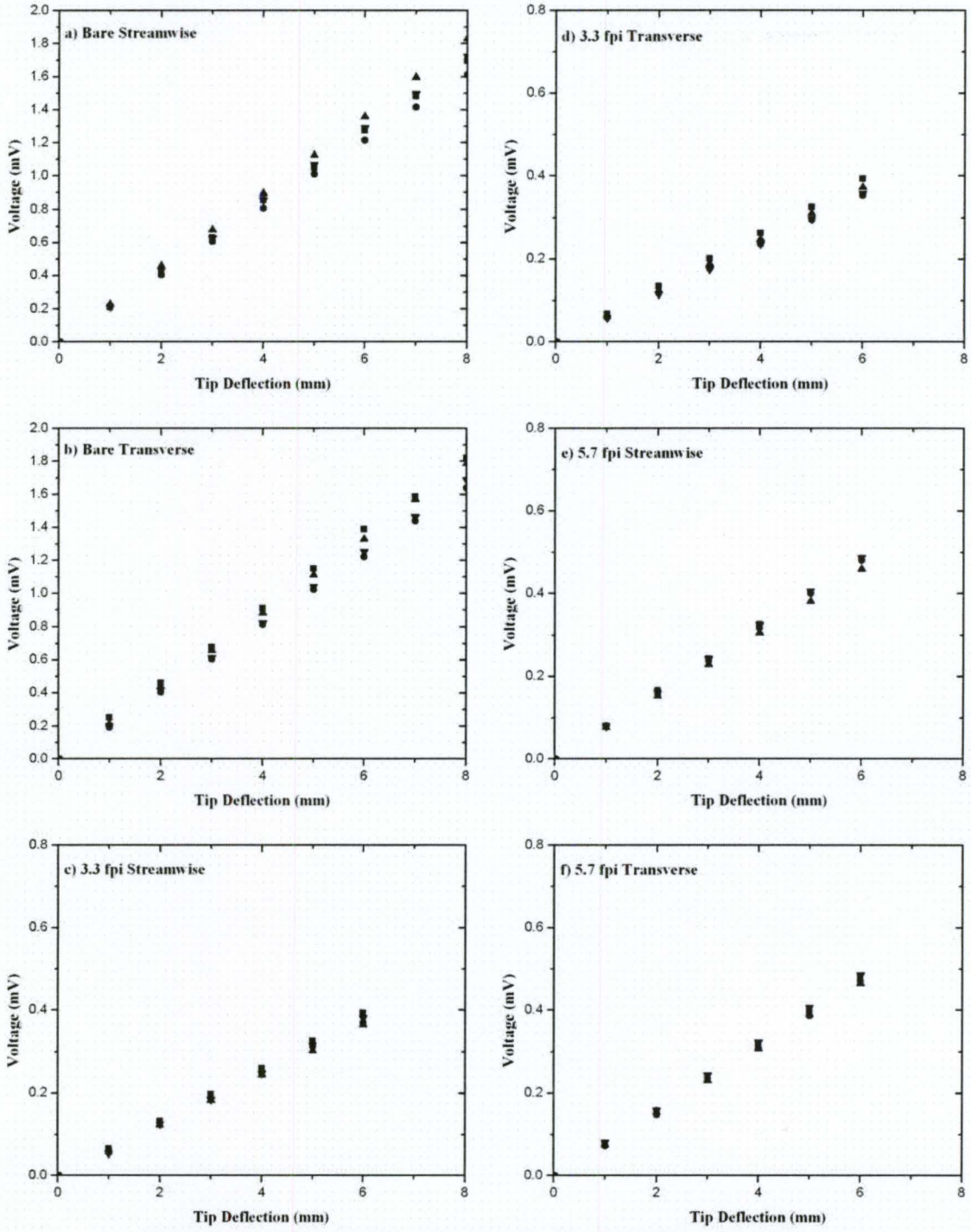

Figure 7.1: Calibration Curves for In-Line Square Arrays, a) bare Streamwise, b) bare Transverse, c) 3.3 fpi Streamwise, d) 3.3 fpi Transverse, e) 5.7 fpi Streamwise, f) 5.7 fpi Transverse ■ – 1, ● – 2, ▲ – 3, ▼ – 4 (refer to Figure 3.2)

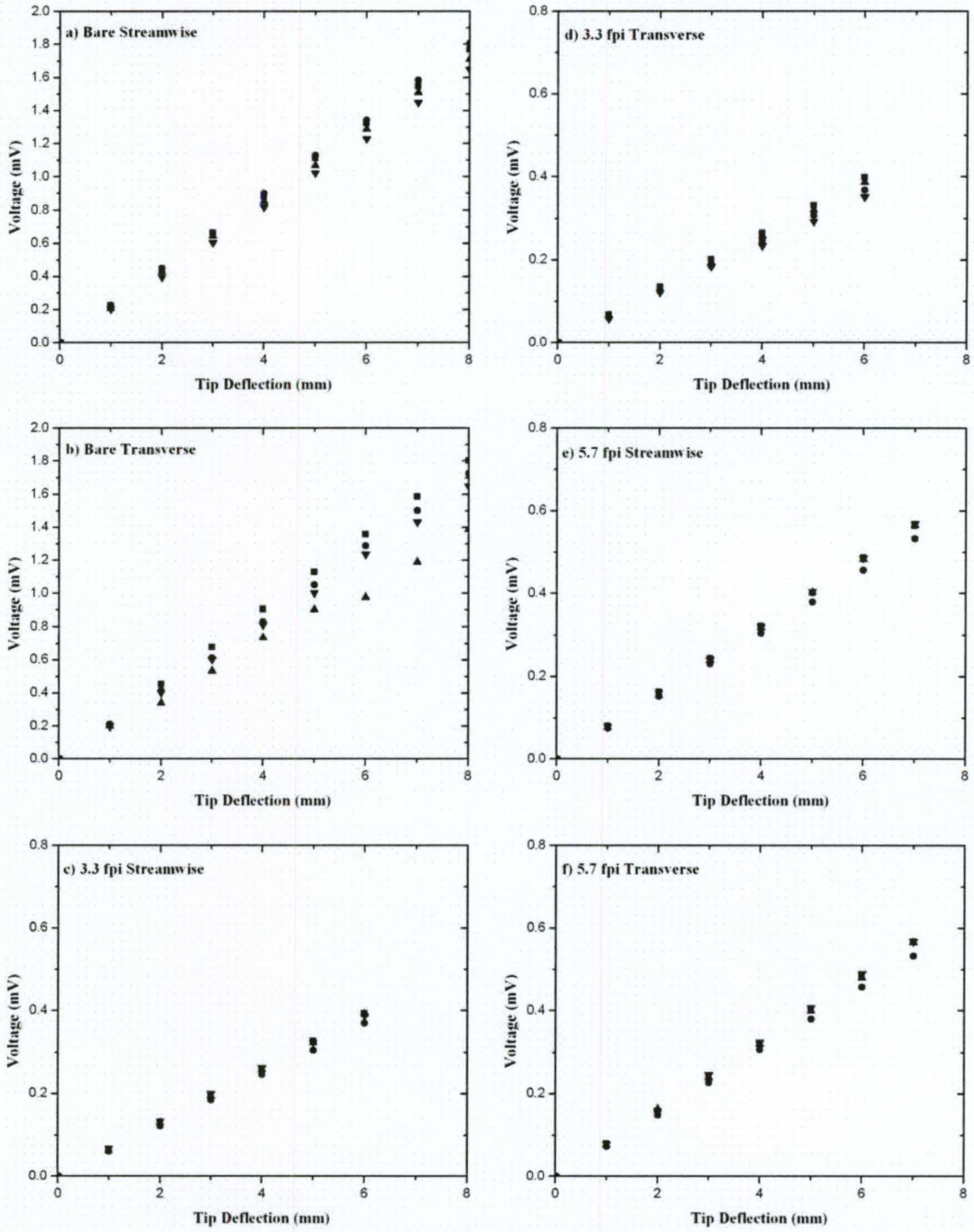

Figure 7.2: Rotated Square Arrays,
a) bare Streamwise, b) bare Transverse, c) 3.3 fpi Streamwise,
d) 3.3 fpi Transverse, e) 5.7 fpi Streamwise, f) 5.7 fpi Transverse
■ – 5, ● – 6, ▲ – 7, ▼ – 8 (refer to Figure 3.2)

Table 7.1: In-Line Square Strain Gauge Calibrations (mm/V)

	Streamwise				Transverse			
Tube	**1**	**2**	**3**	**4**	**1**	**2**	**3**	**4**
Bare	4.710	4.974	4.390	4.648	4.409	4.860	4.459	4.752
3.3 fpi	15.308	16.183	16.440	15.632	15.331	16.949	16.110	16.733
5.7 fpi	12.394	12.505	13.090	12.302	12.448	12.740	12.878	12.334

Table 7.2: Rotated Square Strain Gauge Calibrations (mm/V)

	Streamwise				Transverse			
Tube	**5**	**6**	**7**	**8**	**5**	**6**	**7**	**8**
Bare	4.531	4.428	4.653	4.835	4.411	4.628	5.881	4.852
3.3 fpi	15.216	16.241	15.358	15.507	15.102	16.288	15.590	17.072
5.7 fpi	12.396	13.141	12.340	12.305	12.334	13.075	12.426	12.249

Note: all calibration trends are linear except for tube #7 in the bare tube rotated square array (Figure 7.2 b)). These plots are the calibrations for the strain gauge voltage versus tube tip deflection.

7.3 Friction Factor

The friction factor across each tube array is presented in Figure 7.3 for the in-line and in Figure 7.4 for the rotated square arrays. The figures are plots of the friction factor per row versus the Reynolds number. The friction factor is calculated based on the definitions in Weierman (1977) and Weierman *et al.* (1978) so that they can be compared with the predicted results discussed below. The friction factors for each array are presented in Table 7.3. It can be seen from the data that the addition of fins causes an increase in the friction factor. This result is expected due to the increase in flow blockage. When comparing the bare tube array results it can be seen that the friction factor for the rotated square array is only slightly higher, which is expected with such a

large tube pitch ratio. The friction factor for the rotated square finned tube arrays is higher than the in-line square finned arrays, which agrees with existing literature. The results indicate that the rotated square finned tube arrays have a friction factor twice that of the in-line square finned tube arrays. Note that the wind tunnel measurements were only obtained for the velocities that span the fluidelastic instability experiments and the array was fully fixed during these experiments.

Table 7.3: Friction Factor

Tube	P_t/D_{eff}	In-Line	Rotated
Bare	2.32	0.04-0.05	0.04-0.05
3.3 fpi	2	0.06-0.07	0.10-0.13
5.7 fpi	1.78	0.11-0.14	0.21-0.25

Further in this Appendix, the equations are provided for the friction factor predictions for the finned tube arrays. The comparison between these calculations and the experimental results are presented in Figures 7.5 to 7.8. In all cases except for the 5.7 fpi in-line square array, the predicted value is higher than the experimental results. For the 5.7 in-line square array the predictions are slightly lower. The difference between the experimental friction factor and the predicted results are presented in Table 7.4.

Table 7.4: Difference between Experimental and Predicted Results

Tube	In-Line	Rotated
3.3 fpi	15-30%	40-60%
5.7 fpi	5-25%	30-35%

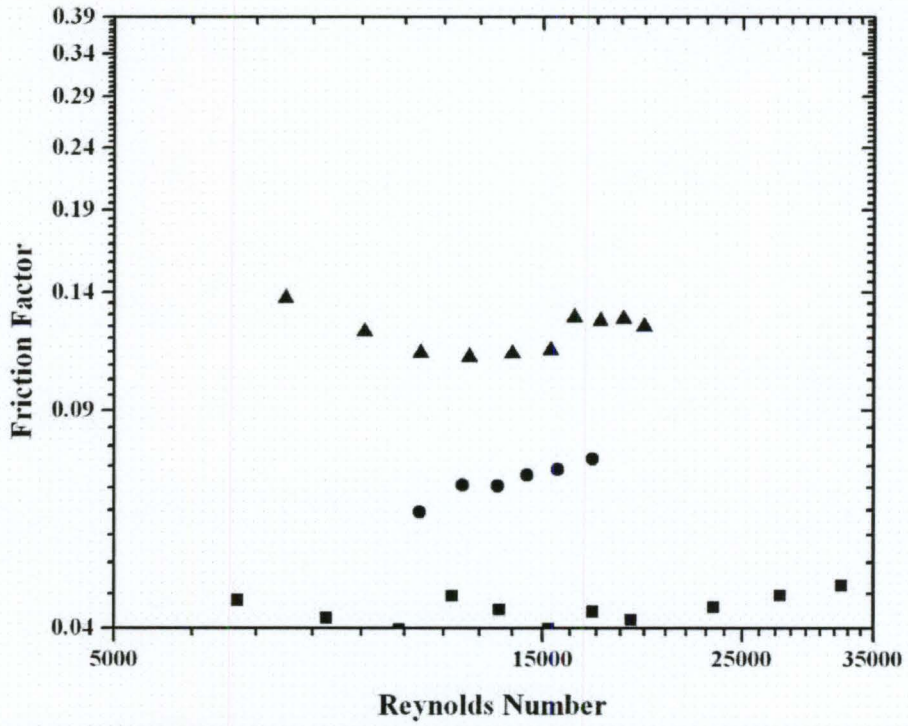

Figure 7.3: Friction Factor, In-Line Square, ■ – Bare, ● – 3.3 fpi, ▲ – 5.7 fpi

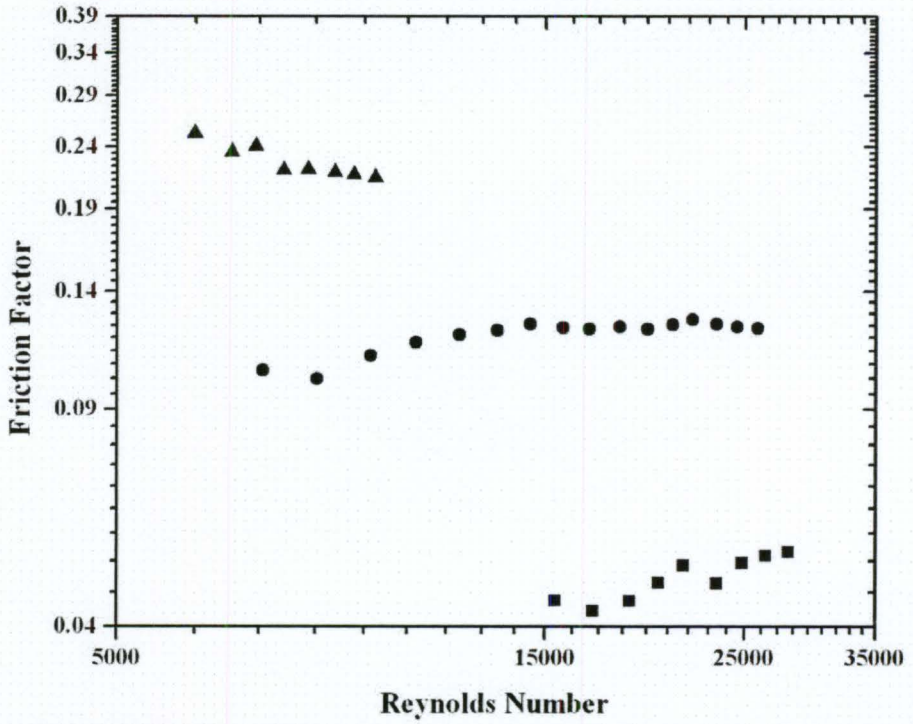

Figure 7.4: Friction Factor, Rotated Square, ■ – Bare, ● – 3.3 fpi, ▲ – 5.7 fpi

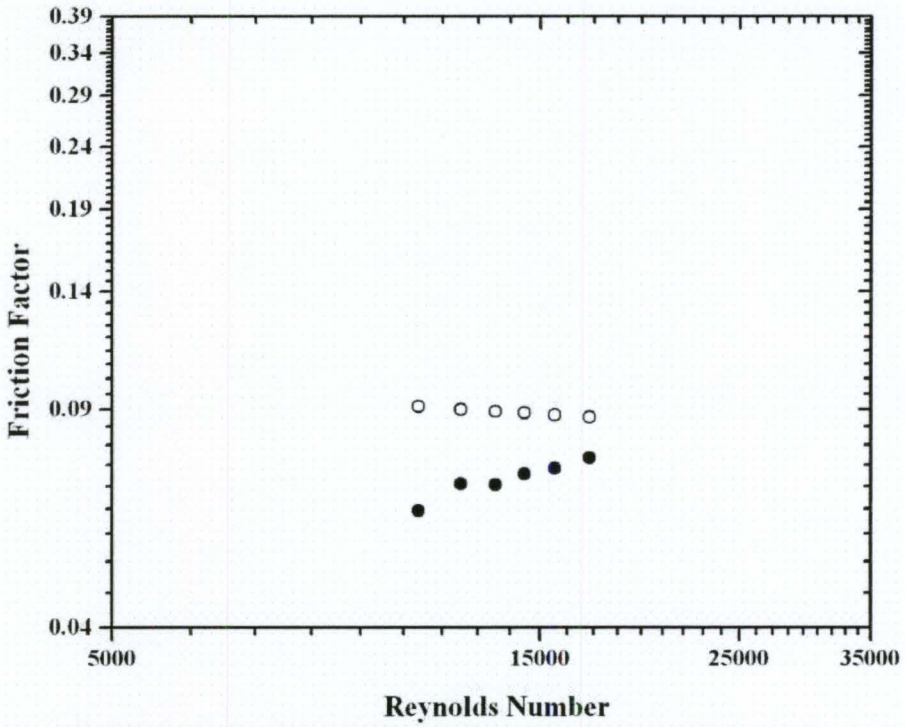

Figure 7.5: Friction Factor, 3.3 fpi In-Line Square, ● – Experiment, ○ – Analytical

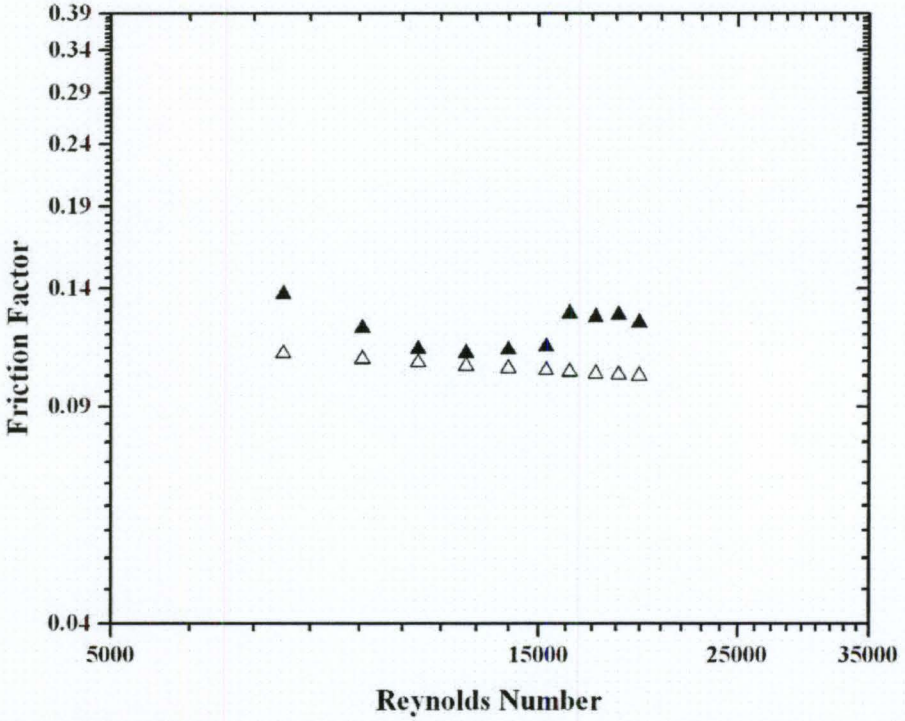

Figure 7.6: Friction Factor, 5.7 fpi In-Line Square, ▲ – Experiment, Δ – Analytical

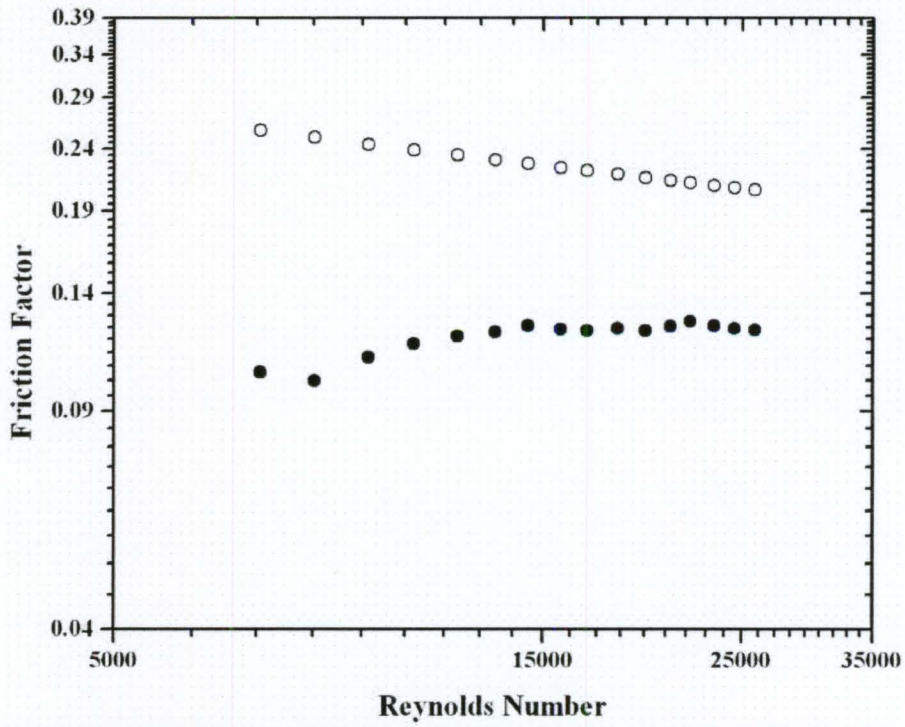

Figure 7.7: Friction Factor, 3.3 fpi Rotated Square, ● – Experiment, ○ – Analytical

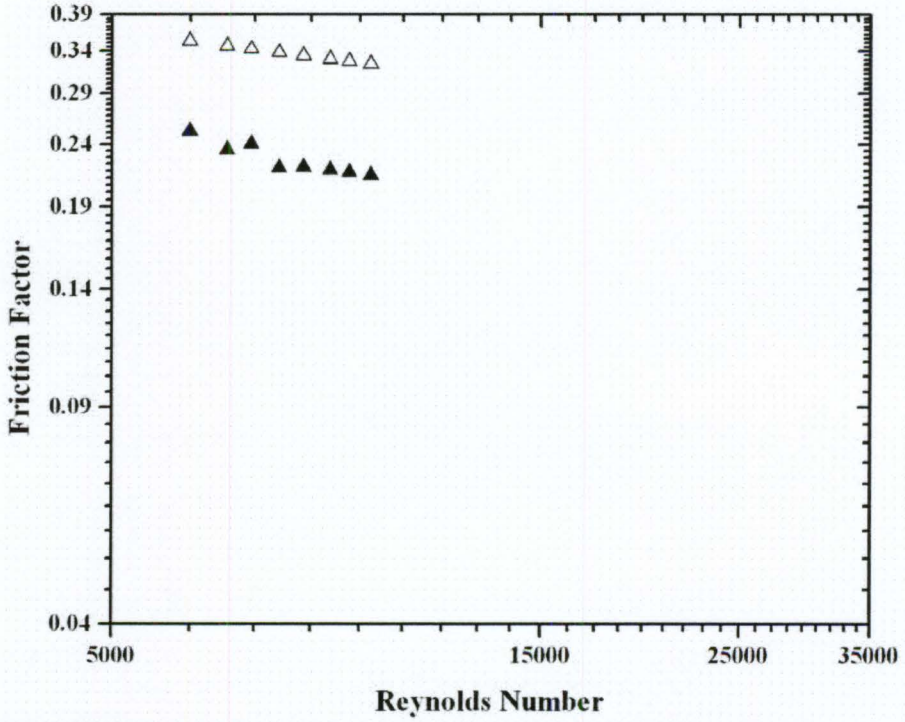

Figure 7.8: Friction Factor, 5.7 fpi Rotated Square, ▲ – Experiment, Δ – Analytical

Calculation of the Fanning Friction Factor using ESCOA Calculations for finned tube arrays. NOTE: The Fanning Friction Factor is 4 times less than the more familiar Darcy Friction Factor.

In-Line (ESCOA)

$$C_2 = 0.11 + 1.4\,\mathrm{Re}_D^{-0.40}$$

$$C_4 = 0.08\left[0.15\frac{P_t}{D_b}\right]^{\left(-1.1\left\{\frac{l_f}{s_f}\right\}^{0.15}\right)}$$

$$s_f = \frac{1}{n_f} - t_f$$

$$C_6 = 1.6 - \left[0.75 - 1.5e^{-0.7N}\right]e^{-0.2\left(\frac{P_l}{P_t}\right)^2}$$

$$f_f = C_2 C_4 C_6 \frac{D_f}{D_b}\left(\frac{T_b - 460}{T_s - 460}\right)^{0.25}$$

Staggered (ESCOA)

$$C_2 = 0.075 + 1.85\,\mathrm{Re}_D^{-0.30}$$

$$C_4 = 0.11\left[0.05\frac{P_t}{D_b}\right]^{\left(-0.7\left\{\frac{l_f}{s_f}\right\}^{0.2}\right)}$$

$$C_6 = 1.1 + \left[1.8 - 2.1e^{-0.15N^2}\right]e^{-2\frac{P_l}{P_t}} - \left[0.7 - 0.8e^{-0.15N^2}\right]e^{-0.6\frac{P_l}{P_t}}$$

$$f_f = C_2 C_4 C_6 \sqrt{\frac{D_f}{D_b}} \left(\frac{T_b - 460}{T_s - 460} \right)^{-0.25}$$

Nomenclature:

C_2 – Reynolds number correction

C_4 – Fin Geometry correction

C_6 – Tube Layout correction

D_f – Fin Diameter

D_b – Bare tube Diameter

f_f - Fanning Friction Factor

l_f – Length of fin

N – Number of tube rows in the streamwise direction

n_f – fins per inch

P_t – Tube Pitch in Transverse to flow Direction

P_l – Tube Pitch in longitudinal Direction (streamwise)

s_f – Gap between fins

T_b – Average outside Fluid Temperature

T_s – Average fin surface temperature

t_f – Fin thickness

***FOR TUBE-X HF tubes

Information from www.fintubetech.com/escoa (RE) Accessed April 11, 2006

ESCOA Engineering Manual: TURB-X HF MENU: RATING PROCEDURE

7.4 Damping Trial Results

Several damping trials were taken per instrumented tube. Table 7.5 and 7.6 show the results of each trial in the in-line and rotated square arrays respectively. This information was fed into Table 3.5. The largest difference between a trial value and its trial average was 9%.

Table 7.5: In-Line Square Damping Trial Results

Tube	1		2		3		4	
	Trial Value	**Trial Average**	**Trial Value**	**Trial Average**	**Trial Value**	**Trial Average**	**Trial Value**	**Trial Average**
Bare	0.0039	0.0037	0.0026	0.0024	0.0037	0.0037	0.0023	0.0024
	0.0035		0.0023		0.0036		0.0024	
	0.0038		0.0024		0.0038		0.0024	
3.3 fpi	0.0045	0.0047	0.0046	0.0048	0.0048	0.0046	0.0048	0.0048
	0.0046		0.0050		0.0044		0.0049	
	0.0051		0.0049		0.0046		0.0046	
5.7 fpi	0.0064	0.0064	0.0061	0.0062	0.0049	0.0049	0.0074	0.0073
	0.0064		0.0063		0.0049		0.0076	
	0.0064		0.0061		0.0049		0.0068	

Table 7.6: Rotated Square Damping Trial Results

Tube	5		6		7		8	
	Trial Value	**Trial Average**	**Trial Value**	**Trial Average**	**Trial Value**	**Trial Average**	**Trial Value**	**Trial Average**
Bare	0.0035	0.0035	0.0028	0.0029	0.0061	0.0056	0.0024	0.0026
	0.0034		0.0029		0.0055		0.0027	
	0.0036		0.0029		0.0052		0.0026	
3.3 fpi	0.0052	0.0050	0.0047	0.0048	0.0055	0.0055	0.0051	0.0050
	0.0050		0.0050		0.0053		0.0050	
	0.0049		0.0049		0.0056		0.0049	
5.7 fpi	0.0061	0.0064	0.0049	0.0049	0.0076	0.0075	0.0060	0.0063
	0.0069		0.0049		0.0075		0.0066	
	0.0063		0.0048		0.0074		0.0063	